NASA TECHNICAL NOTE

NASA TN D-3200

c. 1

NASA TN D-3200

INVESTIGATION OF THE USE OF PENETROMETERS TO DETERMINE THE CAPABILITY OF DUST MATERIALS TO SUPPORT BEARING LOADS

by Brantley R. Hanks and John Locke McCarty

Langley Research Center
Langley Station, Hampton, Va.

NATIONAL AERONAUTICS AND SPACE ADMINISTRATION • WASHINGTON, D. C. • JANUARY 1966

INVESTIGATION OF THE USE OF PENETROMETERS TO DETERMINE THE CAPABILITY OF DUST MATERIALS TO SUPPORT BEARING LOADS

By Brantley R. Hanks and John Locke McCarty

Langley Research Center
Langley Station, Hampton, Va.

NATIONAL AERONAUTICS AND SPACE ADMINISTRATION

For sale by the Clearinghouse for Federal Scientific and Technical Information
Springfield, Virginia 22151 – Price $3.00

CONTENTS

INVESTIGATION OF THE USE OF PENETROMETERS TO DETERMINE THE CAPABILITY OF DUST MATERIALS TO SUPPORT BEARING LOADS

By Brantley R. Hanks and John Locke McCarty
Langley Research Center

SUMMARY

The characteristics of accelerometer-equipped spherical projectiles (penetrometers) impacting targets composed of uniformly sized fine particles were examined under atmospheric pressure conditions over a range of impact variables to determine the adequacy of the penetrometer technique to define the load-supporting capability or bearing strength of dust materials. Studies were made of the characteristics which describe the acceleration time history of impact and the characteristics which describe the impact craters. In addition, studies which included multiple quasi-static loading tests were made to evaluate certain physical properties of the dust targets for the purpose of defining their bearing strengths.

The results of this investigation, which was somewhat limited in scope, indicated that the penetrometer technique is amenable to defining characteristics of a dust material. Peak accelerations and characteristic times of the acceleration time histories generated during penetrometer impact into dust targets are related on a gross scale to the target bearing strength and density. Furthermore, the bearing strength of a dust material depends not only upon the density of the medium but also upon less evident factors such as the size and shape of individual particles. Empirical expressions are formulated for peak acceleration and penetration depth in terms of parameters containing the impact test variables.

INTRODUCTION

The long standing scientific interest in the surface structure of the moon has currently advanced to a need for engineering data to support manned landings and explorations. Although the recent photographs of discrete regions of that surface provided by the Ranger spacecraft identify objects of about 3 feet (0.91 meter) in dimension, diverse opinion still exists as to the actual composition or texture of the surface material. However, indications are that the surface of the moon is covered with a layer of dust-like material (for example, refs. 1 to 3), although theories vary considerably as to its formulation, quantity, distribution, behavior, and particle size. Of the various lunar surfaces conjectured, one having a deep dust layer would probably pose the greatest challenge to landing and surface operations. Unless the bearing strength (load-supporting capability) of the lunar surface at and near prospective landing sites is adequately defined, hardware design requirements for surface landing and exploration must consider all potential types of landing surfaces; therefore, a need exists to determine the bearing strength of tentative lunar landing sites. Furthermore, this information should be obtained by direct measurement techniques employing engineering tools that are designed to perform such tasks.

Techniques used to determine the bearing strength of terrestrial soils or materials, such as the bevameter and shear tests, generally require in situ personnel operations. In view of the limitations of such methods, the Langley Research Center has been engaged in the development of the dynamic penetrometer technique for measuring physical properties of remote surfaces such as that of the moon. This technique consists of impacting acceleration-measuring instruments, called penetrometers, onto the surface in question and analyzing the accelerations generated during impact. The results of penetrometer studies conducted on terrestrial materials ranging in hardness or penetrability from that of concrete to that of coarse sand indicated that sufficient information could be derived from impact acceleration time histories to define adequately certain physical properties of the target materials examined. (See ref. 4.) Considerable attention (refs. 5 and 6) has since been given to the application of this technique to investigate properties of lunar and planetary surfaces.

The target materials of reference 4 were not intended to be representative of anticipated lunar surface media but were chosen to study different classes of the impact phenomena. Indeed, should the lunar surface prove to have the load-supporting strength of concrete, sod, or even sand, the lunar landing and surface operational problems would be greatly alleviated. However, in view of the lunar dust concept, a study was undertaken to investigate the applicability of the penetrometer technique to determine the bearing strength of dust-like media. The results of this investigation, which was performed under atmospheric conditions, are reported herein. Beds of uniformly sized fine particles were impacted with various accelerometer-equipped projectiles for purposes of relating the resulting impact characteristics to data from bearing strength tests conducted on the same beds.

SYMBOLS

The units used for the physical quantities defined in this paper are given both in the U.S. Customary Units and in the International System of Units (SI). Factors relating the two systems are given in reference 7.

a_{max}	peak acceleration, g units (1 g = 9.8 meters per second^2)
D	penetrometer diameter, inches (centimeters)
d	diameter of blast crater, inches (centimeters)

k	penetration parameter
m	penetrometer mass, pound-second^2 per inch (kilograms)
t_r	rise time for peak acceleration in acceleration time history, milliseconds
t_t	total time for acceleration time history, milliseconds
V	penetrometer impact velocity, inches per second (centimeters per second), unless otherwise indicated
y	penetration depth of impacting penetrometer, inches (centimeters)
l	average particle size, microns ($1\mu = 0.001$ millimeter)
γ	dust density, pounds per cubic foot (kilograms per meter^3)

APPLICABILITY OF PREVIOUS RESEARCH

The objective of the tests described herein was to relate impact characteristics of accelerometer-equipped projectiles to the load-supporting capability of certain dust-like materials which may pose landing difficulties if encountered on the surface of the moon. In meeting this objective it was necessary to conduct a twofold test effort: tests to define the bearing strength of each of the examined dusts and tests to collect data on the resulting characteristics of penetrometers impacting those materials. The possible applicability to this study of previous efforts in these areas is briefly discussed in the following paragraphs.

Bearing-Strength Tests

The bearing strength of a surface is defined as the maximum load per unit area which may be applied to that surface without causing penetration beyond prescribed limits. Experimental bearing-strength studies to date have been performed primarily in the field of soil mechanics on naturally occurring earth materials to evaluate those materials for such structural applications as buildings, highways, and runways. (See, for example, refs. 8, 9, and 10.) The subject has been theoretically treated (for example, refs. 11 to 14); however, these studies, at best, predict only the bearing capacity of a material - that is, the pressure necessary to cause plastic failure. Furthermore, these theories cannot predict load-penetration profiles or penetration depths at which plastic failure will occur. Hence, the results of these experimental and theoretical studies are not directly applicable to defining the resistance to penetration of the lunar surface, or of a simulated lunar surface, while undergoing loading such as that incurred during and following a spacecraft landing. Because of this lack of information, bearing-strength studies have been included in several programs intended to evaluate the mechanics of potential lunar-type soils. For example, references 15 and 16 include the results of experimental studies to determine the resistance of powdered pumice, and silica and olivine flours, respectively, to penetration by small rectangular probes (i.e., loading plates) under both atmospheric and vacuum conditions. The results of measurements of bearing capacity on powdered olivine basalt in various states of packing obtained in both air and vacuum by means of small cylindrical probes are presented in reference 17. Although the information obtained from these reports was valuable in describing test procedures and in interpreting the data, no direct application of these data could be made to the present tests because data in each case are unique to the particular material tested.

Impact Tests

Studies treating various aspects of impact phenomena have received considerable attention in recent years. Research in the field of ordnance and ballistics (refs. 18 and 19, for example) has included studies to evaluate the impact characteristics of projectiles, bombs, and missiles striking a variety of targets. Research is also under way to study new impact problems which arose with the advent of space flight, such as the effects of impact of meteoric particles on space vehicles. The primary objective of these efforts has been to evaluate impact damage mechanisms. The Langley Research Center has been engaged for several years in impact research for the purpose of utilizing impact data to evaluate the physical characteristics of the target. This research (ref. 4) supported the development of penetrometers as potential devices for measuring characteristics of remote surfaces such as that of the moon. Such measurements entail a study of the acceleration time history at impact and include comparisons with acceleration time histories measured for known materials such as those which occur on the earth's surface.

Prior research to obtain impact acceleration data has been restricted to firm targets (e.g., concrete, lead, sod, etc.) which have fairly distinct physical characteristics in relation to each other. Impact tests on targets composed of dust media (for example, ref. 20), which are of significant interest in lunar surface evaluation studies, have been concerned primarily with penetration characteristics and not with impact accelerations. The present tests are directed at measuring the acceleration characteristics of various penetrometers impacting into dust-like materials by utilizing the experimental and data reduction techniques previously established.

APPARATUS AND TEST PROCEDURE

Test Bed

Description of material.- The dust material used in the bearing strength and impact tests consisted of different grades of aluminum oxide particles (specific gravity 3.89) and one grade of ground pumice (specific gravity 2.20). Aluminum oxide was chosen because it is relatively inert and is commercially available in large quantities of closely graded particle sizes, and pumice was selected to provide a material of low density. The characteristics of these materials are given in table I. These characteristics, like the test data, were obtained in an atmospheric, room-temperature environment in which the moisture content of each dust grade never exceeded 0.3 percent.

The average particle size of each dust grade was evaluated by means of the sieving technique discussed in reference 21. This technique yields the weight distribution of the particle sizes within a dust grade, from which the average particle size can be determined. The results of the sizing measurements performed on the dusts of these tests are presented in figure 1. For the grade having the smallest dust particles, the average particle size was determined by means of a different technique which is based upon an air permeability principle (ref. 22). The average particle size for this grade was 5μ.

Table I also includes the angle of repose for each of the dust sizes examined. The angle of repose as used herein is the average slope of several piles of particles formed by pouring from just above the pile. Photographs of typical piles formed during the course of these tests are presented as figure 2. The angles formed by the 5μ dust exceed those formed by the larger dust sizes. The angles in the region of the pile apex for such a dust, which can be in excess of 90°, were not considered because the pouring process introduces material packing and other possible dynamic effects in that vicinity of the pile. The angles of repose measured from these and other similar photographs are presented in figure 3 together with measurements obtained from other dust sizes which were examined to provide better insight into the effect of particle size on the angle of repose. Measured angles of repose of the pumice particles are also included in this figure and are somewhat higher than those of the aluminum oxide at the corresponding particle size. Figure 3 shows that the angle of repose tends to decrease slightly with decreasing particle size until particles of about 7μ are reached. The angle of repose for particles below this size is considerably greater, averaging approximately 51°. There are two primary static restraining forces involved in angle-of-repose tests; namely, friction forces which depend upon particle weight, shape, and size and the little understood interparticle cohesive forces which are believed to increase with decreasing particle size. For particle sizes less than 7μ, it is possible that the interparticle cohesive forces influence the particle behavior, whereas the friction forces dominate the behavior of the larger particles. Some of the scatter in the data for the smaller size particles may be attributed to this interparticle cohesion since, as noted in reference 11, angles of repose for material with cohesion are not definitive.

Photomicrographs, such as those shown in figure 4, were taken of representative dust samples to determine general shape characteristics of the different grades of aluminum oxide dust. Measurements were made from the photomicrographs to determine the percentage of oblong particles in each dust size, an oblong particle being arbitrarily defined as one with a length-width ratio of at least 2. Measurements were made on samples which ranged in size from 500 particles for the coarser grades to over 1600 particles for the finer grades. The results of these measurements, presented in table I, indicated a much smaller percentage of oblong particles in the four coarser dusts than in the finer dusts.

Water was also included as a target material in several impact tests to aid in understanding the observed fluid-like behavior of the finer dust particles during impact.

Preparation.- All tests upon dust media were performed in an 18-in-square (45.72 cm) wooden test bin filled to a depth of approximately 12 in. (30.48 cm). A sectional sketch of the bin is presented in figure 5.

The bin was equipped with a dust preparation apparatus which was necessary to assure repeatability of test-bed conditions. The apparatus consisted of a valved manifold, a tubing system, and an air diffuser pad to accommodate a dust aerification process. The aerification process, which was repeated prior to each test, consisted of forcing air under pressure into the dust through the perforated tubes in the bottom of the test bin. Distribution of air to each of the tubes was equalized by the manifold mounted beneath the bin. A felt pad, covering the tubes, served to diffuse the air flow to the dust and to prevent the tubes from becoming clogged. The aerification forced the dust particles to become essentially suspended in the air flow and fall under their own weight when the air flow ceased. Following aerification, the surface of the dust was scraped to provide a level test surface. Measurements of the density of the prepared dust were obtained by weighing a cylindrical sample, 3 in. (7.62 cm) in diameter and 4 in. (10.16 cm) in length, extracted from the top of the bed.

The aerification process for preparing the test bed was employed in both the bearing-strength and the impact phases of this study. Modifications to the process (changing either the aerification pressure or the diffuser pads) permitted the study of different dust densities. The various densities of each dust size examined are given in table I. Bearing-strength tests were performed upon each dust at all densities tabulated; however, impact tests were conducted only upon those dusts whose densities are indicated by asterisks.

Bearing-Strength Tests

Loading apparatus.- The apparatus employed for applying a load to the dust material in the bearing-strength evaluation tests consisted of an air-driven piston and various loading plates. Figure 5 shows a sketch of the apparatus mounted to the test bin. Compressed air bled into a cylinder actuated a piston which in turn forced the loading plate into the dust material. The magnitude of the load and the loading rate were controllable by means of a needle valve which regulated the air pressure behind the piston. For purposes of these tests, the loading rate was controlled such that the average penetration rate was maintained at less than approximately 0.3 in/min (0.0127 cm/sec).

The loading plates were disks having areas of 5, 10, 30, and 50 in^2 $\left(32.26, 64.52, 193.55, \text{ and } 322.58\ \text{cm}^2\right)$ constructed from 1/2-in-thick (1.27 cm) aluminum plate. Bearing-strength tests were also conducted with 2-, 3-, and 4-in-diameter (5.08, 7.62, and 10.16 cm) spheres made of epoxy resin and fiber glass in order to relate the static loads to the dynamic loads incurred during the impact phase of this research.

Both a loading plate and one of the fiber-glass spheres are shown in figure 6, which is a sequence of photographs taken during bearing-strength tests performed on four of the dust grades.

Instrumentation.- The applied force was measured by means of a load cell mounted between the piston and the loading plate; plate penetration was measured by a potentiometer which was actuated by plate displacements through an attached cable. (See fig. 5.) The outputs from these instruments were recorded simultaneously and displayed for continuous observation and subsequent analysis.

Test procedure.- The procedure employed in the bearing-strength tests consisted of forcing loading plates into a bed of dust particles and monitoring the penetration and the corresponding applied load. The loading process was one of regulating the air flow to the cylinder to permit a gradual increase in pressure behind the piston, which directly affected the loading to the plate. Plate loading continued until either the applied load had reached 500 lb (2224 N) or the plate had penetrated to a depth of 6 in. (15.24 cm); these restrictions were imposed by the structural integrity of the apparatus and the size of the dust container. Each loading test was performed at least twice and, for purposes of evaluation, a curve was faired through the composite data as illustrated in figure 7.

Impact Tests

Penetrometers.- Four spherical penetrometers were used in the impact tests. The mass and diameter of each of the penetrometers are given in table II. Aft portions of the basic fiber-glass structure of several of the penetrometers were either replaced with lead or plastic foam or removed altogether to provide the desired penetrometer mass. All penetrometers were equipped with steel inserts to which the necessary impact sensing instruments could be mounted.

Instrumentation.- Each penetrometer was equipped with a crystal accelerometer which was oriented along the impact axis of the penetrometer to sense the accelerations incurred during the impact process. The accelerometers were cable-coupled to an impedance matching cathode follower/amplifier and the signals were displayed as a voltage-time trace on a storage oscilloscope and photographed. Sketches of representative samples of these photographs are shown in figure 8 where the voltage has been converted to acceleration in g (earth gravity) units.

Test procedure.- The testing technique consisted of impacting the penetrometers into the prepared beds of dust particles indicated in table I at velocities ranging from 5 to 30 fps (1.52 to 9.14 m/sec) and recording the measured impact characteristics. The desired impact velocity was obtained by releasing the penetrometers at specified heights above the target surface. Each test was performed at least three times. The impact characteristics measured during and following the tests included the acceleration time histories and, whenever possible, the resulting penetration depths and crater dimensions.

PRESENTATION OF DATA

Bearing-Strength Tests

Load-penetration data from the bearing-strength tests were initially plotted as shown in figure 7. Curves were faired through the composite data points of repeated tests as illustrated in the figure. The faired loadings were converted to loading per unit plate area and plotted as a function of plate penetration for purposes of analysis and interpretation. The results from all bearing-strength tests are presented in this latter form in figure 9.

Impact Tests

Acceleration time histories recorded during the impact of accelerometer-equipped projectiles on target surfaces display various characteristics which are of significance in defining the impacted surface. These characteristics are noted in one of the time histories of figure 8 and include the magnitude of the peak acceleration a_{max}, the rise time required to reach that acceleration t_r, and the total duration of the pulse t_t. The characteristics derived from the impact acceleration time histories are presented in figures 10 and 11. In figure 10 the peak accelerations sensed by each test configuration during impact with each of the target test beds are presented as a function of parameters which were empirically developed by separately examining the variation of peak acceleration with each test variable. These test variables were impact velocity V, penetrometer mass m, and penetrometer diameter D. The rise and total pulse times measured from data obtained for all configurations and targets are presented as a function of the impact velocity in figure 11. In addition to evaluating characteristics of the impact acceleration time histories, measurements were taken whenever possible of certain characteristics of the formed crater - namely, the penetration depth of the impacting projectile and the diameter of the blast crater. These characteristics are summarized for the different penetrometers and dust surfaces and are presented as a function of the pertinent test variables in figures 12 and 13.

DISCUSSION OF RESULTS

Bearing-Strength Tests

The bearing strength of a surface composed of a loose particulate material is defined as the loading pressure required to effect a certain penetration into the material. However, no standards exist which specify the size of the loading plate or the penetration depth required for bearing-strength measurements. Therefore, for a given application, a penetration depth and loading-plate area must be selected which are appropriate to the design objective. Since the objective of this investigation was to correlate the bearing strength of the test materials to the impact characteristics, it was necessary to specify a meaningful definition of bearing strength. Hence, a number of load-penetration tests were conducted on each of the dust materials. The results of these tests are presented in figures 9 and 14.

Loading-plate considerations.- Figure 9 presents the load per unit plate area, or bearing pressure, of the loading plates used in these tests as a function of plate penetration in each of the dusts examined. The figure shows that the bearing pressure necessary to produce a given penetration generally increases with the size of the loading plate which is consistent with the data of reference 23 for these plate sizes. This difference in pressure appears to become more pronounced with increased penetration but has decreasing divergence with decreasing particle size and dust density. Similar trends are also predicted by theoretical considerations for the bearing capacity of footings in such materials (refs. 11, 12, and 13). Comparison of the trends of footing bearing capacity with the trends of the bearing-strength data of this paper appears justifiable, since the pressure-penetration curves of figure 9 may be considered, at least in a first approximation, as a series of incremental plastic failures.

Test-bin considerations.- The interpretation of the results of the bearing-strength tests required a knowledge of the effects due to boundary restrictions imposed by the size of the test bin. Consideration was given to the dust depth and test-bin width relative to the size and the depth of penetration of the loading plates. It was anticipated that the bearing strength of a material would be affected at plate penetration depths where the zone of significant stress in the dust beneath the plate approaches the bottom of the test bin. The sudden upward trends in some of the loading curves of figure 9 indicate that such an interaction may have occurred at deep penetrations. Therefore, in order to avoid possible bottom boundary effects, the bearing strengths of the dusts were defined on the basis of shallow penetrations.

The use of a bin having a finite test surface area also affects the bearing-strength measurements when the size of the loading plate is such that the test results no longer duplicate those which would be obtained from similar tests on an unbounded surface. For example, reference 11 points out that loaded circular plates on a soil surface induce a visible radial heave which extends to approximately $2\frac{1}{2}$ plate diameters. In addition, reference 15, on the basis of limited test data derived from loading small footings (2-in-diameter (5.08 cm) plates), indicated that a ratio of container diameter to footing diameter greater than 8 would assure that the area effect on the bearing capacity measurements would be negligible. Proximity effects between the dust-bin walls and the loading plates of the present tests can be examined with the aid of figure 14. In this figure, loading per unit plate area at arbitrarily selected penetration depths in the 187μ dust ($\gamma = 120$ lb/ft^3 (1922 kg/m^3)) is presented as a function of the ratio of test-bin width to loading-plate diameter. Figure 14(a) presents data for the different loading plates taken directly from figure 9(f). Figure 14(b) presents the results of additional tests on this dust obtained by loading the smallest loading plate (5 in^2 (32.26 cm^2)) in different size bins formed by inserting concentric essentially rigid sleeves into the prepared test bed. The figure shows that the bearing-strength measurements are substantially affected when the diameter of the loading plate approaches one-third the size of the test bin. Furthermore, these effects become more pronounced with increasing penetration depth. Therefore, in performing laboratory bearing-strength tests consideration must be given to the size of the test bin relative to the size and penetration of the loading plate.

Bearing-strength definition and comparison.- As a result of these considerations, test data obtained from the small loading plate at shallow penetration depths are believed to be valid representations of data for a semi-infinite plane surface since interferences from the test-bin boundaries are minimized. Therefore, for the purposes of these tests, bearing strength was arbitrarily defined as the pressure necessary to force the 5 in^2 (32.26 cm^2) plate to penetrate into the test material a distance of 1 in. (2.54 cm). This definition was selected to minimize effects of conditions unique to this particular test apparatus and, as such, is not proposed as a standard definition or convention.

The bearing strengths of the different dust grades, as herein defined, are summarized as a function of dust density in figure 15. The particle size of the dust grade corresponding to each density is identified in the key. Bearing strengths are presented for all grades examined including those evaluated at several densities. The bearing strength of all 10 dust grades, tested in a loosely packed state at densities ranging between 37 lb/ft^3 (593 kg/m^3) and 122 lb/ft^3 (1954 kg/m^3), shows the following variations with respect to density. As the dust density is increased from the lowest tested, the bearing strength increases until it peaks at a density of approximately 112 lb/ft^3 (1794 kg/m^3), then decreases rapidly until the density reaches approximately 118 lb/ft^3 (1890 kg/m^3), then reverses, and again increases throughout the rest of the range of dust densities. Also, as the density of a given dust grade is increased, which in effect corresponds to increased packing, the bearing strength rapidly increases. Figure 16, which presents corresponding data from the 10 in^2 (64.52 cm^2) loading plate, corroborates these trends while providing additional data for the 75μ and 550μ dust grades.

It should be recognized in interpreting the data of figures 15 and 16 that the variation of bearing strength may be due to effects other than dust density. In an effort to evaluate other factors which may have influenced these bearing-strength results, various characteristics of the aluminum oxide dust grades were explored. For example, particle shape measurements were made, as discussed in the section entitled "Apparatus and Test Procedure," and the results are given in table I. Briefly, these measurements indicated a larger percentage of oblong and needle-like particles in the five smaller dust sizes than that of the four larger sizes. Although it is generally agreed (ref. 24, for example) that particle shape and roughness affect the material shear strength and, hence, the bearing strength, no definite correlation could be made between particle shape and bearing strength.

In addition, triaxial compression and direct shear tests were conducted on the dusts to establish a measure of the internal friction associated with each dust sample. The application of the results of these tests to the interpretation of the bearing-strength data was meaningless since it was impossible to duplicate and maintain the state of low compaction which existed in the bearing-strength tests. In an effort to evaluate the internal friction of the dusts at densities corresponding to those of table I, several shear tests were performed with a standard direct shear test apparatus but without the application of an external vertical load to the dust sample. The findings of these tests were inconclusive since the data obtained showed considerable scatter.

Impact Tests

The data obtained from the impact tests are presented in figures 10 to 13. These data include the magnitudes of certain distinguishing features of the impact acceleration time histories (figs. 10 and 11) and measurements of the penetrometer penetration depths (fig. 12) and blast-crater diameters (fig. 13). The paragraphs which follow discuss the impact characteristics of the different penetrometer-dust target combinations as defined by these data.

Peak acceleration.- The peak accelerations are presented in figure 10 as a function of empirical parameters which contain the impact test variables and which were developed for each target surface. Expressions containing these parameters which best fit the test data are also included in the figure. The empirical expression clearly shows the influence of the test variables on the peak acceleration. Unlike the elastic and plastic impacts of reference 4, where the peak acceleration is seen to be essentially a linear function of the impact velocity, the impact velocity appears to have a greater effect on the peak accelerations encountered by penetrometers which penetrate the target such as those of the present paper. The peak acceleration is shown to vary with $V^{15/8}$ in the coarse granular aluminum oxide dusts (average particle size down to 65μ) and to vary with V^2 in the aluminum oxide dust targets of a powdery texture (27μ and 5μ average particle sizes), in pumice (68μ average particle size), and in water. In the case of elastic and plastic impacts, a change in impact velocity is reflected in the acceleration time histories by a corresponding change in peak acceleration; the total pulse time and the basic pulse shape are essentially unaffected. Hence, the linear variation of peak acceleration with impact velocity is consistent since the area encompassed by the acceleration time history is indicative of that velocity. However, in a penetration-type impact, a change in velocity modifies not only the peak acceleration but also the pulse shape of the acceleration time history as illustrated in figure 8. Hence, for such impacts, it is apparent from areal comparisons that a linear relationship would not be expected to exist between peak acceleration and impact velocity. The parameters of figure 10 also show that the peak acceleration in the granular dusts (figs. 10(a) to 10(f)) varies directly with the penetrometer diameter. The effect of penetrometer diameter on peak acceleration in the powdery dusts, pumice, and water (figs. 10(g) to 10(j)) becomes more pronounced with decreasing dust particle size (and dust density). Also, the parameters indicate that the peak accelerations vary inversely with the mass of the penetrometer, regardless of the impacted target.

The peak acceleration data obtained from one penetrometer (configuration 3) are summarized for impacts in all targets (dusts and water) and presented as a function of test-bed density in figure 17. The figure shows that the overall effect of increasing the density of the target medium is to increase the magnitude of the peak impact accelerations. In addition, this figure illustrates more vividly the effect of impact velocity on the peak impact accelerations. Plots constructed from the data of figure 10 for other configurations yield similar trends.

Characteristic times.- The total pulse times presented in figure 11 are, in general, only slightly affected by changes in impact velocity. These effects occur primarily in the low velocity range where the times are somewhat higher than those measured at the higher test velocities. The long total pulse times associated with impacts in the fine, low-density dusts (27μ and 5μ aluminum oxide and pumice) are attributed to an apparent buoyant action in such targets. The incomplete pulse time data for these low-density dust targets result from impacts for which the penetrometer struck the bottom of the dust test bin.

Rise times, or the times required to reach the peak acceleration commencing with the onset of impact, are also included in figure 11. The figure shows that the rise time decreases with increasing impact velocity for all penetrometers and all targets, including water, which agrees with the trends noted in reference 25 for water impacts. Furthermore, these rise times are essentially independent of penetrometer mass and diameter at the higher test velocities.

The depth penetrated by each penetrometer during the rise time, or penetrometer penetration at which peak acceleration occurred, was obtained through an approximate double integration of the accelerations during this time period. These depths are presented in terms of penetrometer diameter in figure 18 as a function of impact velocity. The figure includes data obtained from all four penetrometer configurations impacting 187μ dust (fig. 18(a)), and data from configuration 3 impacting all test targets for which sufficient data were available (fig. 18(b)). The penetration-depth—penetrometer-diameter ratio corresponding to peak acceleration appears to vary linearly with the impact velocity and to increase with decreasing penetrometer diameter. Furthermore, this ratio appears to be independent of penetrometer mass; however, more data are required to verify this trend. The trends of the figure also show that, in general (except for the 187μ dust), the penetration depth at which maximum acceleration is incurred increases with decreasing particle size; however, these penetration depths are the shallowest in water.

Penetration depth.- The penetration depth is plotted in figure 12 as a function of a parameter which contains the test variables. The penetration data from all impacts are shown to be described by the general empirical expression

$$y = \frac{km^{1/2}V^{2/3}}{D}$$

where the value of the penetration parameter k depends upon the test dust. This general expression for penetration depth is the same expression developed from the impact tests on sand and aluminum oxide dust targets, described in references 4 and 20, respectively. Penetration data in the 27μ and 5μ dusts are described by two expressions: one which fairs the data of the 4-in-diameter (10.16 cm) penetrometer and one which fairs the data of the other three penetrometers. The shallower penetrations of the 4-in-diameter (10.16 cm) penetrometer are the result of the buoyant nature of these targets which caused this projectile to rebound or "float" to the measured depth following a much deeper penetration. This rebound was readily apparent from both visual observation and high-speed photographic coverage. Buoyancy is believed to be the phenomenon involved because the action of these dusts during impact was observed to be very similar to that of water and because the mass density of the 4-in-diameter (10.16 cm) penetrometer was less than that of the two finer aluminum oxide dusts. Only limited penetration data were obtained for pumice because the penetrometer struck the bottom of the test bin in most tests. However, the relatively shallow penetrations of the 4-in-diameter (10.16 cm) penetrometer in pumice, which had a density much less than that of the penetrometer, indicated that factors other than bouyancy (for example, resistance resulting from compression of pore air) possibly affect penetration in these fine particle targets.

Blast crater.- As noted in reference 20, the impact of projectiles into dust media, whether granular or powdery, produces a blast effect under an atmospheric pressure environment wherein the dust particles are expelled from the impacted area. From the standpoint of lunar landings and impacts, the reference states that there is no effect of environmental pressure on the blast behavior of granular particles. In the present tests, only the ejecta from the three largest dust sizes produced a blast crater of any significance; the expulsion of particles of the finer dusts extended over a wide area and formed no discernible crater. The diameters of the blast craters, which were measured following impacts of the different penetrometers into the three largest dust sizes, divided by the corresponding penetrometer diameters are presented as a function of impact velocity in figure 13. The trends of the data for these configurations agree with those noted in reference 4; namely, that the crater-to-penetrometer diameter ratio increases with increasing impact velocity and decreasing penetrometer diameter and is essentially independent of penetrometer mass. Note that at low impact velocities where the penetration depth was considerably less than the penetrometer radius, as for the 4-in-diameter (10.16 cm) penetrometer, this ratio can be less than 1.

Correlation of Results

To bring about a meaningful correlation between data from the impact tests and the static bearing-strength tests on dust media, the test media in both cases must be identical. The test-bed preparation technique of circulating air through the dust prior to a test proved to be excellent for providing repeatable test conditions. However, since these tests were performed in an atmospheric environment, the behavior of the dust undergoing a static loading may differ from that of the dust undergoing a dynamic loading because voids in the dust contain entrapped air. During the bearing-strength tests, the rate of penetration of the loading plates is essentially negligible and it is likely that sufficient time is provided for this entrapped air to escape from the voids through gradual diffusion prior to further plate penetration. Hence, it seems reasonable to assume that the presence of air in the dust bed for the bearing-strength tests did not appreciably influence the test results. Thus, similar bearing-strength tests performed on these dusts in a vacuum environment are expected to produce the same results as those obtained for the same dust densities in the atmosphere. However, as discussed in reference 26, the entrapped air is rapidly expelled from the voids in the dust bed during penetration of the projectiles in the impact tests. This sudden expulsion of the air may influence the behavior of the dust particles and hence affect the projectile impact characteristics. Consequently, test beds of dust-like materials may, under atmospheric conditions, pose one type of target to static tests and another to dynamic tests due to the action of the entrapped air. The results of earlier projectile impact tests conducted on identical dust grades of aluminum oxide (ref. 20) indicate that penetration characteristics, and hence possibly other impact characteristics, are dependent upon the environmental pressure for certain characteristics of the test material. The dusts tested in reference 20 were described in terms of the manufacturer's stated nominal particle sizes rather than actual measured values. The 600μ, 266μ, 86μ, 44μ, and 32μ dusts of that report correspond, respectively, to the 550μ, 187μ, 75μ, 32μ, and 27μ dusts of the present report. On the basis of particle size, it was concluded in reference 20 that the penetration depth of projectiles impacting dusts having an average particle size of 27μ or greater appeared to be unaffected by the pressure environment. For impacts into smaller particle sizes, the depth of penetration increased with decreasing particle size and was dependent upon the environmental pressure in the range between atmospheric and approximately 1 mm Hg. However, since during the course of the tests reported herein and in references 20 and 26 the penetration characteristics of dusts were observed to be influenced by their density (i.e., their state of packing), the penetration data of reference 20 were reexamined with respect to test density. On a density basis, penetration depths in the dusts of reference 20 become pressure dependent at densities between 104 lb/ft^3 (1666 kg/m^3) and 111 lb/ft^3 (1778 kg/m^3), the latter being the test density of the 27μ dust. During the performance of the tests discussed in this paper, the density of the 27μ dust was maintained at 93 lb/ft^3 (1490 kg/m^3) and, in this state, demonstrated penetration characteristics and a fluid-like behavior (similar to that of water) which suggested susceptibility to environmental pressure effects. Hence it appears that a density exists, at least for the 27μ dust, between 93 lb/ft^3 (1490 kg/m^3) and 111 lb/ft^3 (1778 kg/m^3) at which a transition occurs wherein impact characteristics become independent of the environmental pressure. This transition has not been explored experimentally. However, the density at which this transition occurs for different dust grades may be a function of particle size, since particle weight and interparticle cohesion may be important factors, and a function of penetrometer impact velocity, since higher velocities may induce higher pore pressures within the test bed. In view of the observations of the present tests, the 27μ and 5μ dusts at the densities examined are affected by environmental pressure. Therefore, a correlation of the results of static bearing-strength and dynamic impact tests conducted in atmosphere on these dusts may not be indicative of what would happen in a vacuum environment. No data are available which relate the dynamic penetration characteristics of the particular pumice grade tested with environmental pressure. However, because the pumice displayed the same fluid-like behavior during impact tests as the fine aluminum oxide dusts, the results of the correlation of the atmospheric static and dynamic tests in this material are also subject to change under vacuum conditions.

Comparison of dynamic and static data.- Figures 19 and 20, respectively, show the variation of peak acceleration and total pulse time characteristics of the impact acceleration time histories, obtained from data presented in figures 10 and 11, with the dust target bearing strength. The data of these figures are presented for configuration 3; however, data for the other penetrometers (also available from figs. 10 and 11) show similar trends. The data of figure 19 show that the peak accelerations encountered by penetrometers impacting dust targets do not uniquely define the static bearing strength of those targets; however, there is a general increase in peak acceleration with increasing bearing strength. The fact that peak acceleration data do not precisely define dust target bearing strengths suggests that the resistance of such targets to static penetration (bearing strength) is not fully realized in impact until the projectile has penetrated beyond the shallow depths at which the peak acceleration occurs. However, on the basis of the data presented in figure 17, it may be concluded that the peak impact acceleration (which is linked to the blast phenomenon) is directly related to the dust target density.

The data for impact total pulse times, as exemplified in figure 20 for configuration 3, exhibit two distinct duration levels. Long acceleration pulse times are associated with the low-bearing-strength powdery dusts, whereas impacts into the more dense granular dusts are defined by relatively short pulse times. The data from tests in the powdery dusts indicate that the pulse time is velocity dependent, and it is expected that these results would change for similar tests in a vacuum environment. The figure also shows that total pulse times for impacts in the granular dusts are essentially independent of impact velocity and dust bearing strength.

Figure 21 presents the impact penetration parameter $\left(k = \frac{y}{m^{1/2}V^{2/3}/D}\right)$ obtained from the impact data of figure 12 as a function of the bearing strength of the dust targets. No value of the penetration parameter is shown for pumice because of the limited penetration data obtained in that material. The figure shows that, under atmospheric conditions, the penetration parameters, and hence the penetration depths, associated with powdery dusts are much greater than those for the granular dusts. It can be inferred from the data of reference 20 that this variation of the penetration parameter with bearing strength would exist in a vacuum environment although the magnitude of the parameter may be somewhat less in the finer, lower bearing strength dusts.

Energy considerations.- In an effort to relate directly penetration depths of dynamic tests to those of static tests, bearing-strength tests were performed in several dusts with spheres similar to the penetrometers of the impact tests replacing the loading plates.

The results of these tests together with corresponding data taken from the impact tests are exemplified in figure 22 for one penetrometer configuration and summarized for all configurations in figure 23. In figure 22 the static and dynamic penetrations of configuration 3 into selected dusts are presented as a function of the energy expended, or work required, to produce those penetrations. The energy corresponding to a static penetration was obtained by integrating, to successive penetration depths, the area under load-penetration curves similar to those shown in figure 7 for the conventional loading plates. The energy corresponding to a dynamic penetration refers to the change in the potential energy of the penetrometer in coming to rest at the designated penetration depth following release at some preselected height above the test surface. The figure shows that both the static and dynamic penetrations vary linearly with the expended energy when plotted on logarithmic coordinates. The different dynamic energy levels result from the different penetrometer drop heights necessary to obtain the different test impact velocities, and the various data points at each level result from variations in measured penetration depths in repeated impact tests. Figure 22 shows that for given input energy, static penetrations, in general, exceed dynamic penetrations in the granular dusts, whereas in dusts which are powdery in nature the dynamic penetrations exceed the static penetrations. The relative differences in these penetrations are better illustrated in figure 23, which presents the ratio of dynamic to static penetrations as a function of expended energy for all penetrometers.

Apparently the energy required to produce the blast phenomenon associated with dynamic penetration in the granular dusts is sufficient to reduce dynamic penetration below that resulting from a static loading at the same overall energy level. Conversely, powdery dusts offer less resistance to dynamic penetration than to static penetration because of the action of the air entrapped in the dust target. During the impact process this air is compressed ahead of the penetrometer and forced to permeate the adjacent dust particles. Since the dust particles in the powdery grades are light, the material is possibly placed in a fluid state by the expanding air flow which reduces the dust shearing strength and hence its resistance to penetration. However, during the static loading process, the air entrapped in the dust is given an opportunity to escape as penetration progresses. This phenonmenon is further discussed in reference 26. It may be possible, through energy considerations, to use impact data to determine the approximate strength of dust materials in situations wherein effects of pore air are not present. The impact velocity and hence kinetic energy of an impacting penetrometer can be obtained through a single integration of the impact acceleration time history. This energy, together with a knowledge of the penetration depth acquired through a double integration of the pulse, may then be related to the static energy absorbing capability of the impacted material.

CONCLUDING REMARKS

The following remarks are based upon the results of a study to relate characteristics of acceleration time histories obtained from impacting penetrometers into dust-like materials with the static bearing strength of these materials. Impact and bearing-strength tests were performed under atmospheric pressure conditions on materials which included eight grades of aluminum oxide, which ranged in average particle size from 936μ to 5μ, and one grade of pumice (68μ).

A study of the characteristic features of the impact acceleration time histories indicated that the complete time history is required in order to describe the load-supporting capability and other characteristics of dusts. Both the peak acceleration and the total pulse time reflect, on a gross scale, the bearing strength of a material. Peak acceleration generally increases with the bearing strength and is directly related to the density of the impacted material. Similarly, weak low-density dusts yield long pulse times, whereas stronger more dense dusts are characterized by relatively short pulse durations.

Empirical expressions for the peak acceleration, formulated from the results of the impact tests, indicated that peak acceleration in the granular dusts (936μ to 65μ) varies directly with the impact velocity raised to the 15/8th power and the penetrometer diameter and is inversely proportional to the penetrometer mass. In the aluminum oxide powders (5μ and 27μ), pumice, and water, the peak acceleration is directly proportional to the square of both the impact velocity and penetrometer diameter D (except for the 27μ aluminum oxide dust for which acceleration appears to be better described by $D^{3/2}$) and is inversely proportional to the penetrometer mass.

Penetrometers impacting weak low-density dusts penetrate to a considerable depth, whereas penetration in stronger more dense dusts is relatively shallow. A general empirical expression describes the penetration depths of penetrometers into all dusts. This expression is the same as that developed in other investigations involving penetrometer penetration and indicates that an increase in penetrometer mass or impact velocity or a decrease in penetrometer diameter results in an increase in the depth of penetration.

For the same expended energy, the static penetrations of spheres in dusts which are not affected by pore air generally exceed the dynamic penetrations, whereas in dusts in which environmental pressure effects are involved, the dynamic penetrations exceed the static.

The bearing strength of a dust material depends not only upon the density of the medium but also appears to be a function of less evident factors such as the size and shape of individual particles. The bearing strength of a given dust grade is increased with increased test density or packing.

Langley Research Center,
National Aeronautics and Space Administration,
Langley Station, Hampton, Va., September 30, 1965.

REFERENCES

1. Urey, Harold C.: The Origin of the Moon's Surface Features. Sky Telescope, vol. XV, nos. 3 and 4, Jan.-Feb. 1956, pp. 108-111, 160-163.

2. Gold, Thomas: Dust on the Moon. Vol. II of Vistas in Astronautics, Morton Alperin and Hollingsworth F. Gregory, eds., Pergamon Press, 1959, pp. 261-266.

3. Whipple, Fred L.: On the Lunar Dust Layer. Vol. II of Vistas in Astronautics, Morton Alperin and Hollingsworth F. Gregory, eds., Pergamon Press, 1959, pp. 267-272.

4. McCarty, John Locke; and Carden, Huey D.: Impact Characteristics of Various Materials Obtained by an Acceleration-Time-History Technique Applicable to Evaluating Remote Targets. NASA TN D-1269, 1962.

5. McCarty, John Locke; Beswick, Alfred G.; and Brooks, George W.: Penetrometer Techniques for Lunar Surface Evaluation. A Compilation of Recent Research Related to the Apollo Mission, NASA TM X-890, 1963, pp. 123-130.

6. McCarty, John Locke; Beswick, Alfred G.; and Brooks, George W.: Application of Penetrometers to the Study of Physical Properties of Lunar and Planetary Surfaces. NASA TN D-2413, 1964.

7. Mechtly, E. A.: The International System of Units - Physical Constants and Conversion Factors. NASA SP-7012, 1964.

8. Palmer, L. A.: Field Loading Tests for the Evaluation of the Wheel-Load Capacities of Airport Pavements. Symposium on Load Tests of Bearing Capacity of Soils, Spec. Tech. Publ. No. 79, Am. Soc. Testing Mater., c.1948, pp. 9-40.

9. Campen, W. H.; and Smith, J. R.: Use of Load Tests in the Design of Flexible Pavements. Symposium on Load Tests of Bearing Capacity of Soils, Spec. Tech. Publ. No. 79, Am. Soc. Testing Mater., c.1948, pp. 51-64.

10. McLeod, Norman W.: A Canadian Investigation of Load Testing Applied to Pavement Design. Symposium on Load Tests of Bearing Capacity of Soils, Spec. Tech. Publ. No. 79, Am. Soc. Testing Mater., c.1948, pp. 83-127.

11. Terzaghi, Karl: Theoretical Soil Mechanics. John Wiley and Sons, Inc., c.1943.

12. Terzaghi, Karl; and Peck, Ralph B.: Soil Mechanics in Engineering Practice. John Wiley & Sons, Inc., c.1948.

13. Scott, Ronald F.: Principles of Soil Mechanics. Addison-Wesley Pub. Co., Inc., c.1963.

14. Housel, William S.: A Generalized Theory of Soil Resistance. Papers on Soils, Spec. Tech. Publ. No. 206, Am. Soc. Testing Mater., c.1957, pp. 13-33.

15. Halajian, John D.: Laboratory Investigation of "Moon-Soils." Rept. No. ADR 04-04-62.1, Grumman Aircraft Eng. Corp., May 1962. (Also available as IAS Paper No. 62-123.)

16. Vey, E.; and Nelson, J. D.: Studies of Lunar Soil Mechanics - Final Report. Contract No. NASr-65(02), IIT Res. Inst., Feb. 1965.

17. Bernett, E. C.; Scott, R. F.; Jaffe, L. D.; Frink, E. P.; and Martens, H. E.: The Bearing Capacity of Simulated Lunar Surfaces in Vacuum. Tech. Rept. No. 32-326 (Contract No. NAS 7-100), Jet Propulsion Lab., California Inst. Technol., Aug. 15, 1963.

18. Anon.: Penetration of Projectiles Into Concrete, Rock, and Soil. Ch. 3 of Testbook of Air Armament, Pt. I, Brit. Air Min., Feb. 1949. (Available from ASTIA as AD No. 145925.)

19. Sanford, Robert B.: Penetration Properties of Inert 500 lb GP Bombs Dropped on Sand. AFAC Tech. Rept. 53-54, Air Res. Dev. Command, Dec. 1953. (Available from ASTIA as AD 23962.)

20. Clark, Leonard V.; and McCarty, John Locke: The Effect of Vacuum on the Penetration Characteristics of Projectiles into Fine Particles. NASA TN D-1519, 1963.

21. Anon.: Sieves for Testing Purposes. ASTM Designation E 11-61, Pt. 4 of 1961 Book of ASTM Standards Including Tentatives. Am. Soc. Testing Mater., c.1961, pp. 1479-1486.

22. Gooden, Ernest L.; and Smith, Charles M.: Measuring Average Particle Diameter of Powders - An Air-Permeation Apparatus. Ind. Eng. Chem., vol. 12, no. 8, Aug. 15, 1940, pp. 479-482.

23. Bekker, M. G.: Theory of Land Locomotion. Univ. of Michigan Press, c.1956, pp. 180-182.

24. Housel, William S.: Interpretation of Triaxial Compression Tests on Granular Mixtures. Triaxial Testing of Soils and Bituminous Mixtures, Spec. Tech. Publ. No. 106, Am. Soc. Testing Mater., c.1951, pp. 267-295.

25. Kornhauser, M.: Structural Effects of Impact. Spartan Books, Inc., c.1964, pp. 25-28.

26. Roddy, David J.; Rittenhouse, John B.; and Scott, Ronald F.: Dynamic Penetration Studies in Crushed Rock Under Atmospheric and Vacuum Conditions. Tech. Rept. No. 32-242 (Contract No. NAS 7-100), Jet Propulsion Lab., California Inst. Technol., Apr. 6, 1962.

TABLE I

CHARACTERISTICS OF TEST-BED MATERIAL

Grade	Average particle size, l, μ	Dust density, γ		Angle of repose, deg	Percentage of oblong particles
		lb/ft^3	kg/m^3		
A	936	*116	1858	41	<5
B	550	118 *119 122	1890 1906 1954	38.5	6.7
C	187	119 *120	1906 1922	38.2	12.5
D	149	*114	1826	36.5	12.5
E	75	111 *112	1778 1794	35.5	24
F	65	*107	1714	37	18.3
G	32	93	1490	35.5	21
H	27	*93	1490	33.5	20
I	5	*73	1169	53	15.5
Pumice	68	*37	593	44	----

*Dust density used for impact tests.

TABLE II

DESCRIPTION OF PENETROMETERS

Configuration	Diameter, D		Mass, m	
	in.	cm	lb-sec^2/in.	kg
1	3	7.62	0.0026	0.455
2	2	5.08	.0020	.350
3	3	7.62	.0020	.350
4	4	10.16	.0020	.350

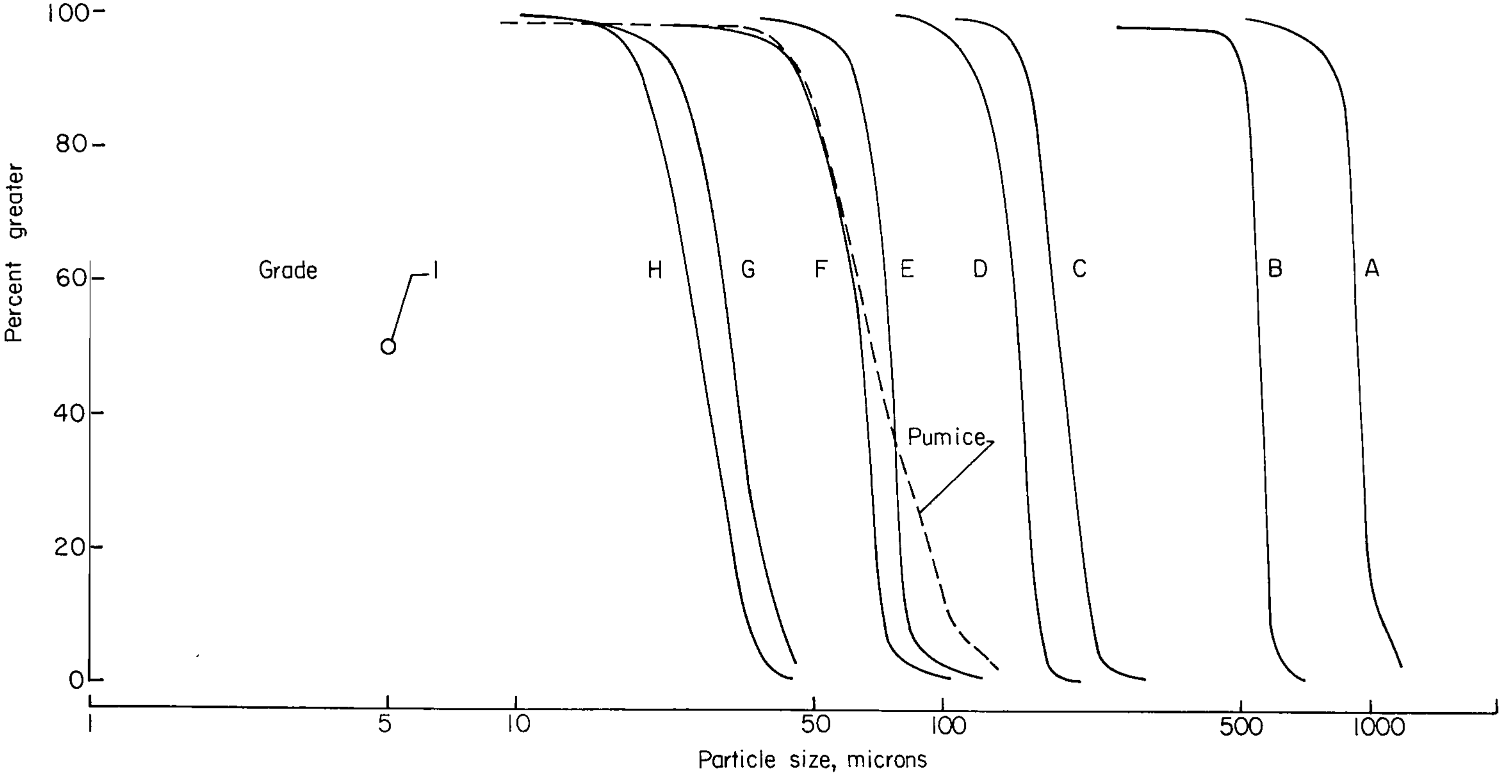

Figure 1.- Particle size distributions of dust grades.

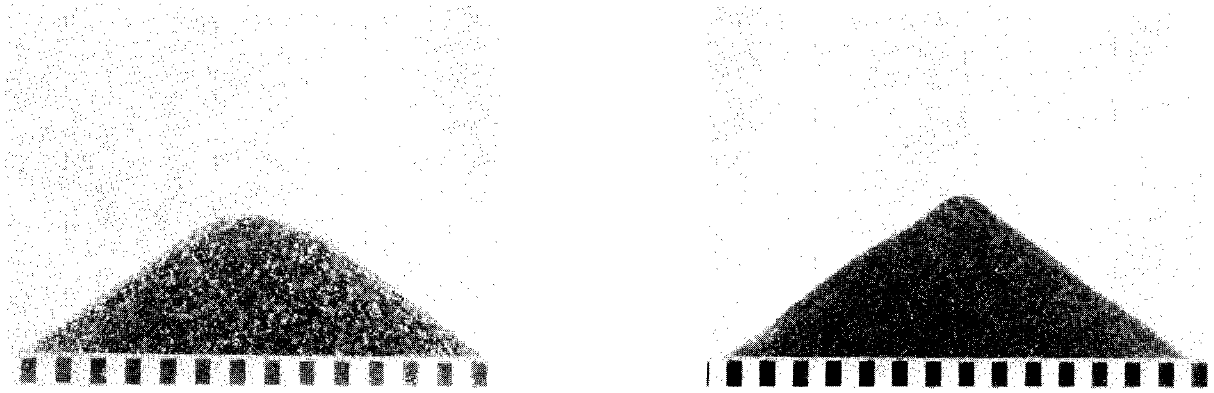

(a) Grade B; $l = 550\mu$.

(b) Grade C; $l = 187\mu$.

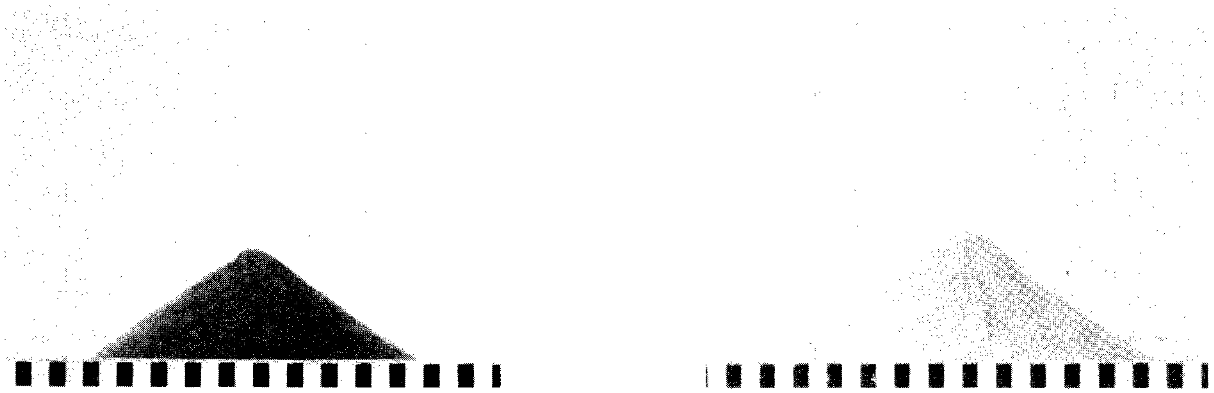

(c) Grade E; $l = 75\mu$.

(d) Grade G; $l = 32\mu$.

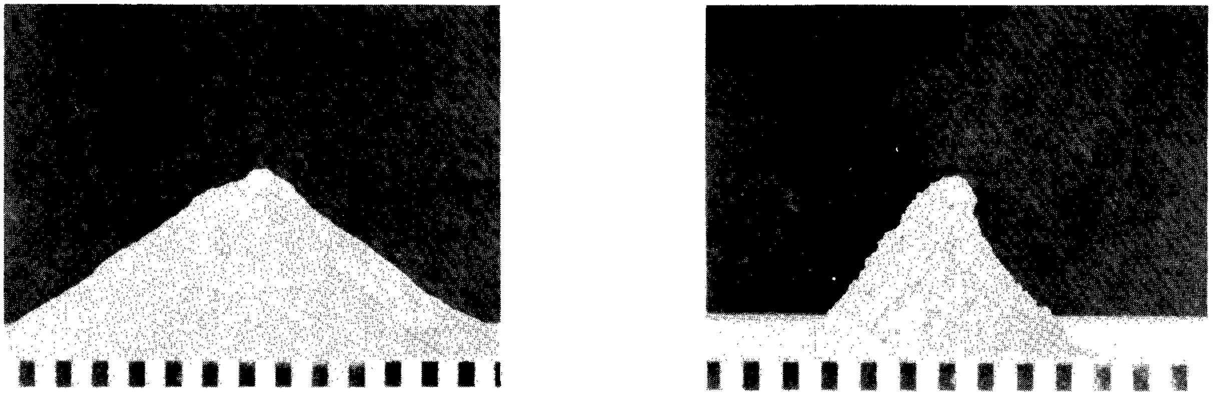

(e) Grade H; $l = 27\mu$.

(f) Grade I; $l = 5\mu$.

Figure 2.- Typical piles formed for measurements of angle of repose.

L-65-7946

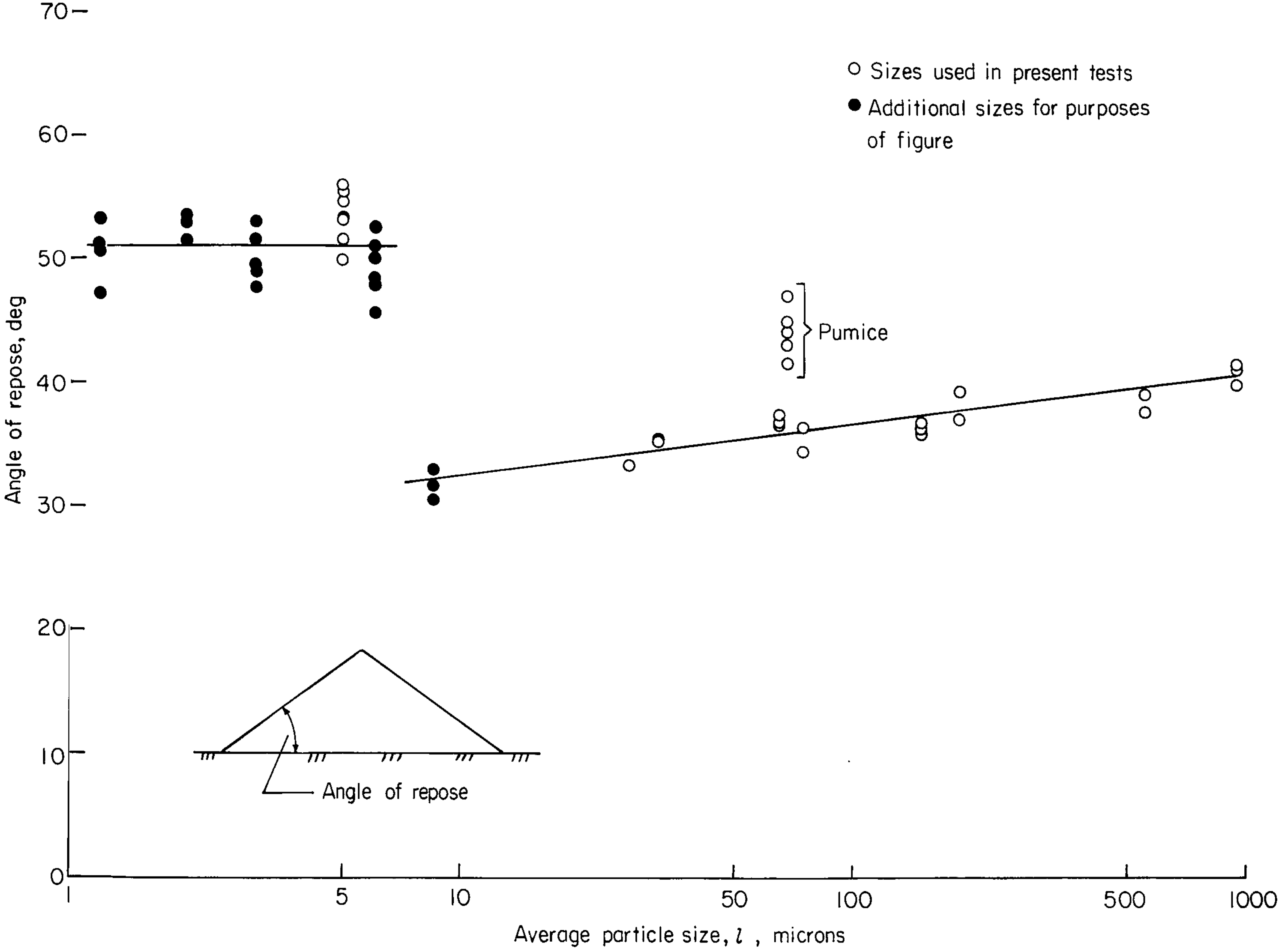

Figure 3.- Measured angles of repose for aluminum oxide and pumice particles.

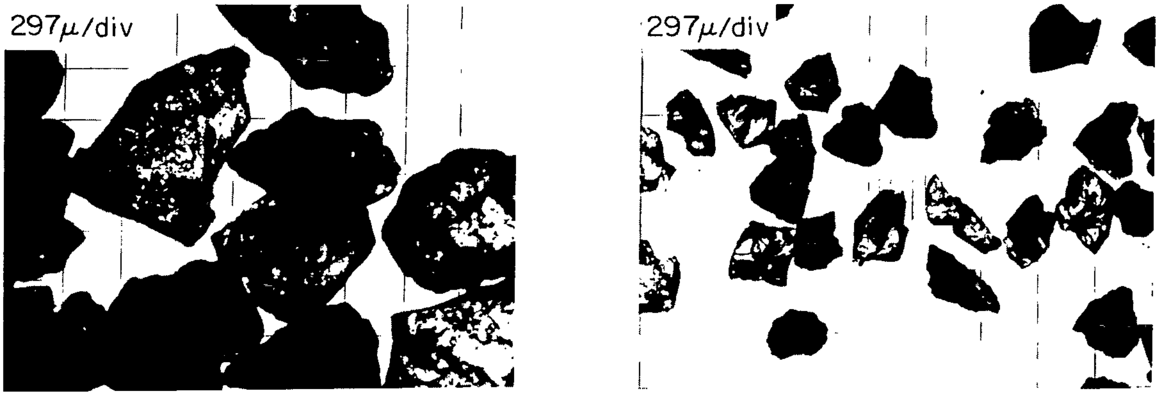

(a) Grade B; $l = 550\mu$.

(b) Grade C; $l = 187\mu$.

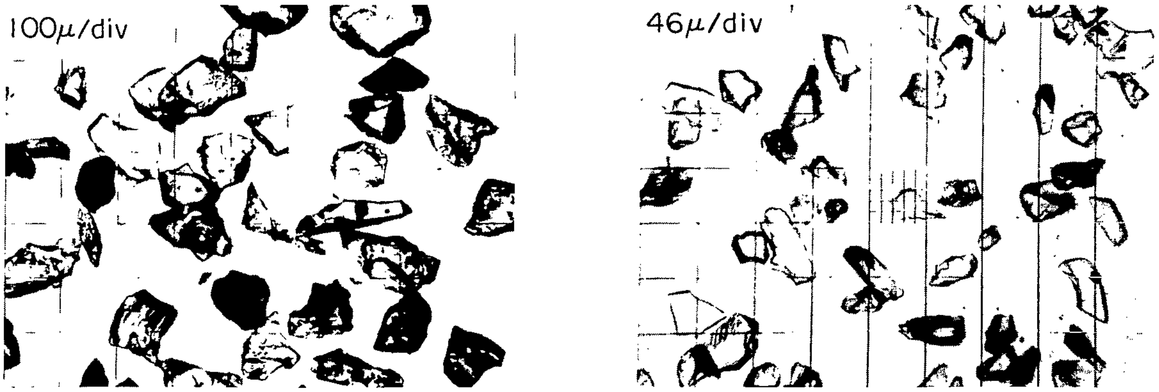

(c) Grade E; $l = 75\mu$.

(d) Grade G; $l = 32\mu$.

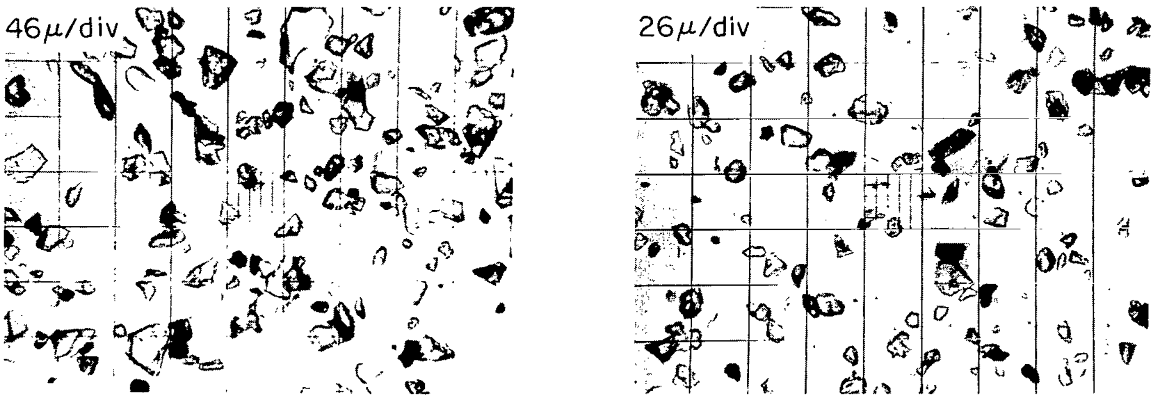

(e) Grade H; $l = 27\mu$.

(f) Grade I; $l = 5\mu$.

Figure 4.- Photomicrographs of samples taken from dust grades.

L-65-7947

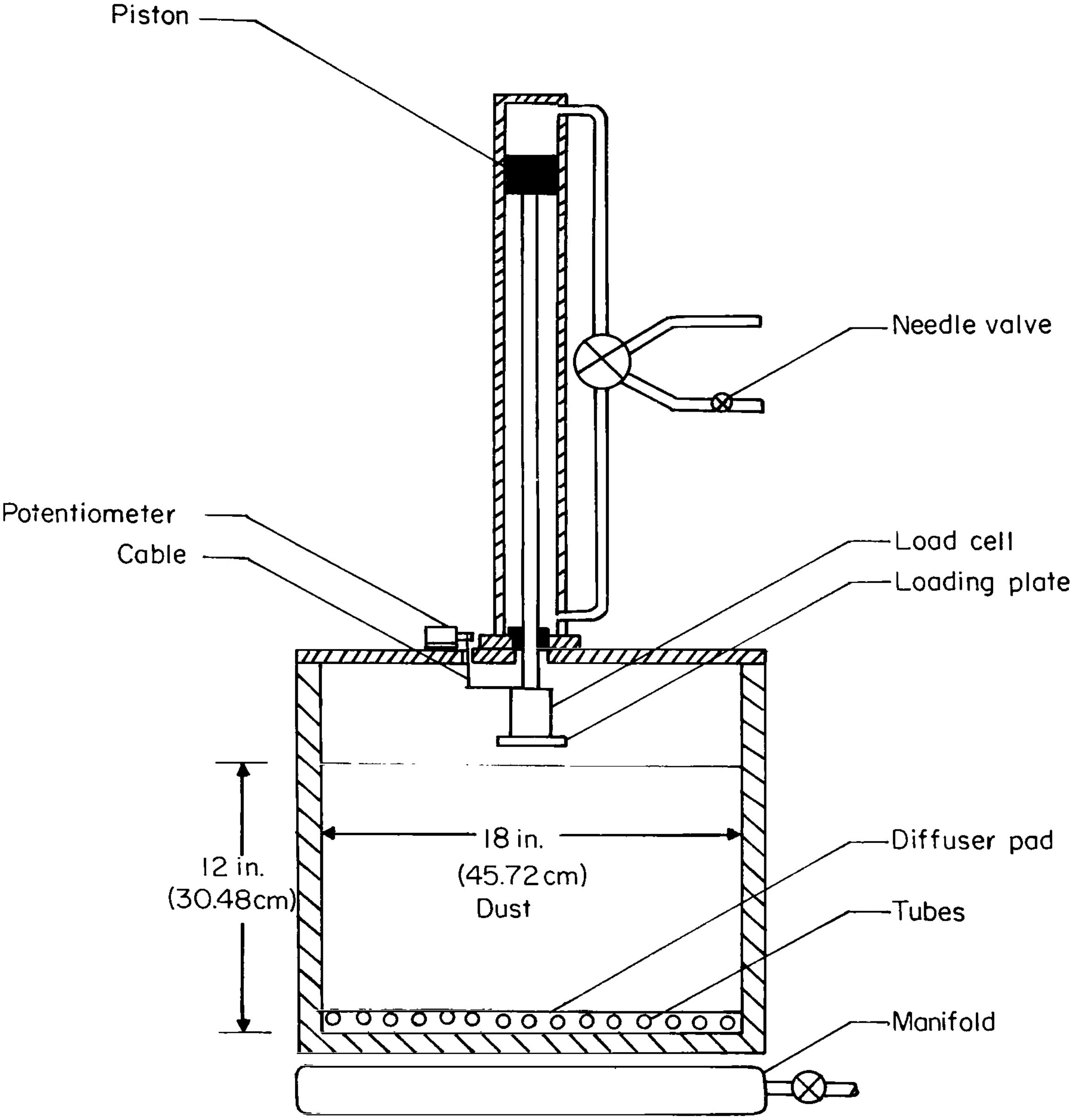

Figure 5.- Section of bearing-strength test apparatus showing details of dust preparation bin.

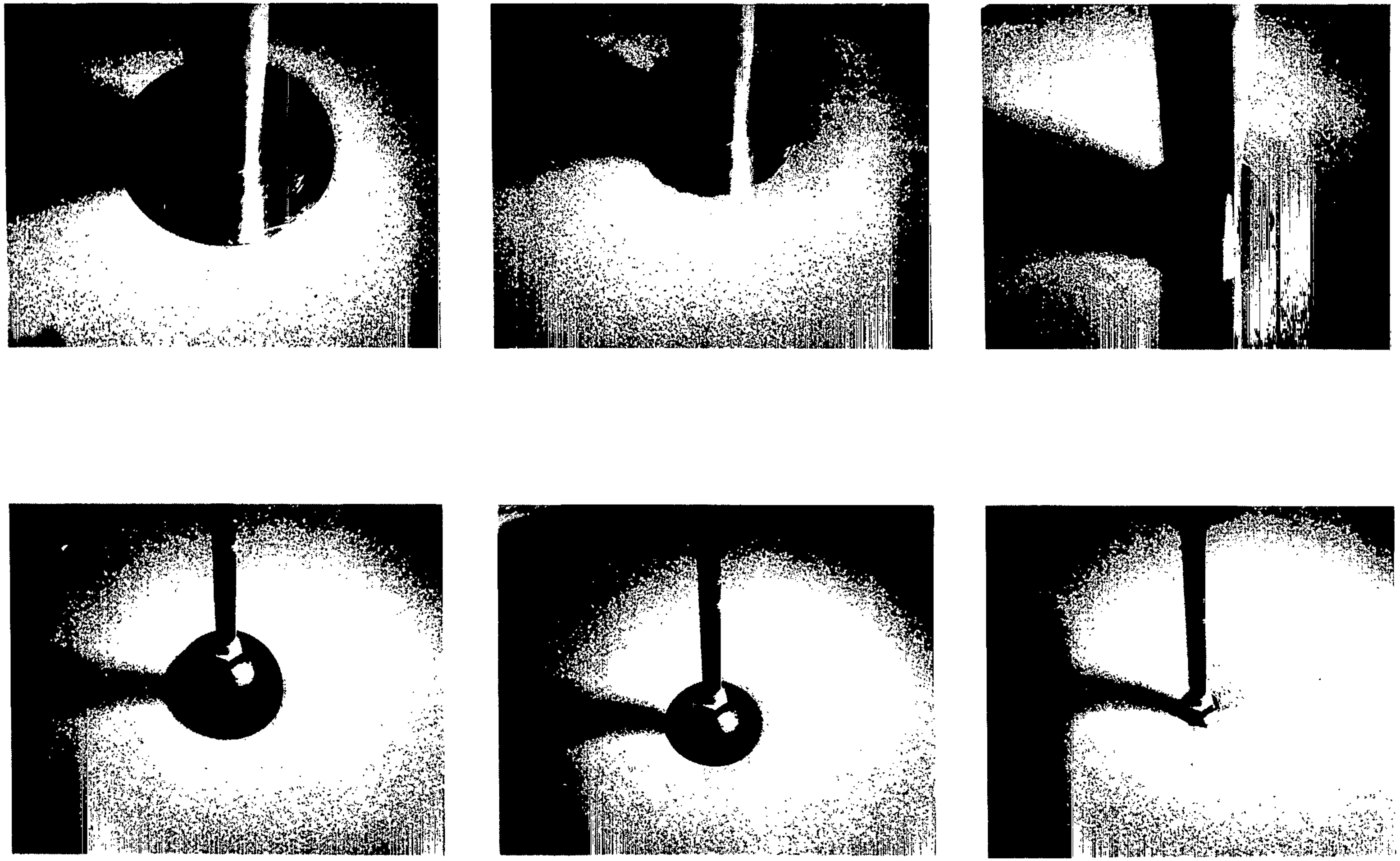

(a) $l = 187\mu$; $\gamma = 119$ lb/ft^3 (1906 kg/m^3).

L-65-7948

Figure 6.- Photographs taken during bearing-strength tests conducted on dusts of several sizes showing 30 in^2 (193.55 cm^2) loading plate and 3-in-diameter (7.62 cm) sphere at various stages of loading process.

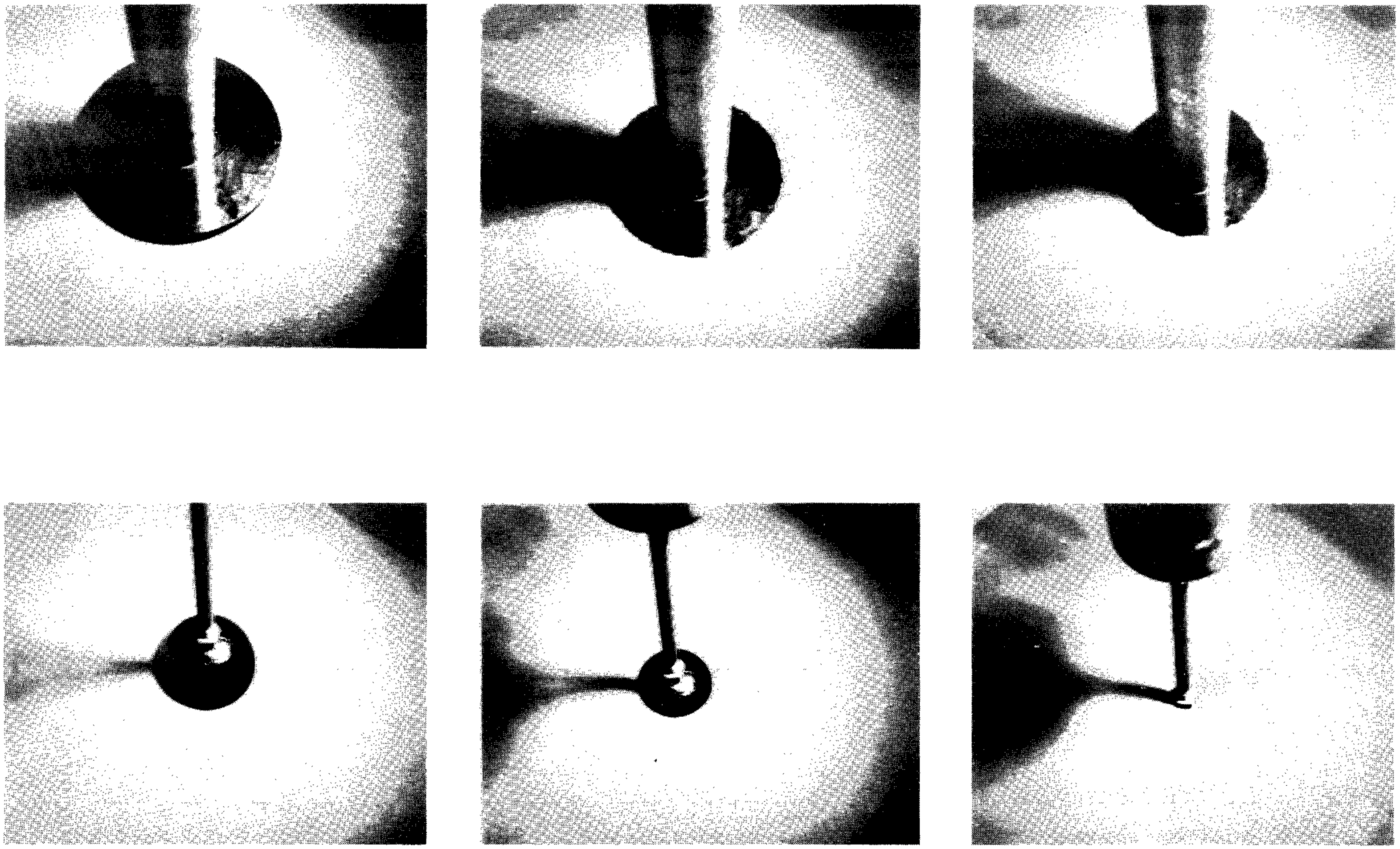

(b) $l = 75\mu$; $\gamma = 112$ lb/ft^3 (1794 kg/m^3).

L-65-7949

Figure 6.- Continued.

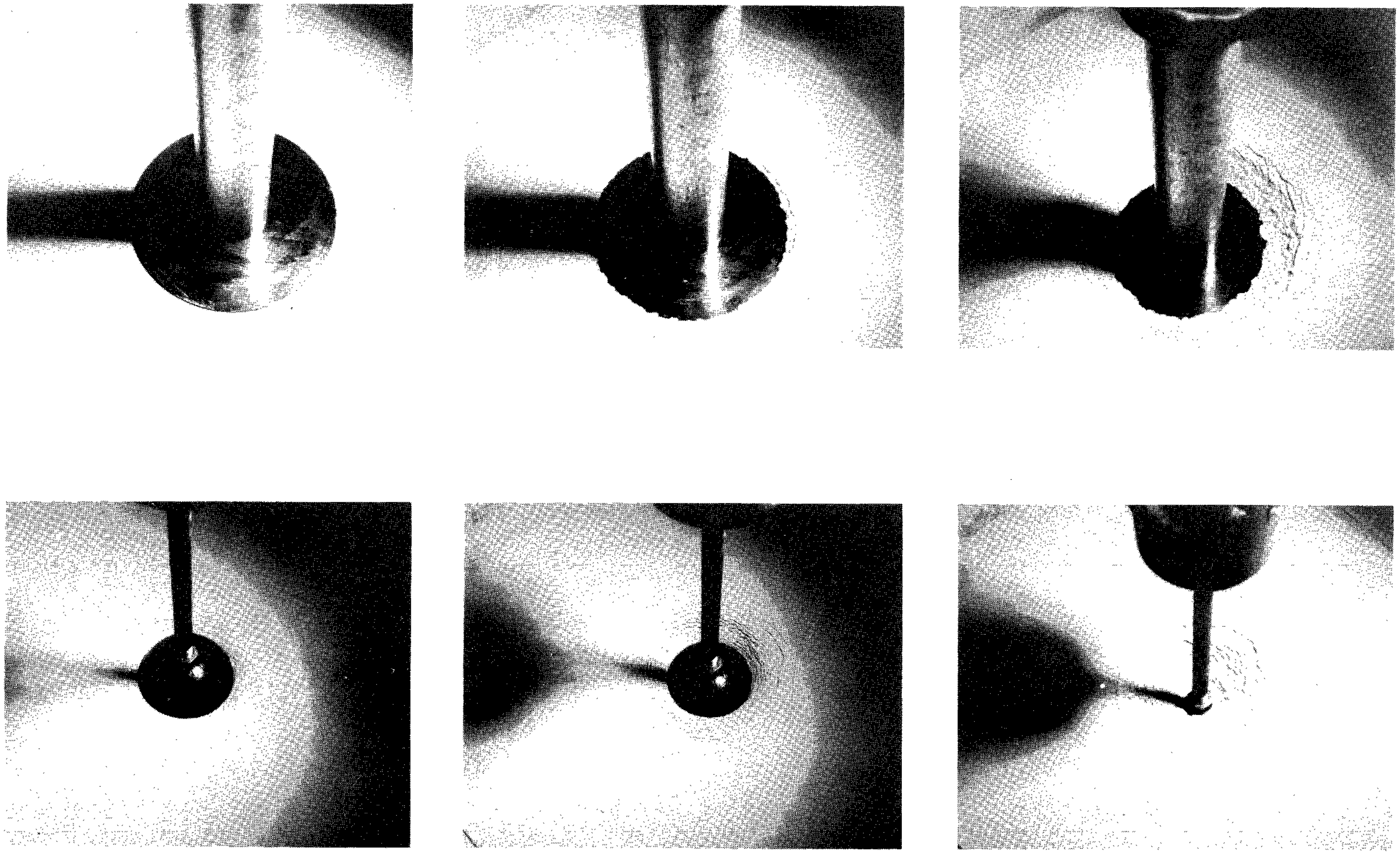

(c) $l = 27\mu$; $\gamma = 93$ lb/ft^3 (1490 kg/m^3).

L-65-7950

Figure 6.- Continued.

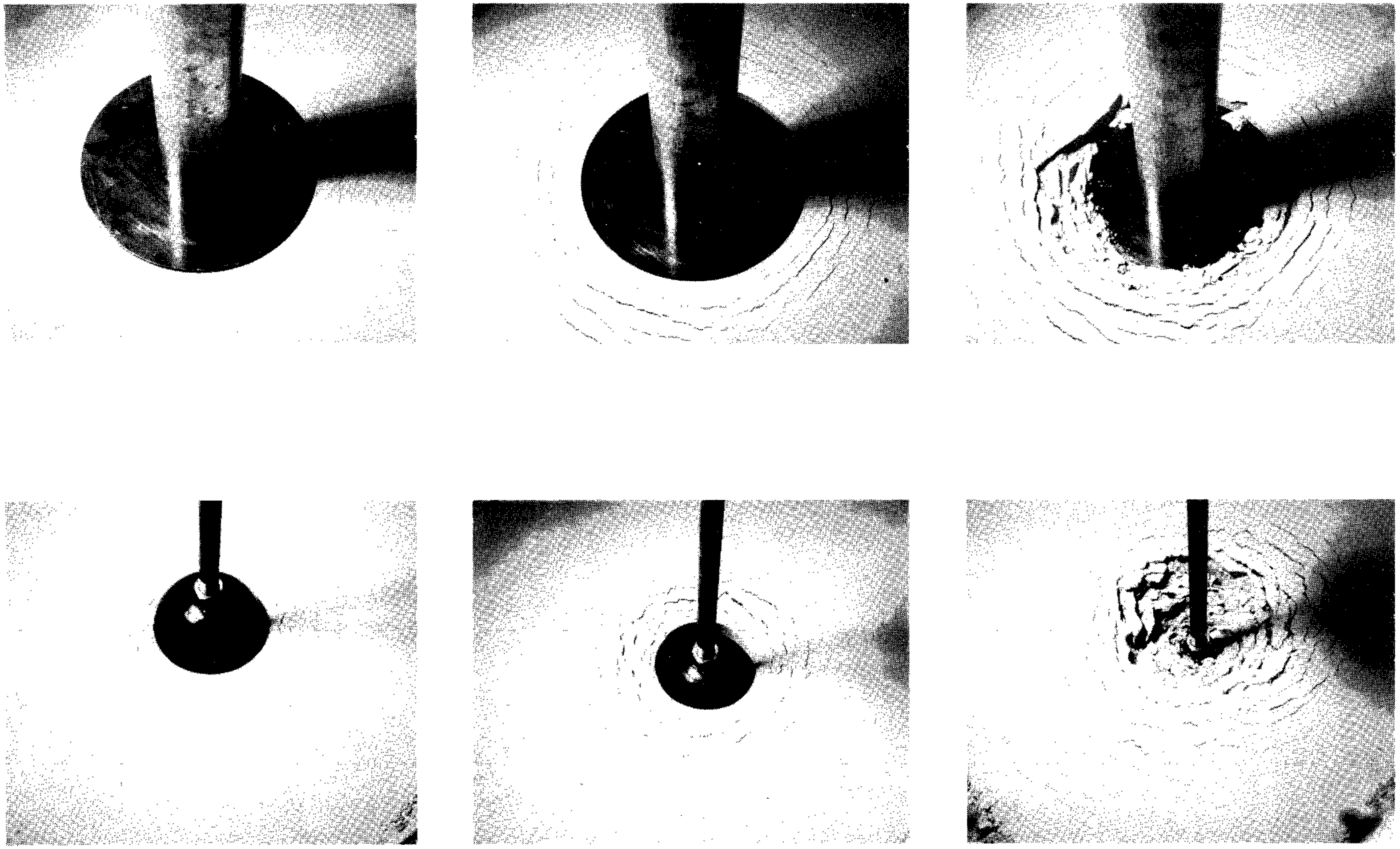

(d) $l = 5\mu$; $\gamma = 73$ lb/ft^3 (1169 kg/m^3).

L-65-7951

Figure 6.- Concluded.

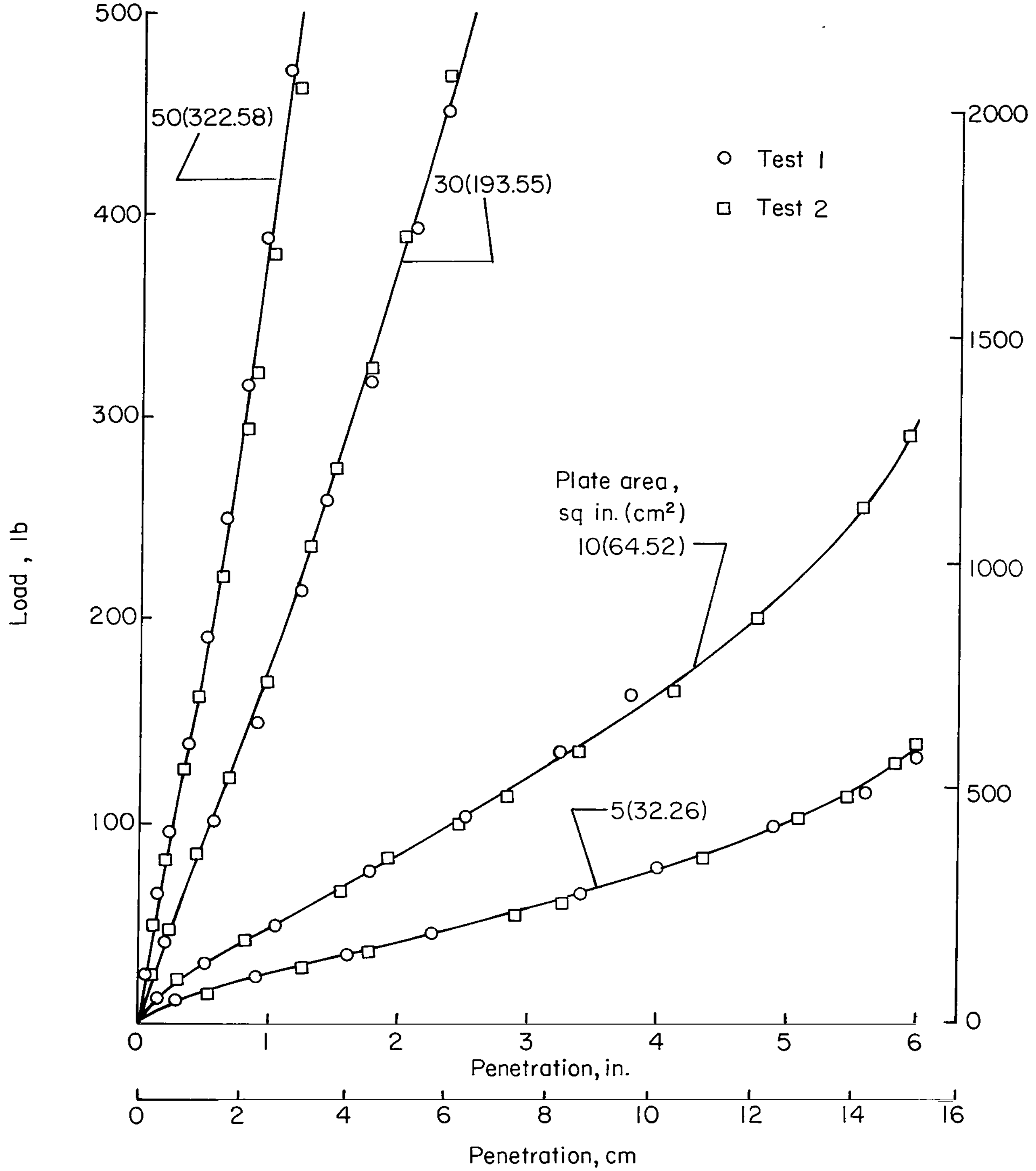

Figure 7.- Typical data from bearing-strength tests. $l = 550\mu$; $\gamma = 119$ lb/ft^3 (1906 kg/m^3).

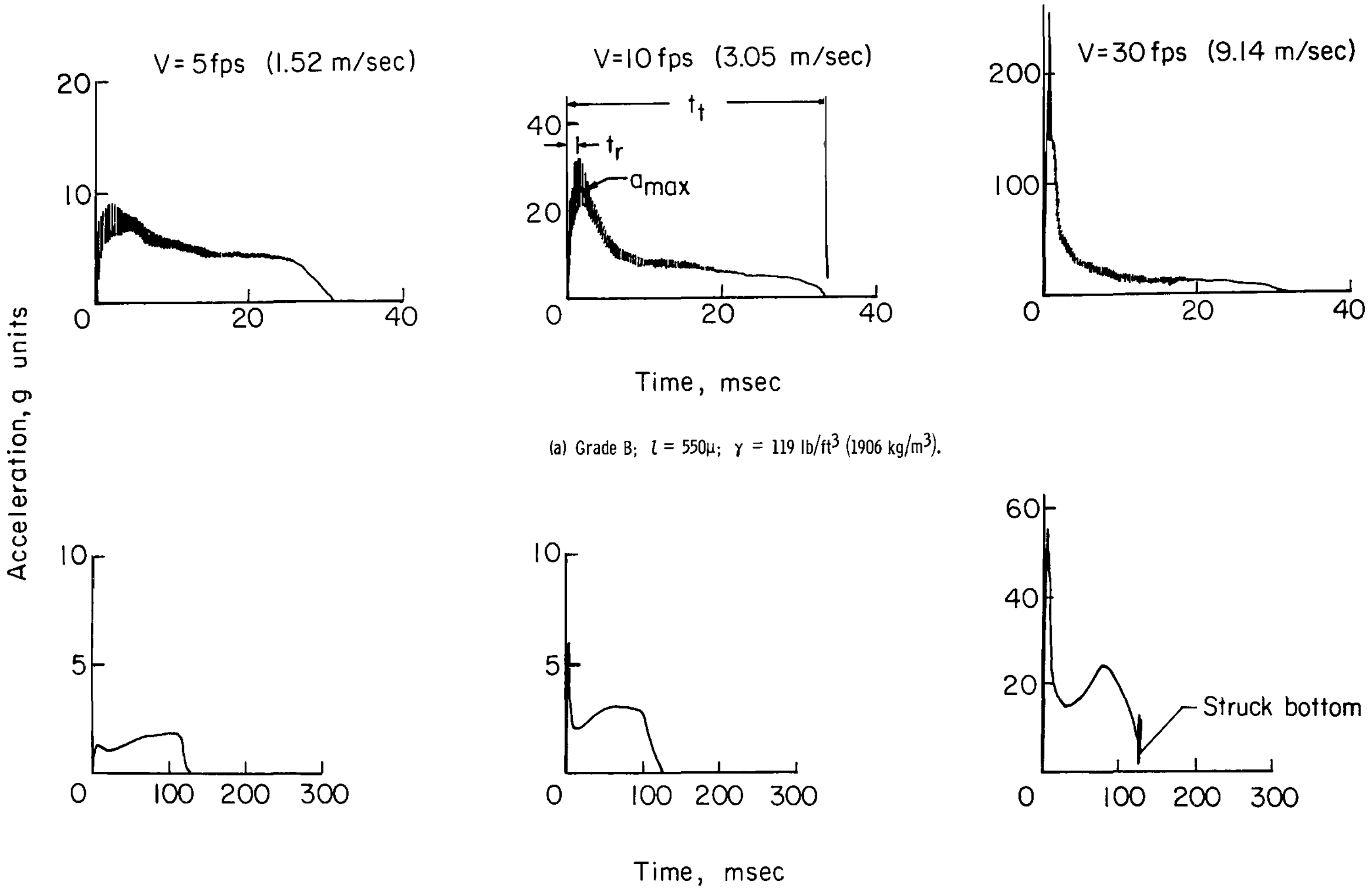

(a) Grade B; l = 550μ; γ = 119 lb/ft^3 (1906 kg/m^3).

(b) Grade I; l = 5μ; γ = 73 lb/ft^3 (1169 kg/m^3).

Figure 8.- Reproductions of typical acceleration time histories recorded during impact tests on two grades of dust particles. D = 3 in. (7.62 cm); m = 0.0020 lb-sec^2/in. (0.350 kg).

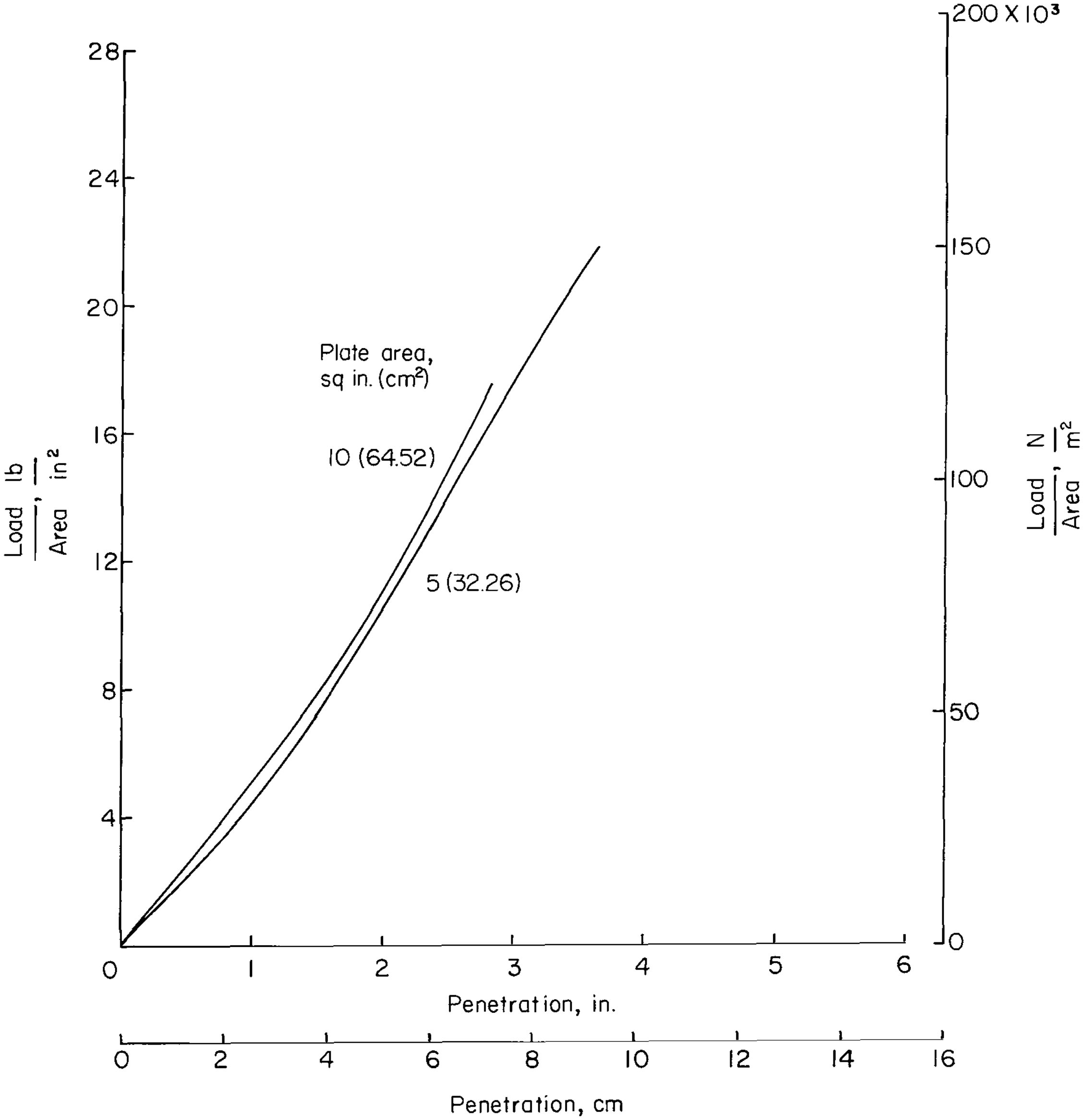

(a) l = 936μ; γ = 116 lb/ft^3 (1858 kg/m^3).

Figure 9.- Summary of bearing-strength test results.

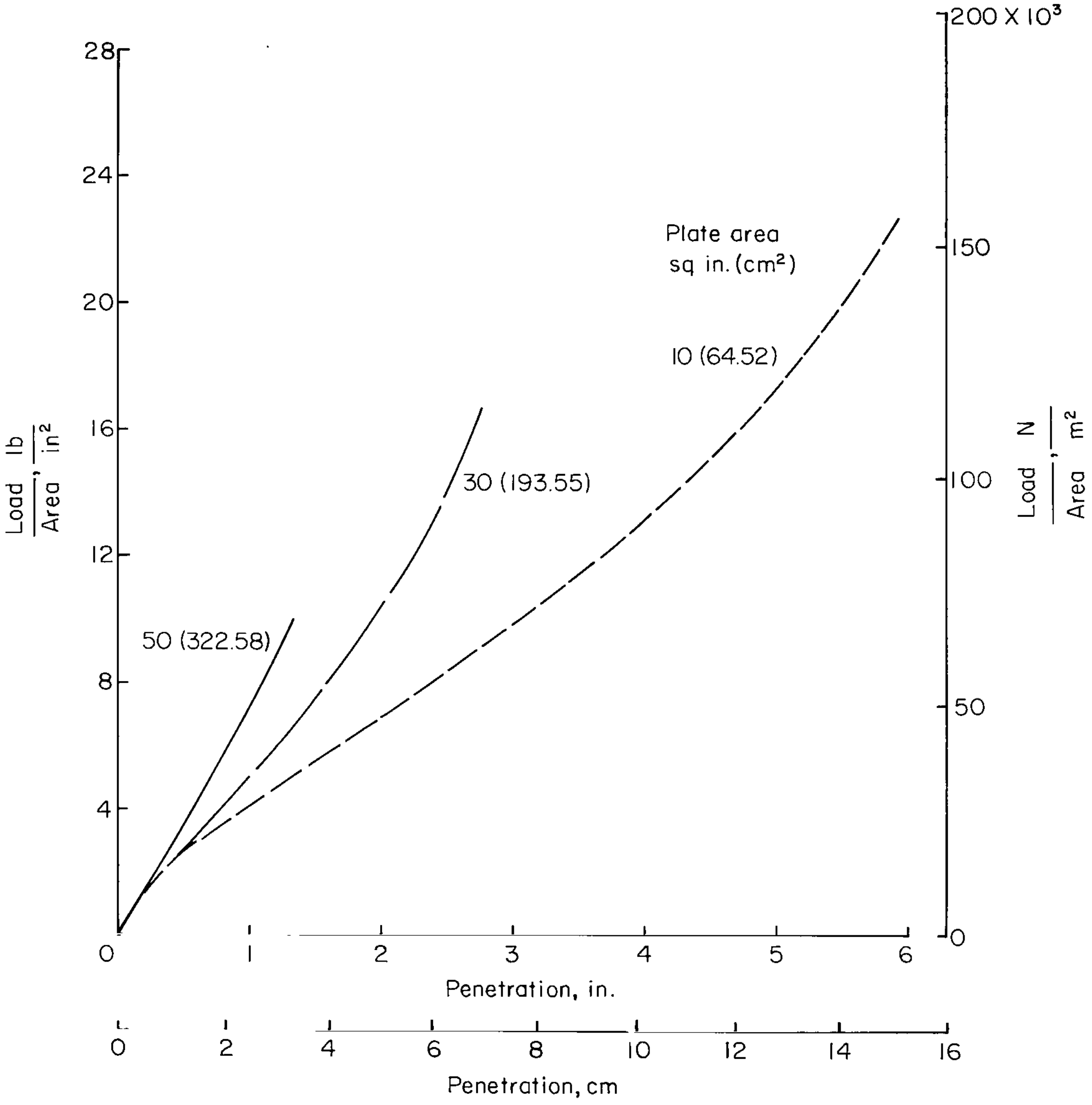

(b) $l = 550\mu$; $\gamma = 118$ lb/ft³ (1890 kg/m³).

Figure 9.- Continued.

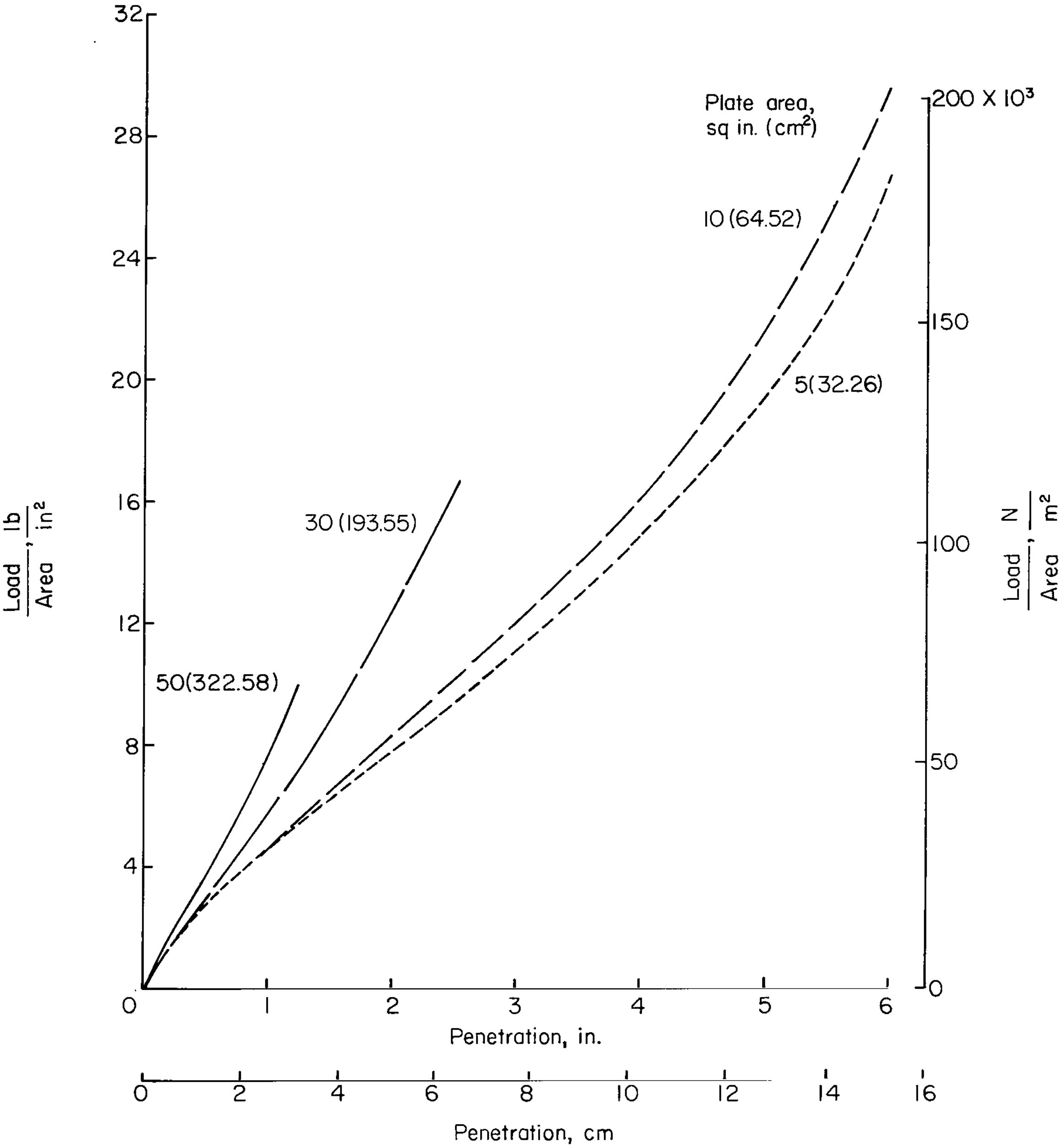

(c) l = 550μ; γ = 119 lb/ft^3 (1906 kg/m^3).

Figure 9.- Continued.

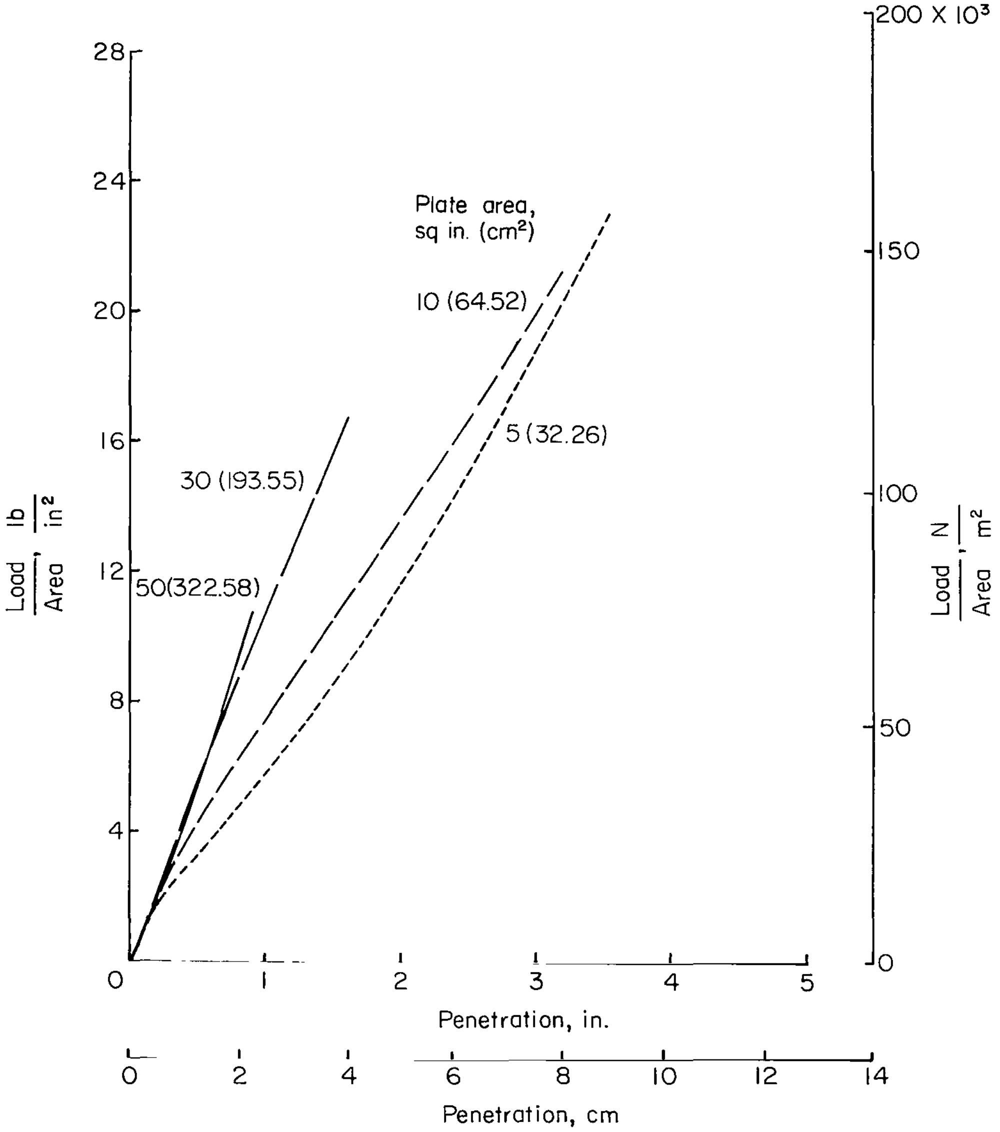

(d) $l = 550\mu$; $\gamma = 122$ lb/ft^3 (1954 kg/m^3).

Figure 9.- Continued.

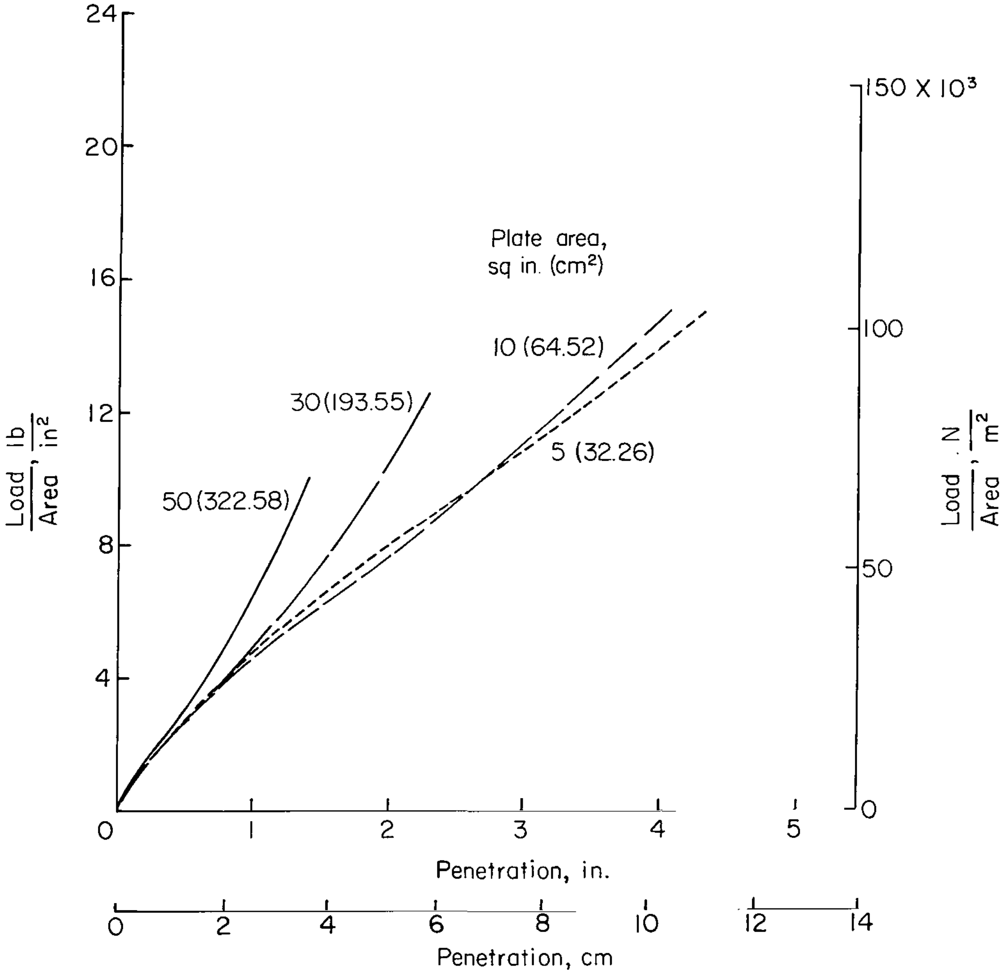

(e) l = 187μ; γ = 119 lb/ft³ (1906 kg/m³).

Figure 9.- Continued.

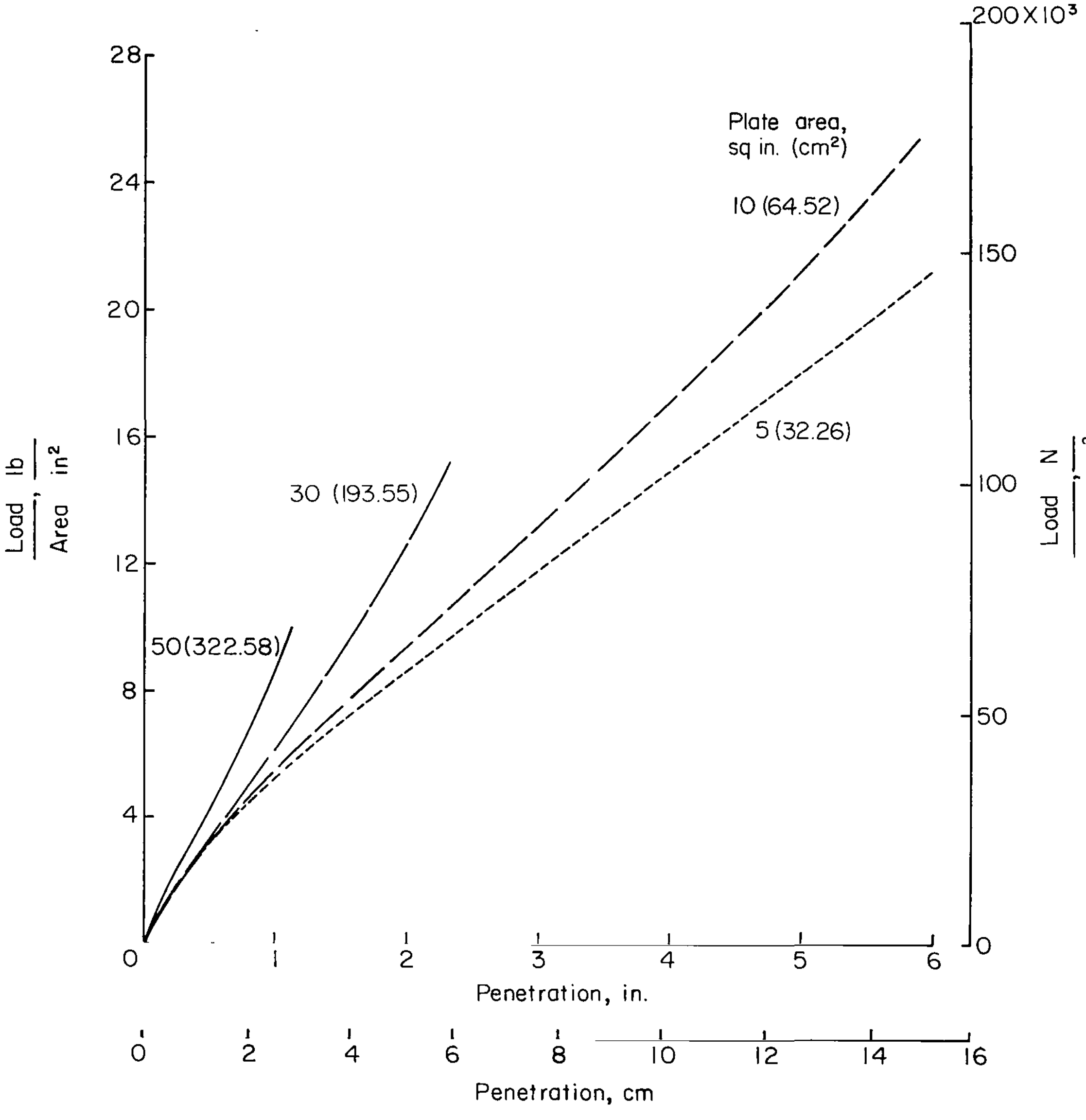

(f) $l = 187\mu$; $\gamma = 120$ lb/ft^3 (1922 kg/m^3).

Figure 9.- Continued.

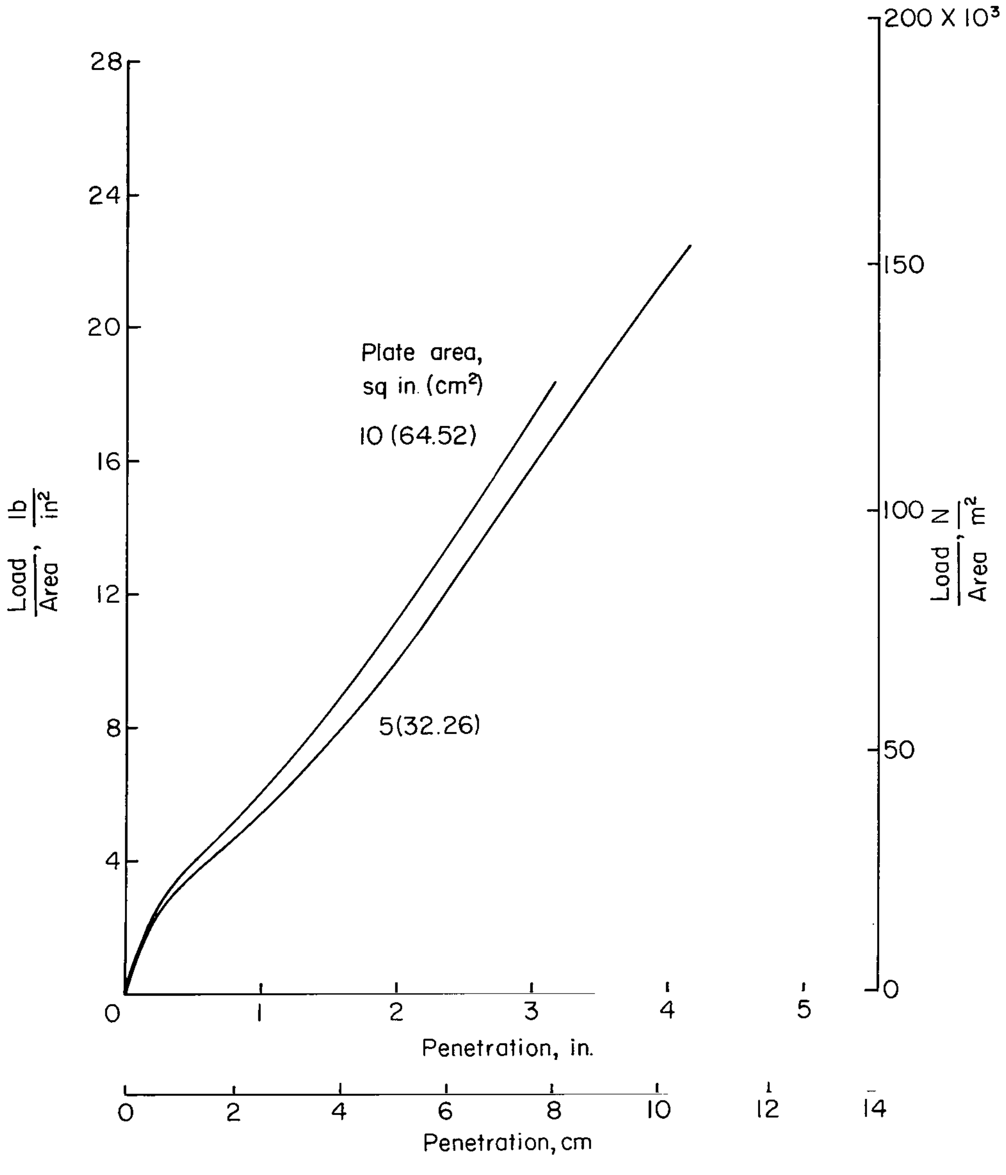

(g) l = 149μ; γ = 114 lb/ft^3 (1826 kg/m^3).

Figure 9.- Continued.

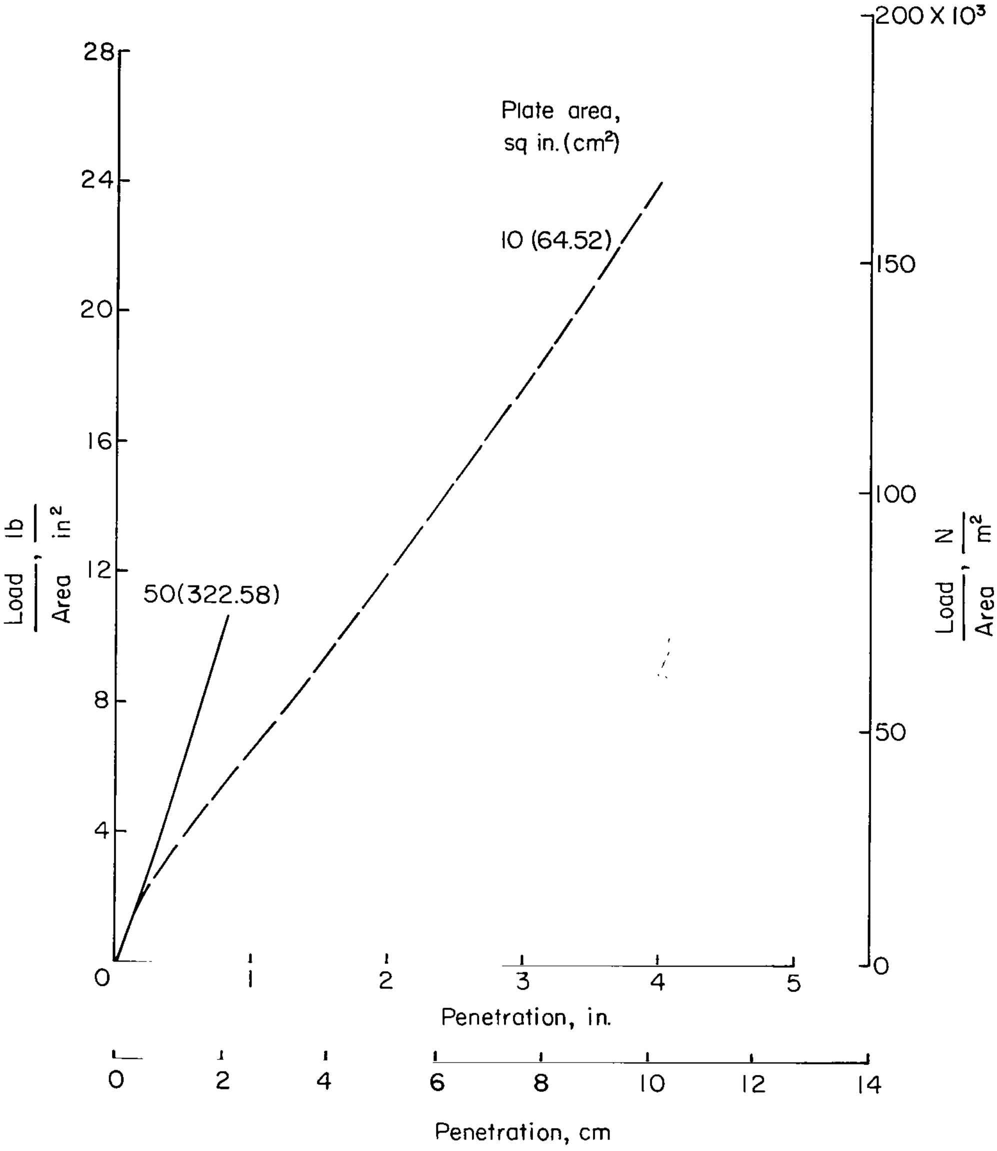

(h) $l = 75\mu$; γ = 111 lb/ft³ (1778 kg/m³).

Figure 9.- Continued.

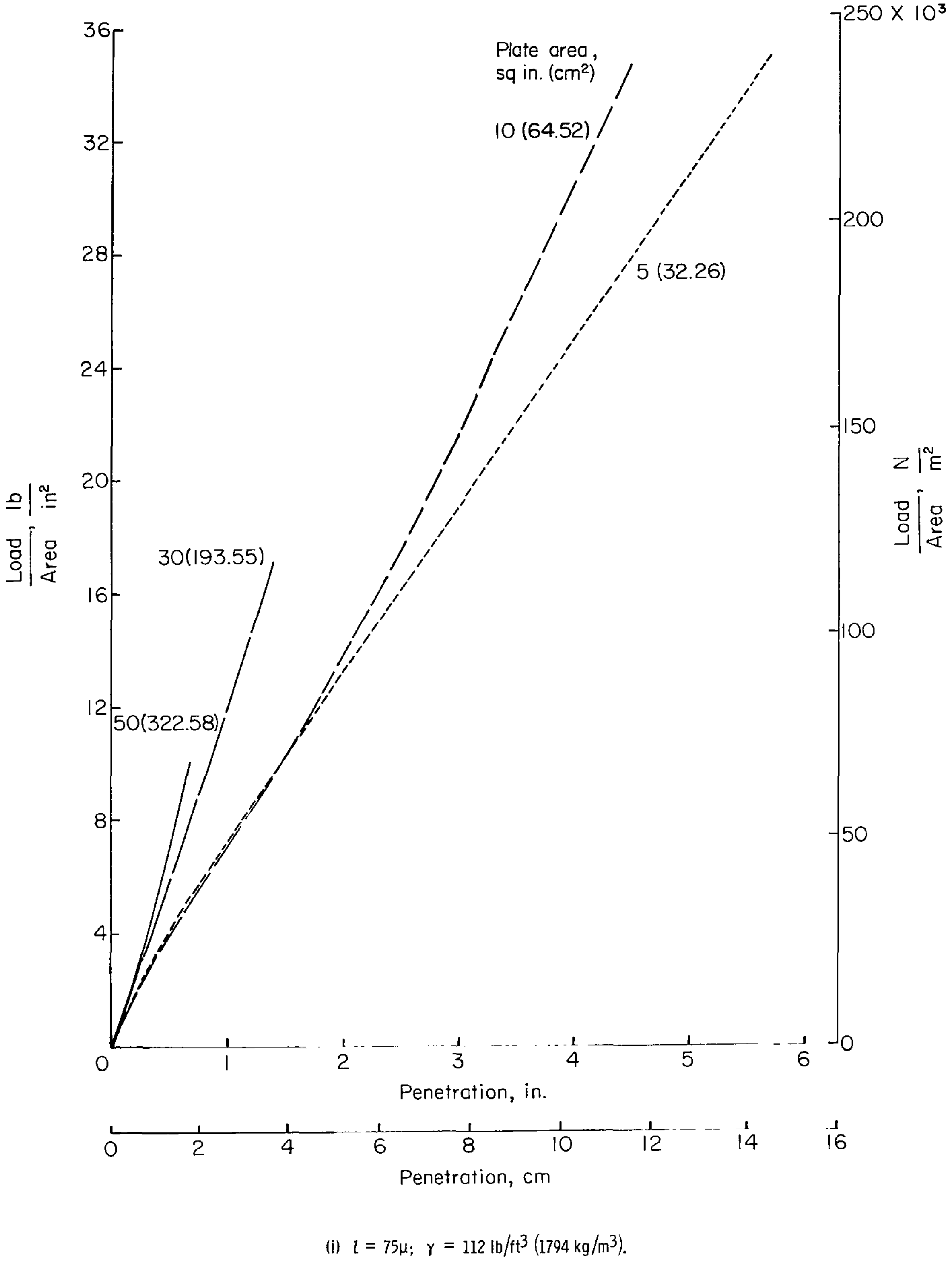

(i) l = 75μ; γ = 112 lb/ft^3 (1794 kg/m^3).

Figure 9.- Continued.

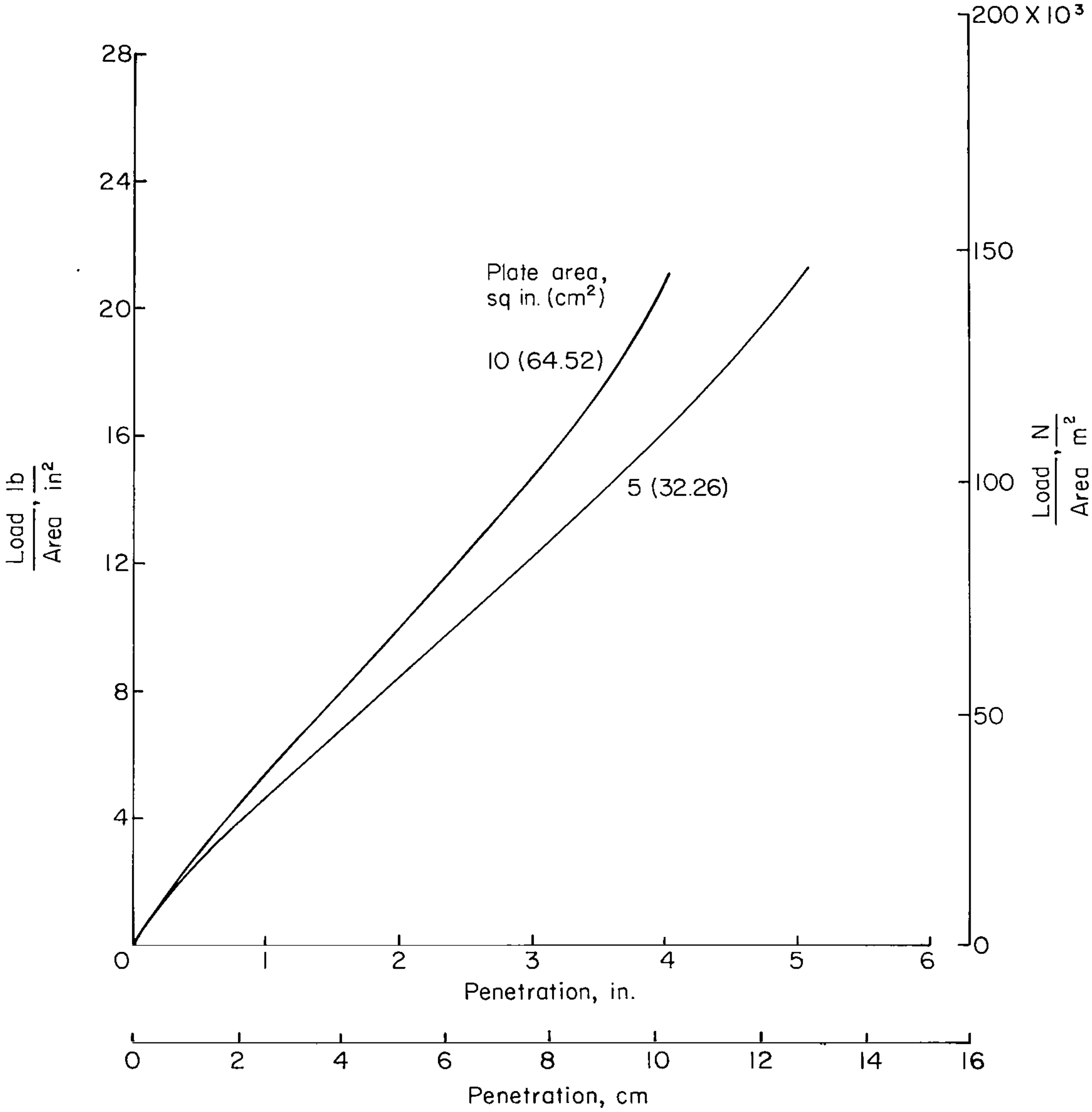

(j) l = 65μ; γ = 107 lb/ft³ (1714 kg/m³).

Figure 9.- Continued.

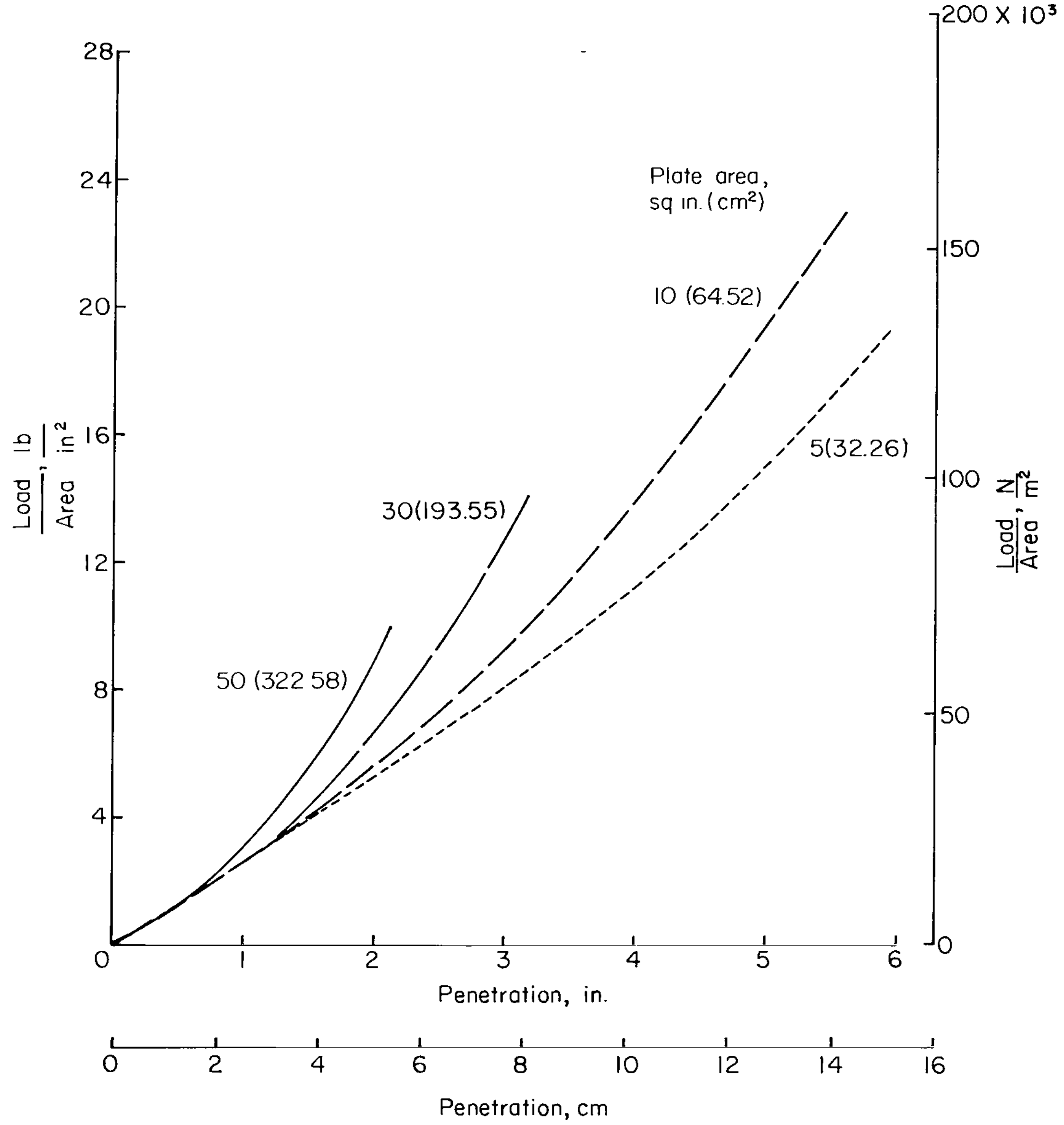

(k) $l = 32\mu$; $\gamma = 93$ lb/ft³ (1490 kg/m³).

Figure 9.- Continued.

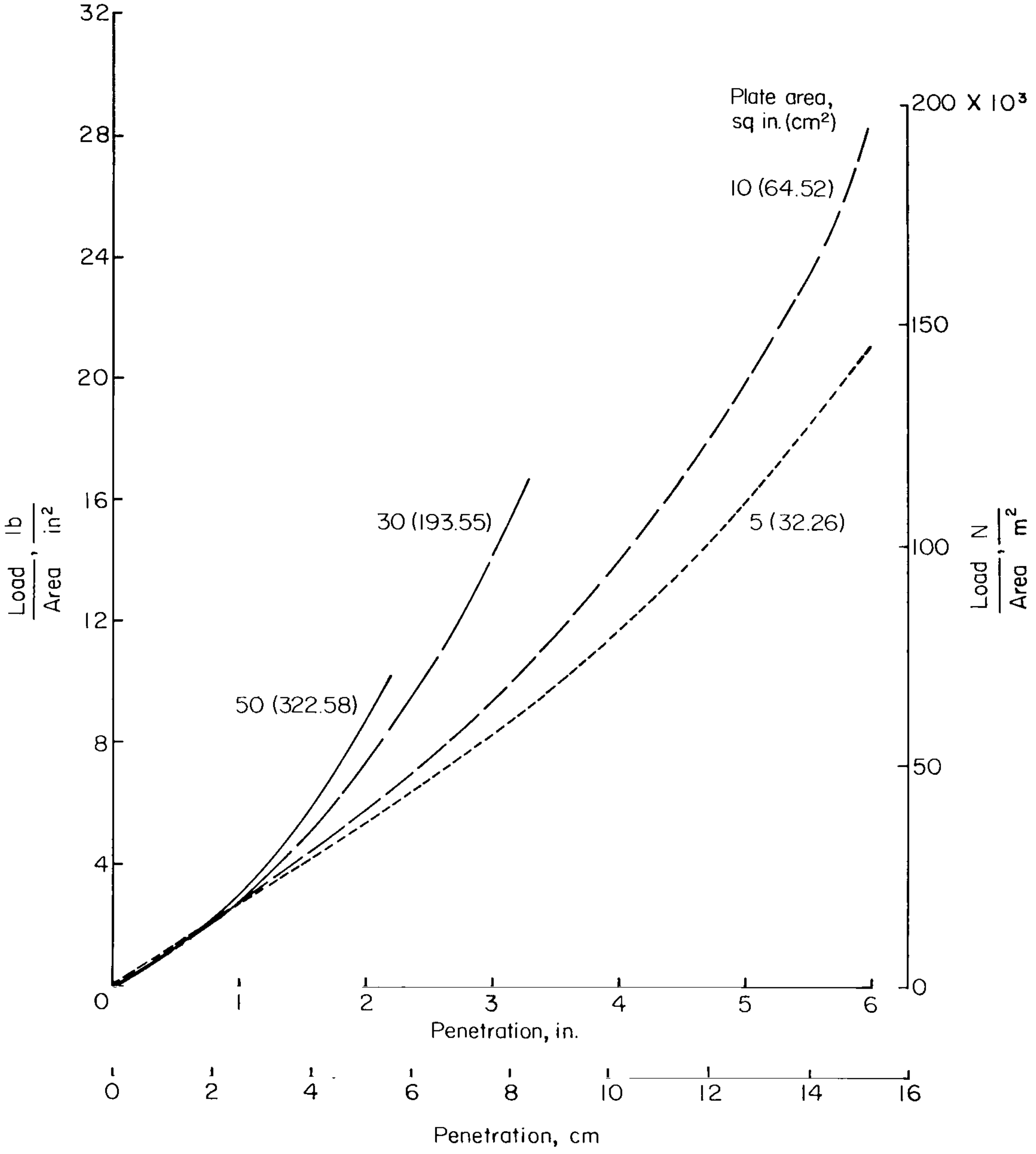

(l) $l = 27\mu$; $\gamma = 93$ lb/ft³ (1490 kg/m³).

Figure 9.- Continued.

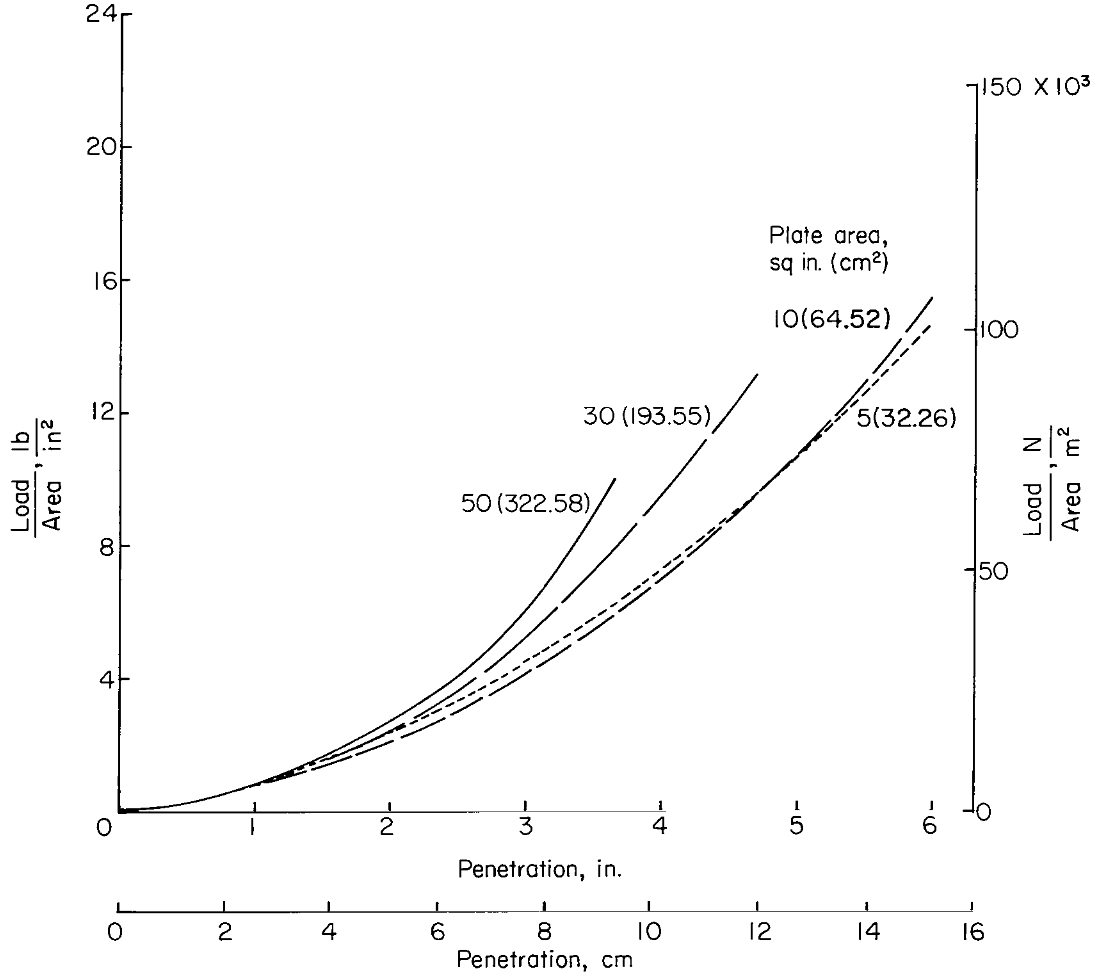

(m) $l = 5\mu$; $\gamma = 73\ \mathrm{lb/ft^3}$ $(1169\ \mathrm{kg/m^3})$.

Figure 9.- Continued.

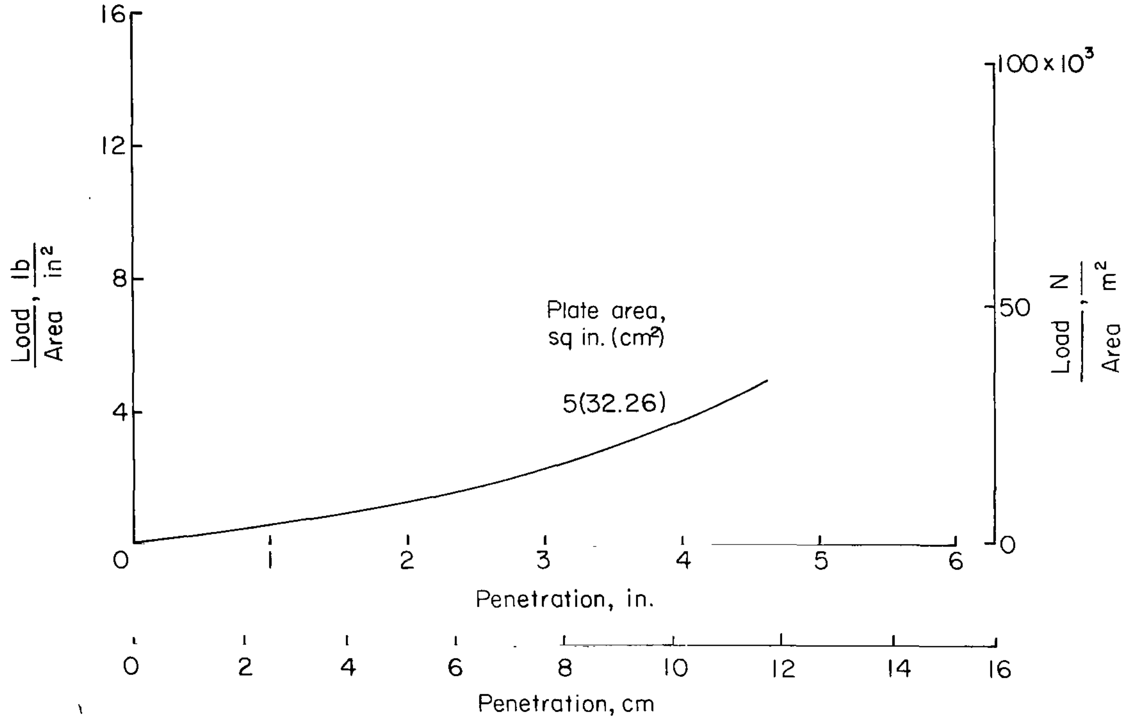

(n) Pumice; l = 68μ; γ = 37 lb/ft³ (593 kg/m³).

Figure 9.- Concluded.

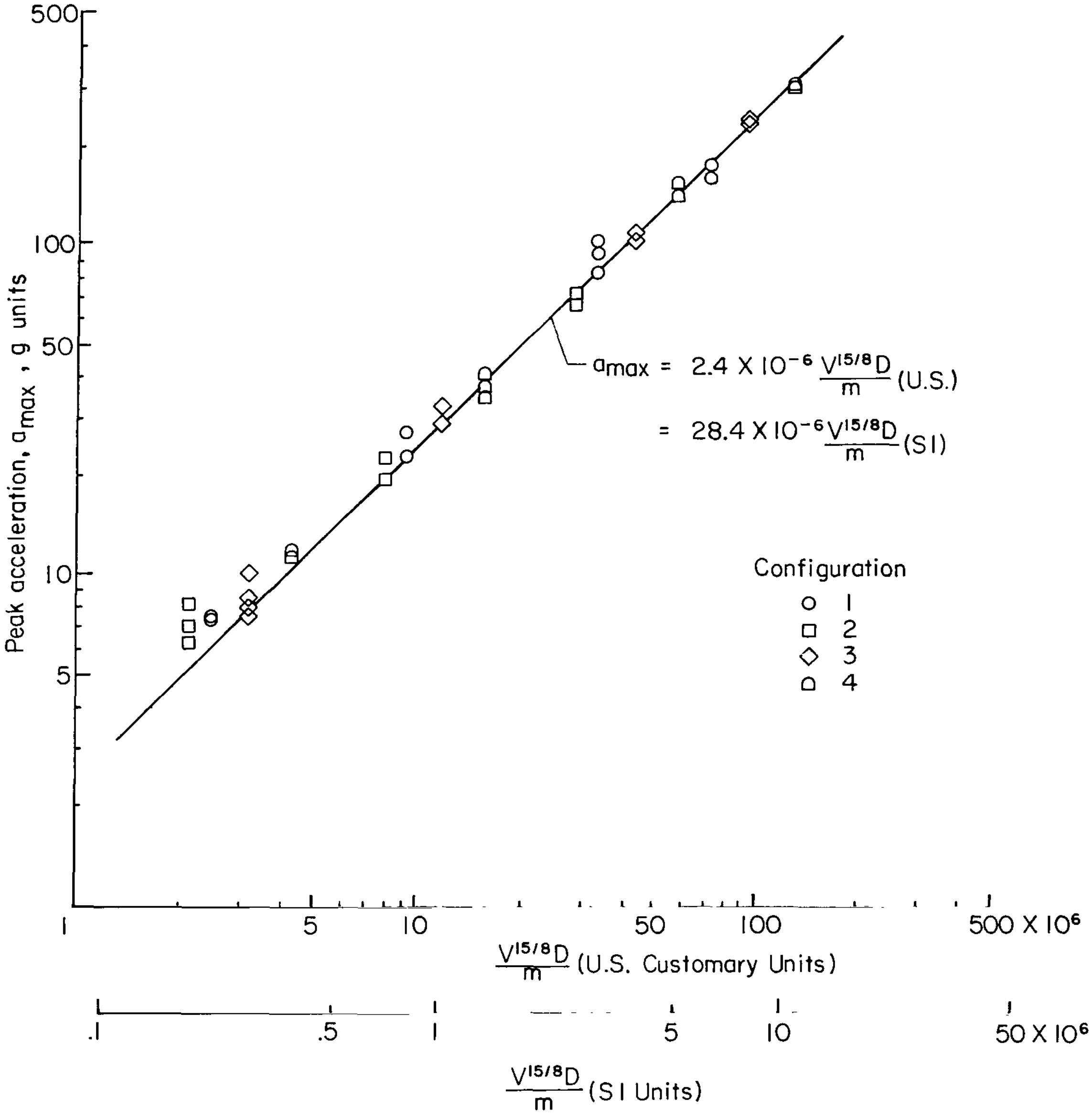

(a) l = 936μ; γ = 116 lb/ft^3 (1858 kg/m^3).

Figure 10.- Summary of peak acceleration data from penetrometer impact tests.

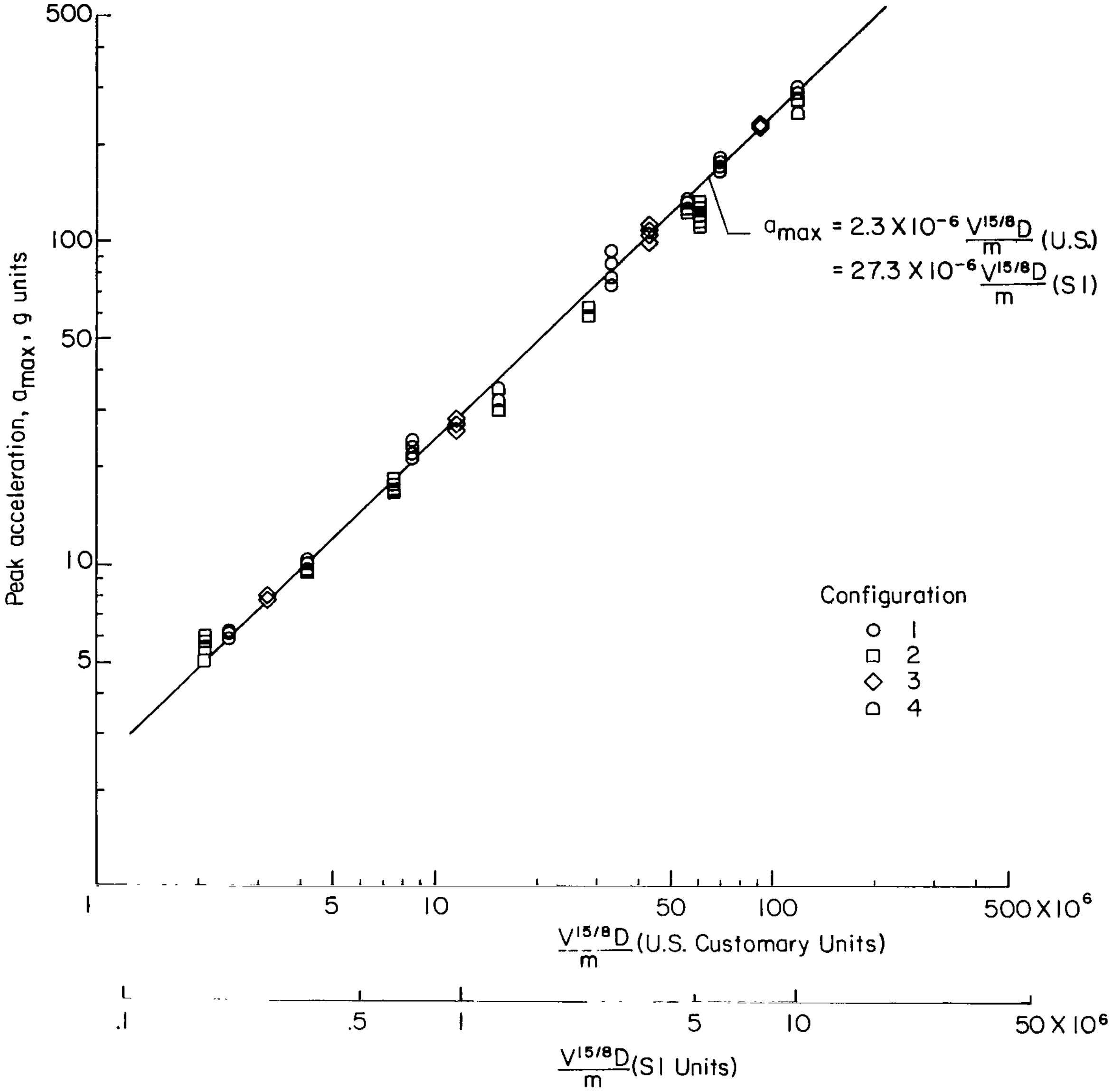

(b) l = 550μ; γ = 119 lb/ft^3 (1906 kg/m^3).

Figure 10.- Continued.

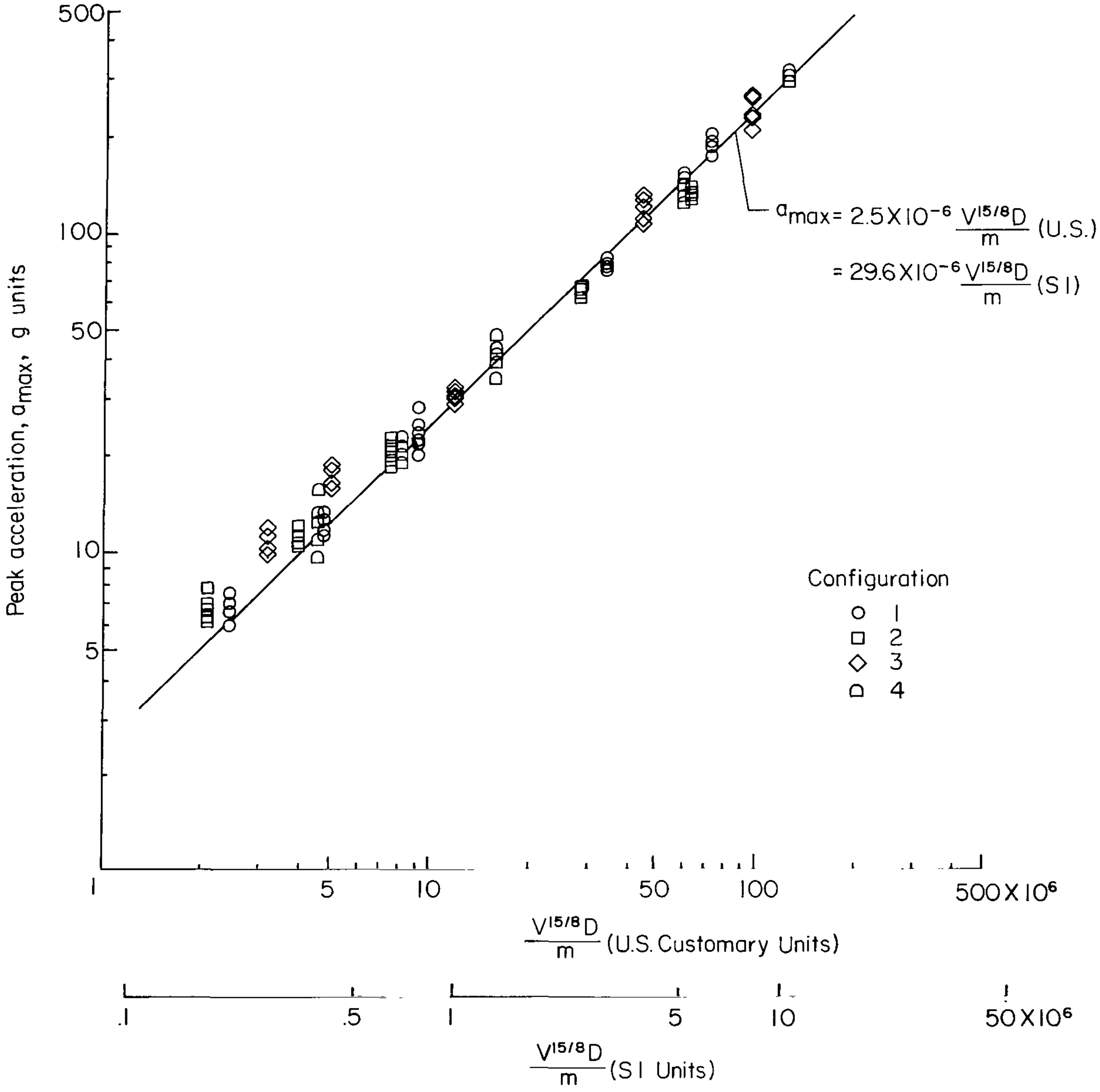

(c) l = 187μ; γ = 120 lb/ft³ (1922 kg/m³).

Figure 10.- Continued.

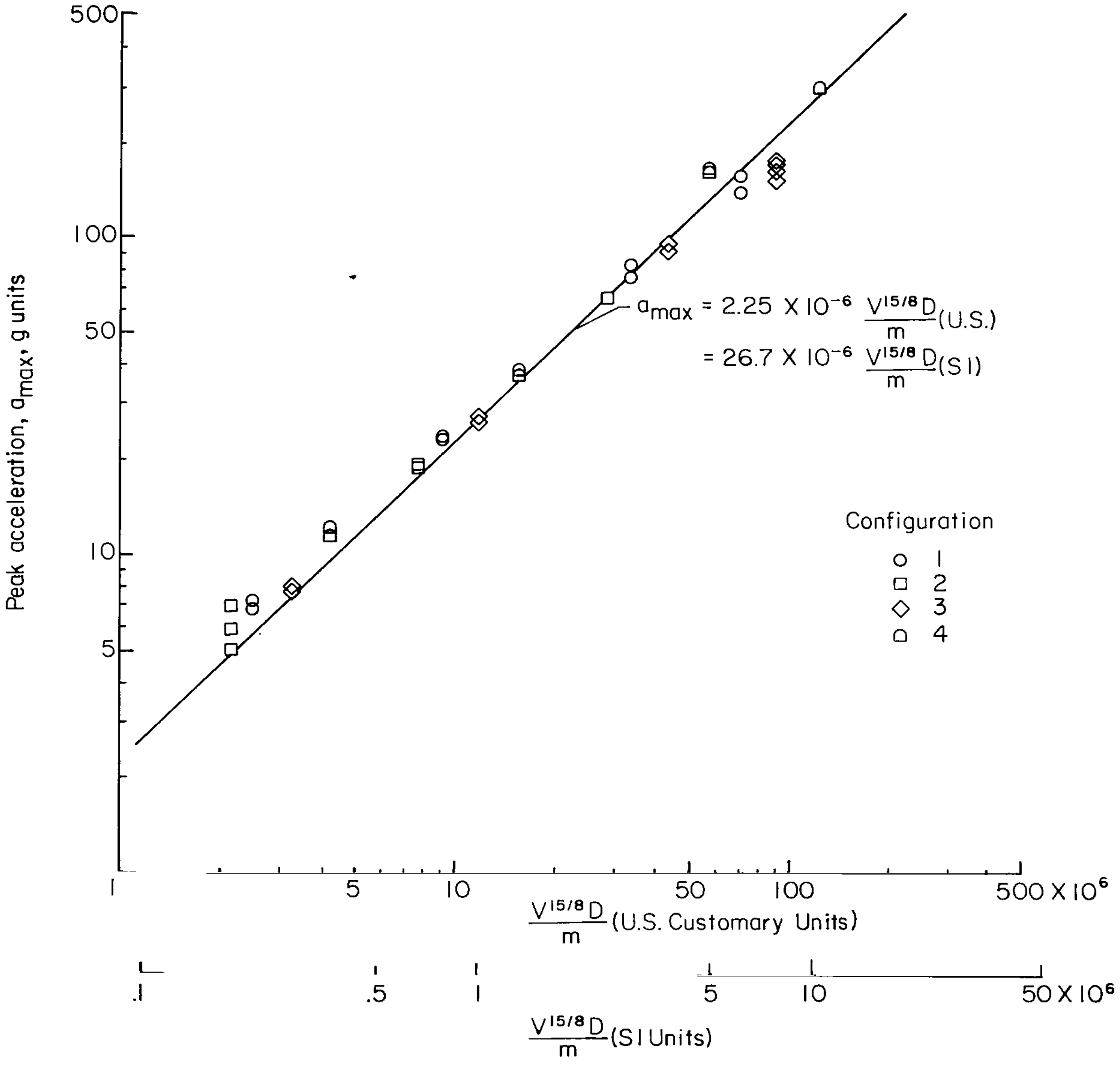

(d) l = 149μ; γ = 114 lb/ft³ (1826 kg/m³).

Figure 10.- Continued.

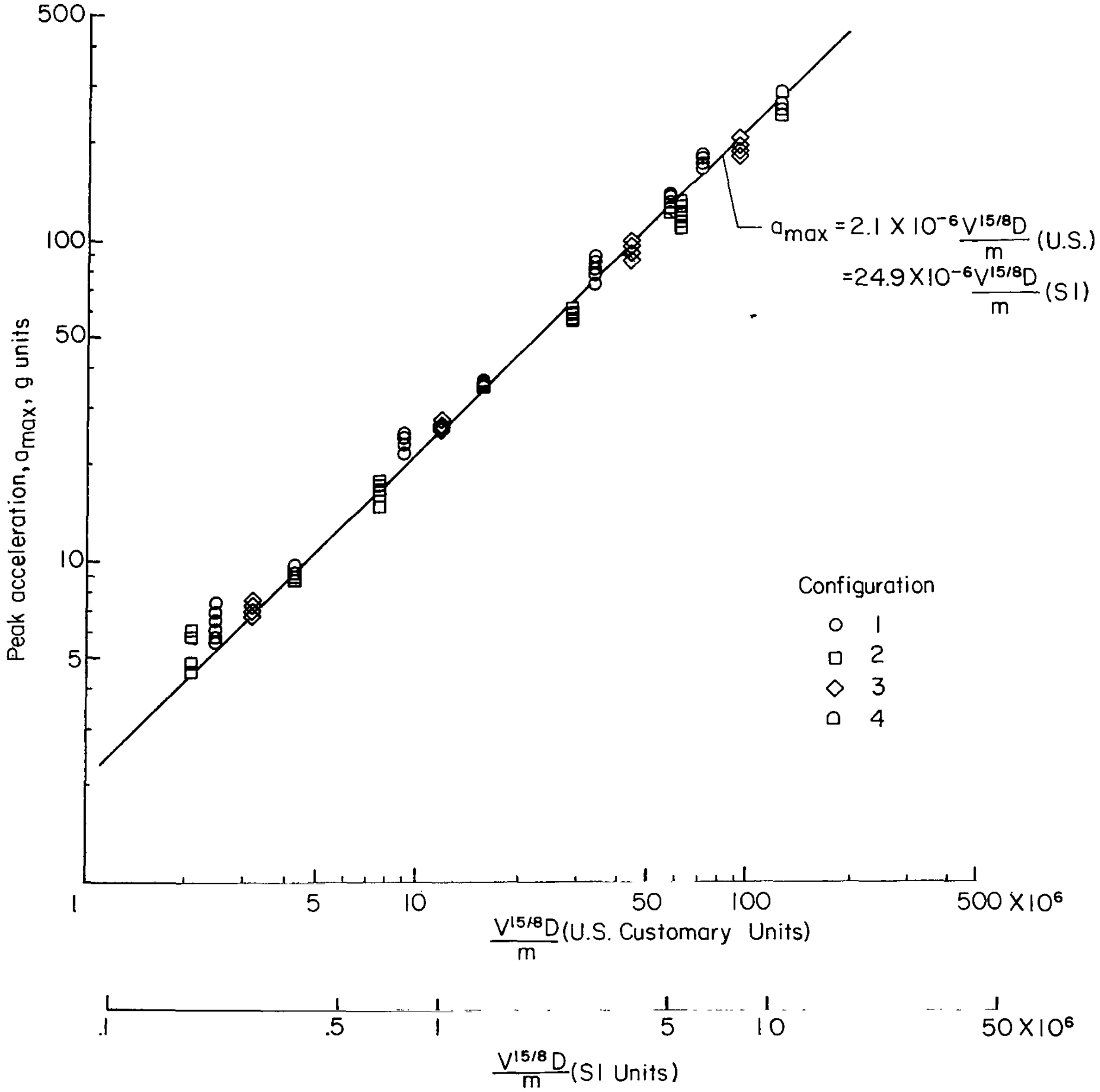

(e) $l = 75\mu$; $\gamma = 112$ lb/ft^3 (1794 kg/m^3).

Figure 10.- Continued.

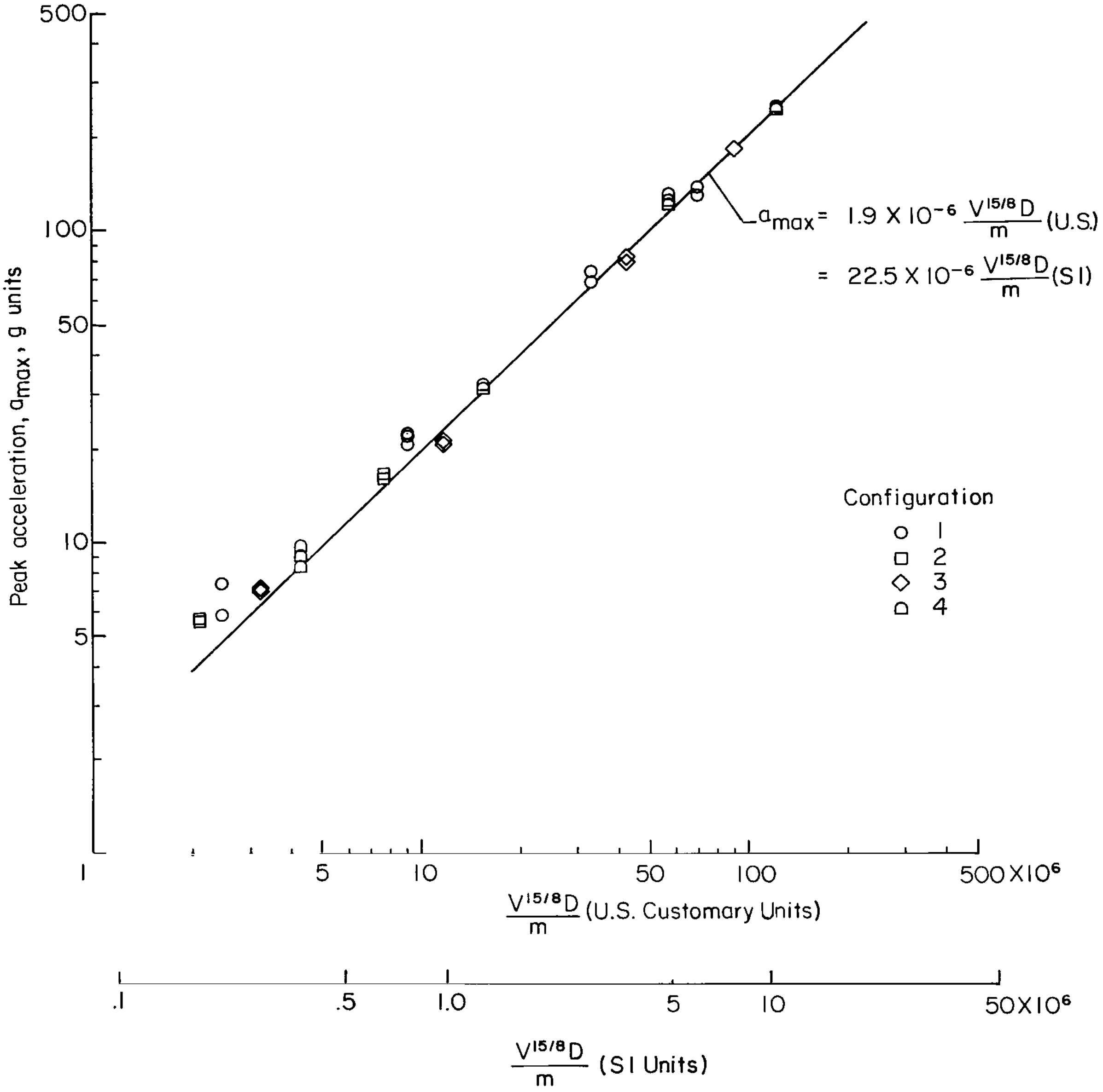

(f) $l = 65\mu$; $\gamma = 107$ lb/ft^3 (1714 kg/m^3).

Figure 10.- Continued.

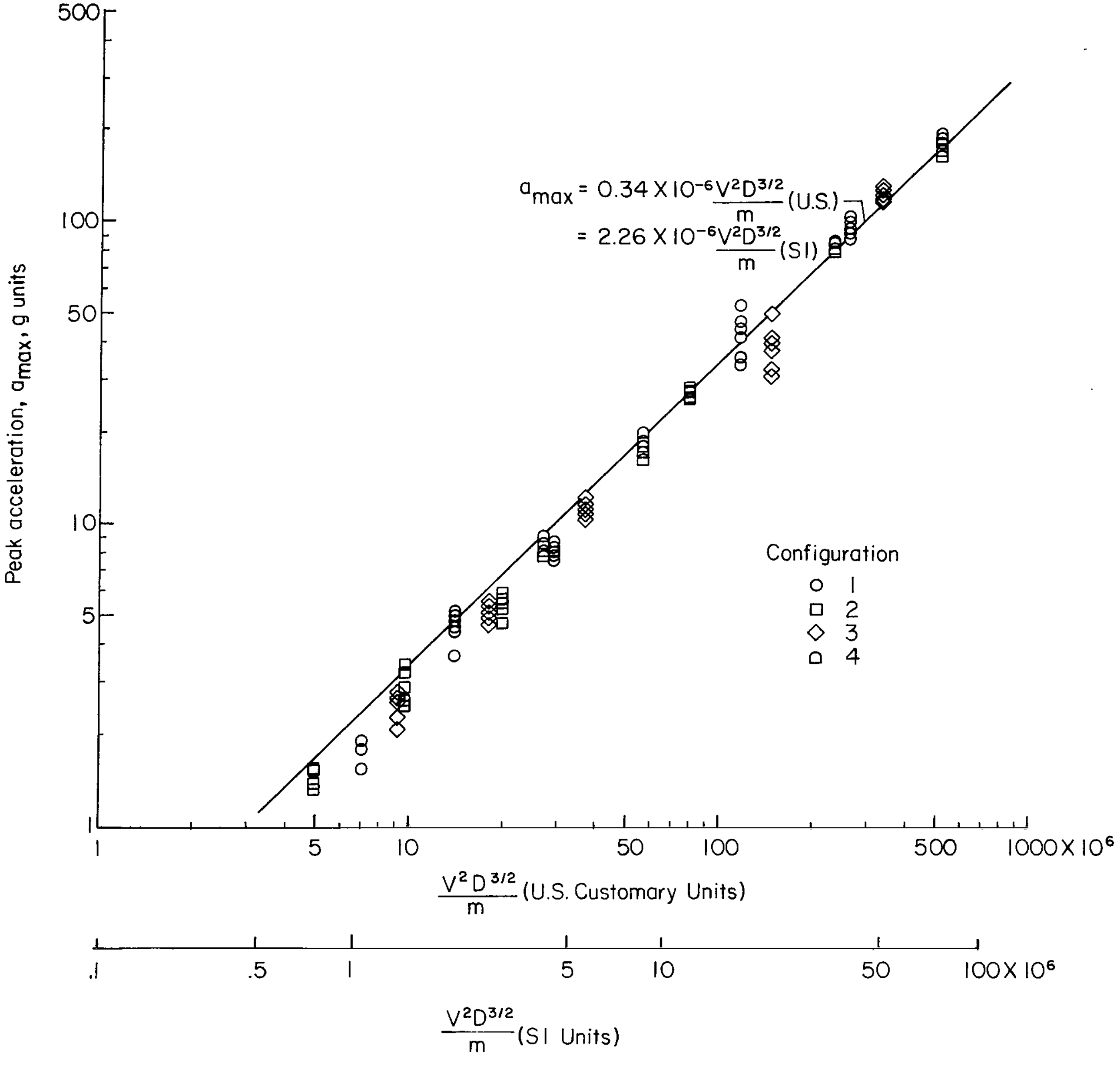

(g) $l = 27\mu$; $\gamma = 93$ lb/ft^3 (1490 kg/m^3).

Figure 10.- Continued.

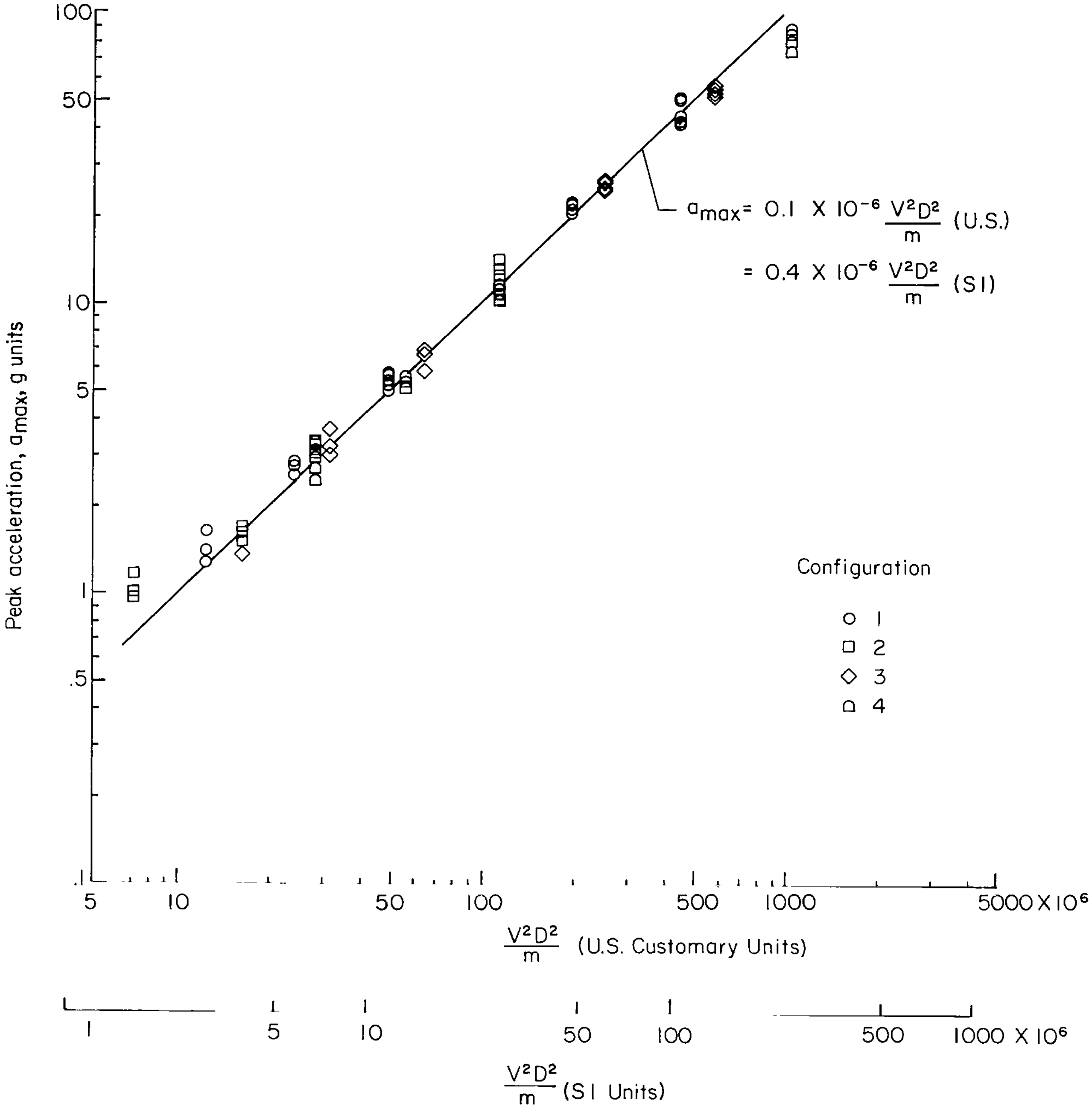

(h) $l = 5\mu$; $\gamma = 73$ lb/ft^3 (1169 kg/m^3).

Figure 10.- Continued.

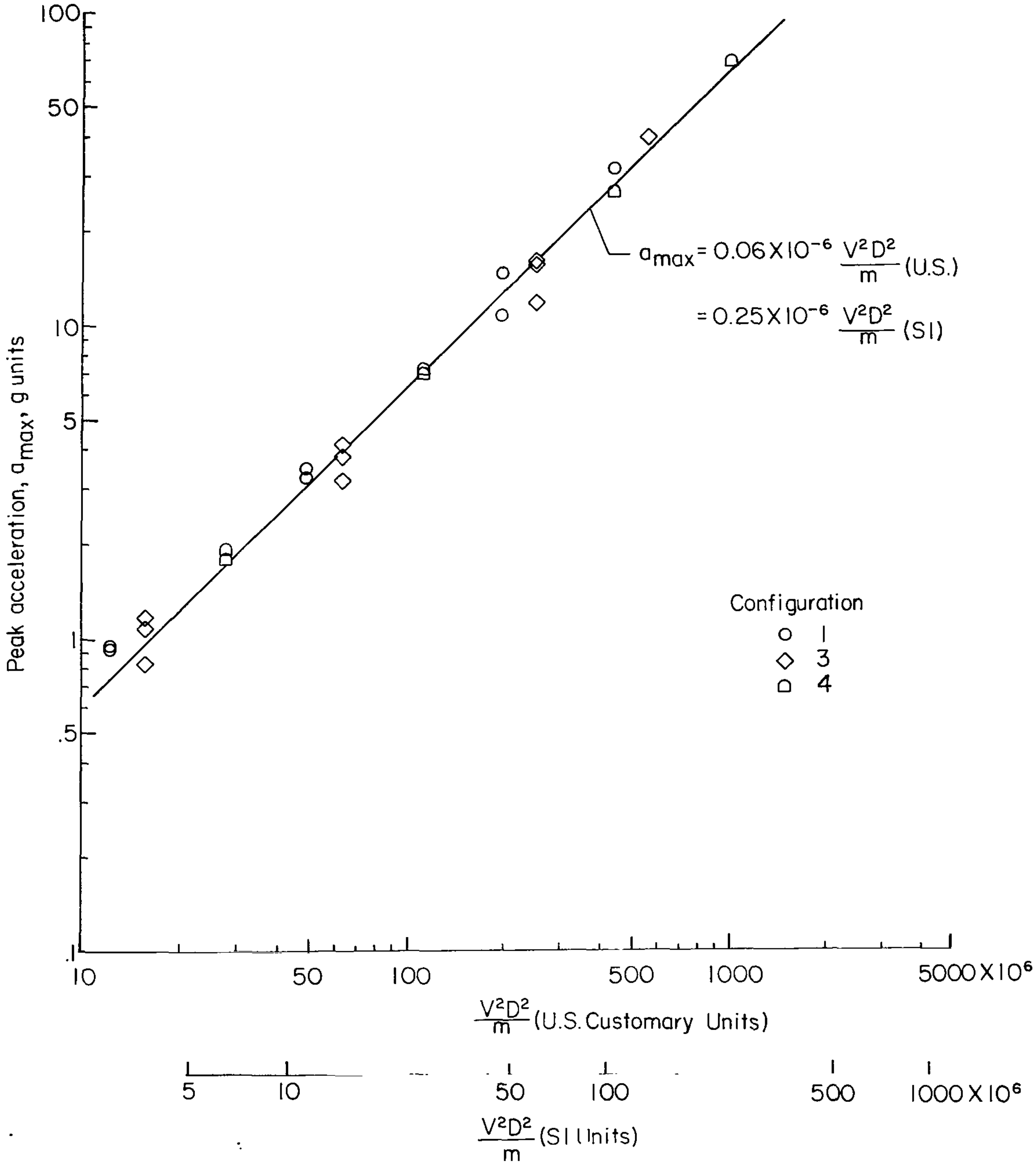

(i) Pumice; l = 68μ; γ = 37 lb/ft^3 (593 kg/m^3).

Figure 10.- Continued.

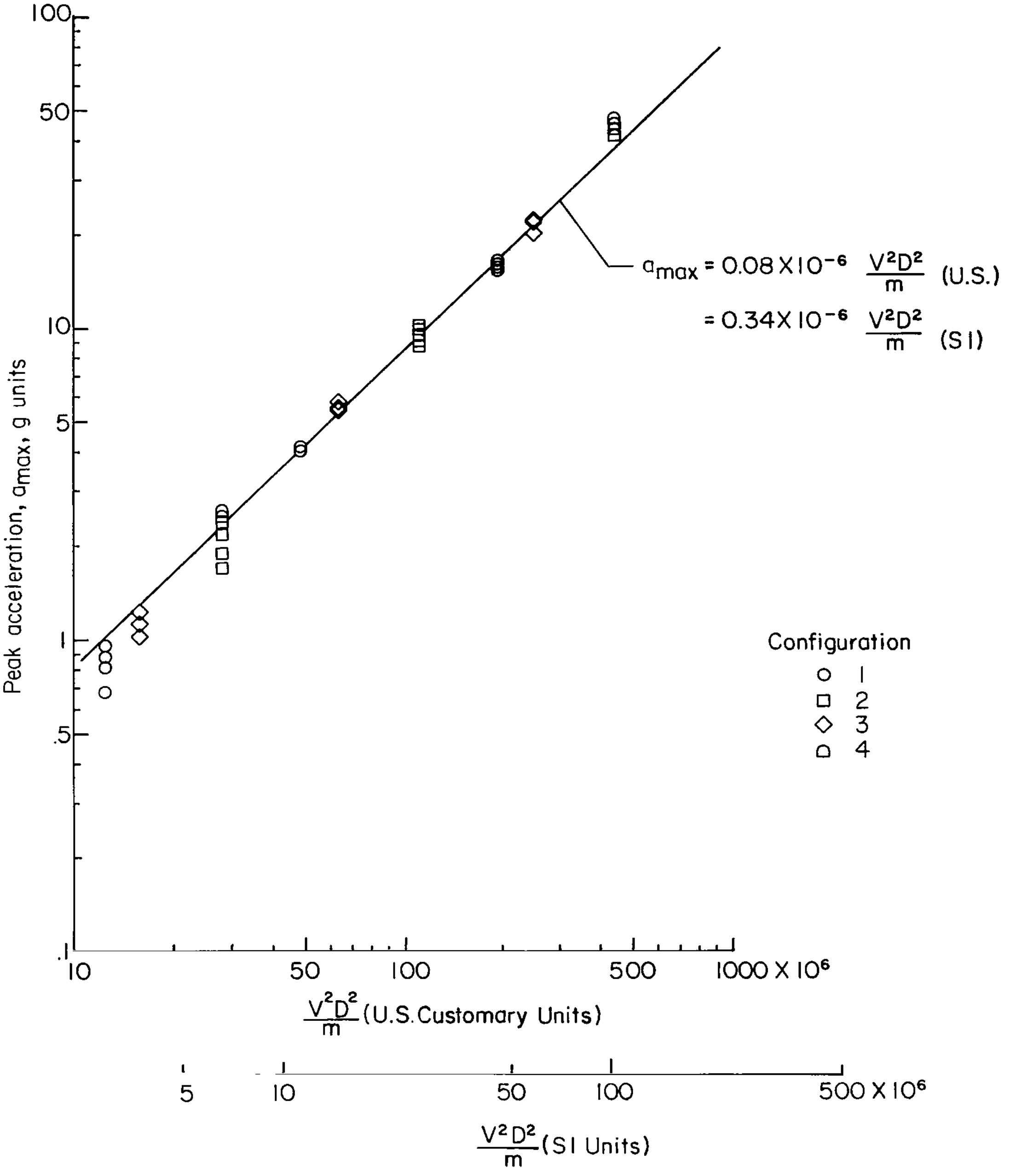

(j) Water.

Figure 10.- Concluded.

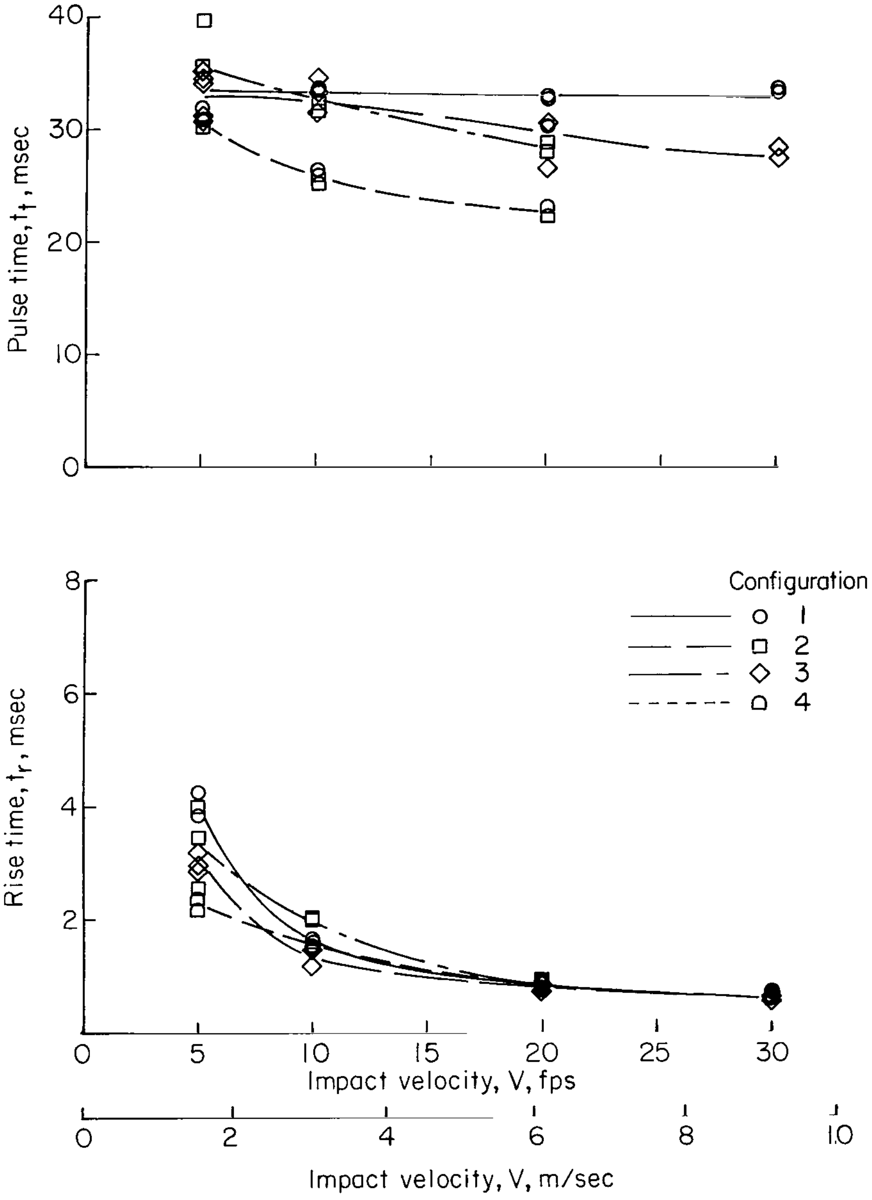

(a) l = 936μ; γ = 116 lb/ft^3 (1858 kg/m^3).

Figure 11.- Characteristic times from acceleration time histories recorded during penetrometer impact tests.

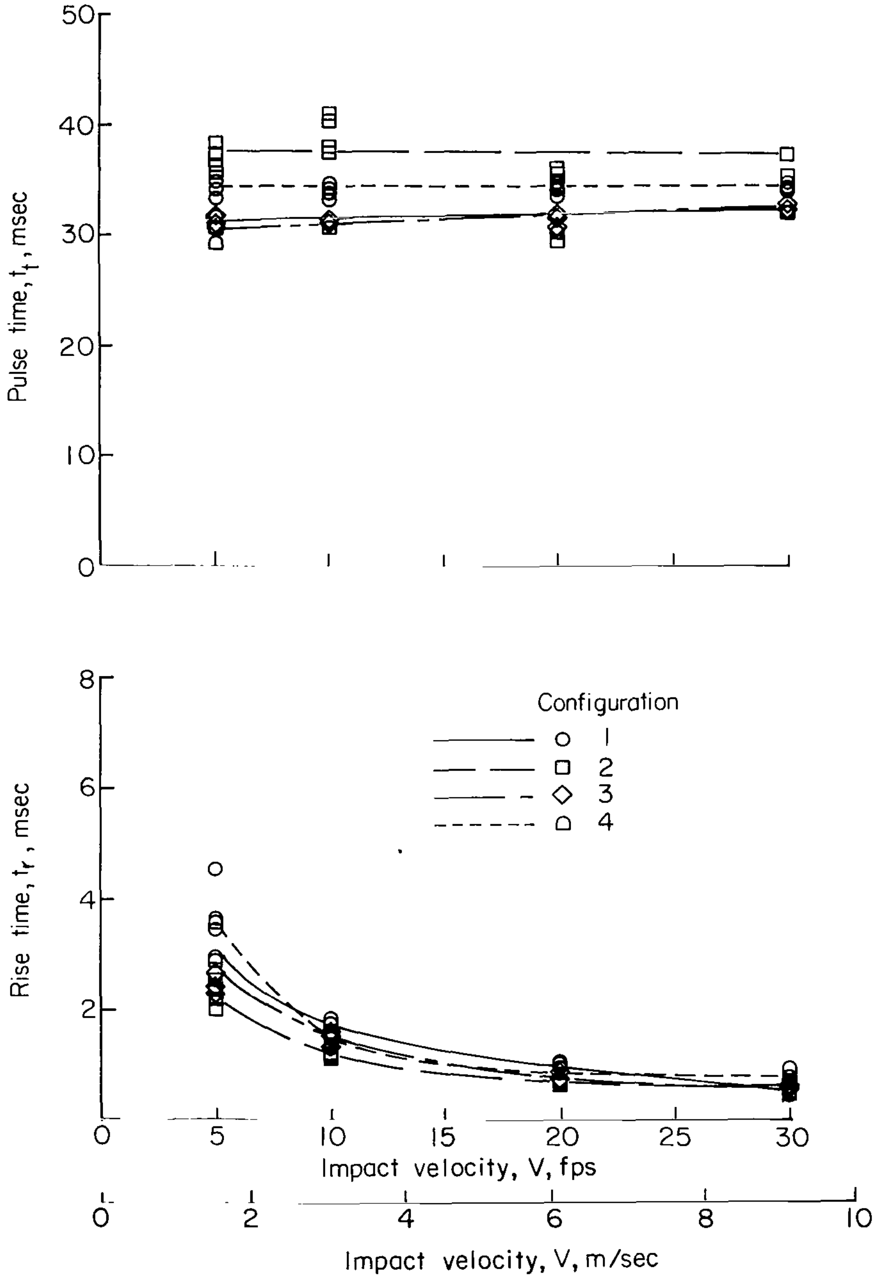

(b) $l = 550\mu$; $\gamma = 119$ lb/ft^3 (1906 kg/m^3).

Figure 11.- Continued.

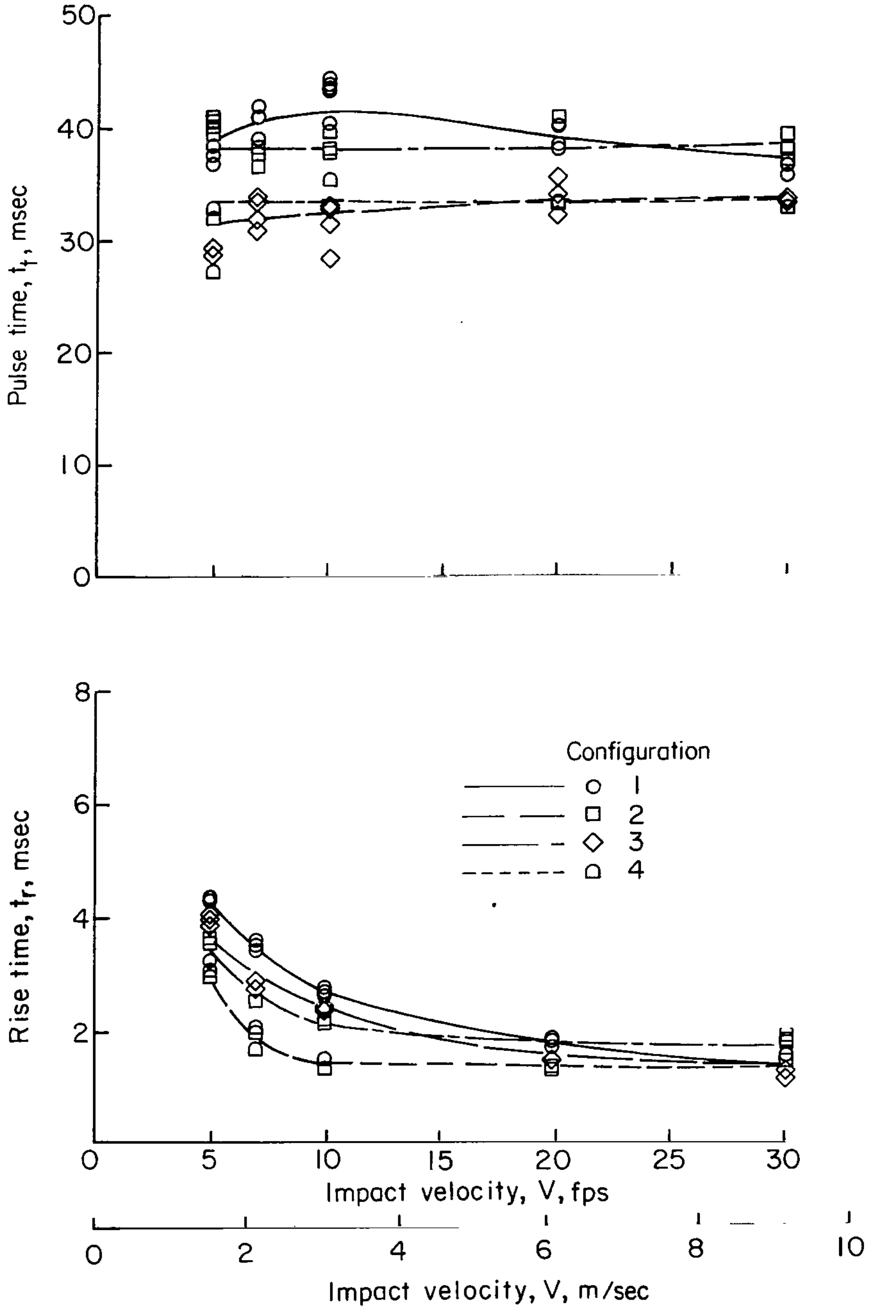

(c) l = 187μ; γ = 120 lb/ft^3 (1922 kg/m^3).

Figure 11.- Continued.

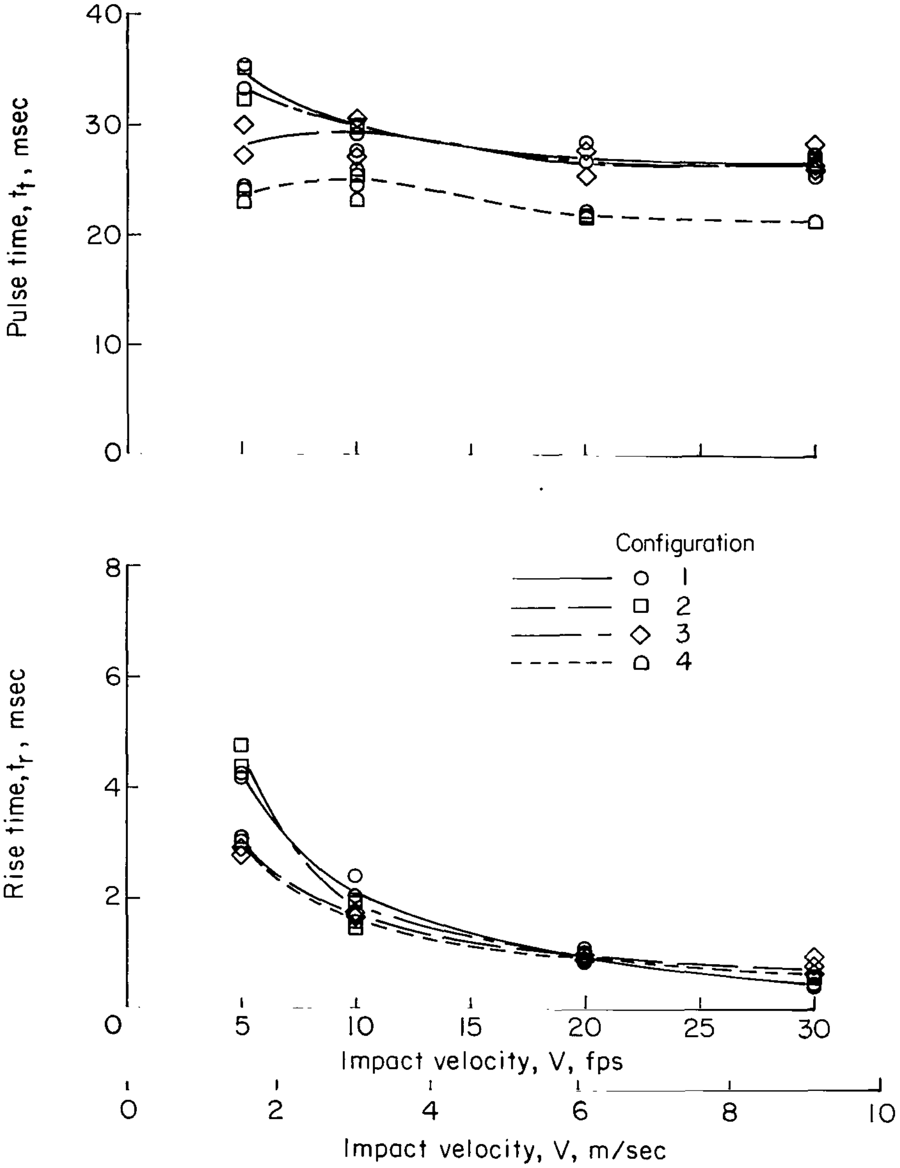

(d) $l = 149\mu$; $\gamma = 114$ lb/ft^3 (1826 kg/m^3).

Figure 11.- Continued.

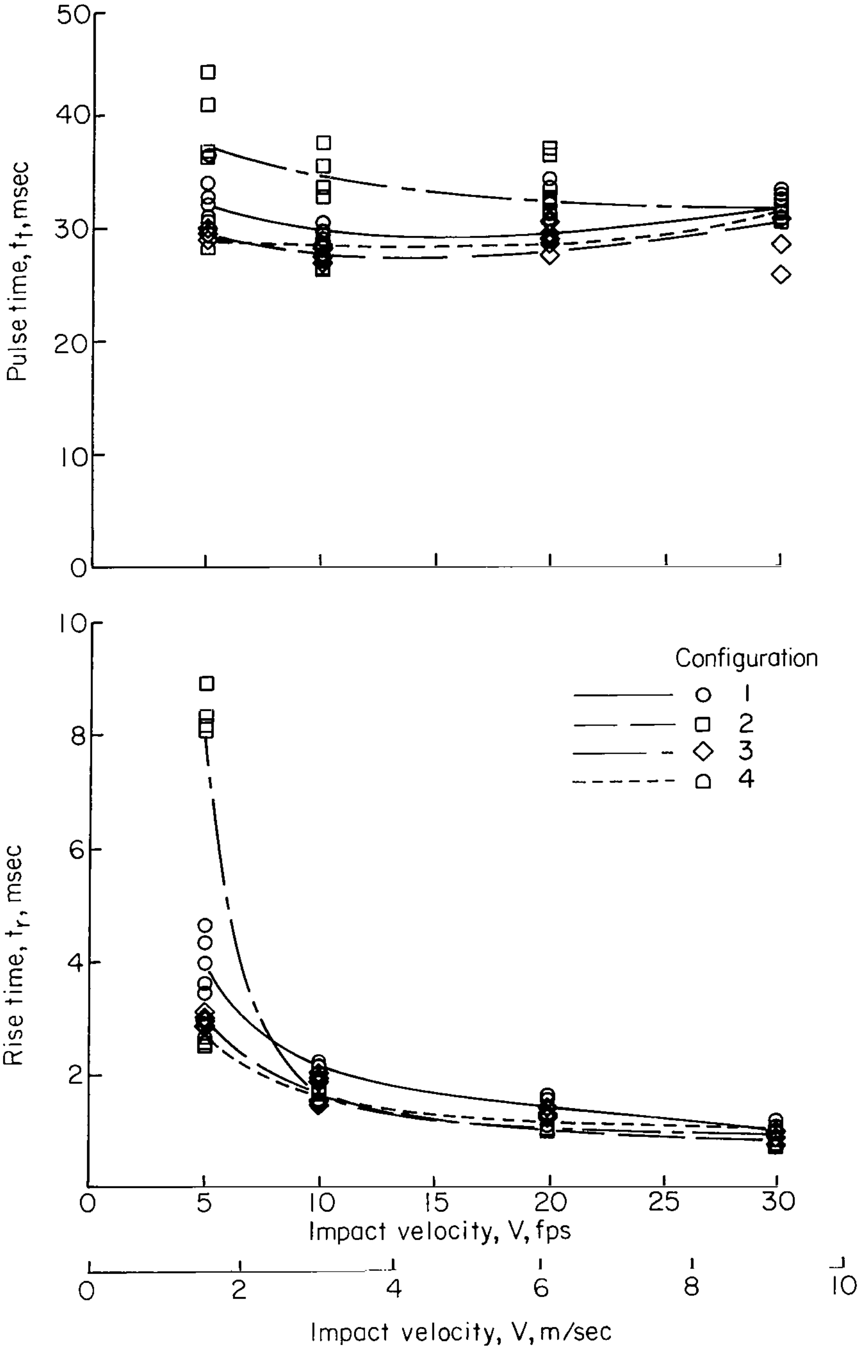

(e) $l = 75\mu$; $\gamma = 112$ lb/ft^3 (1794 kg/m^3).

Figure 11.- Continued.

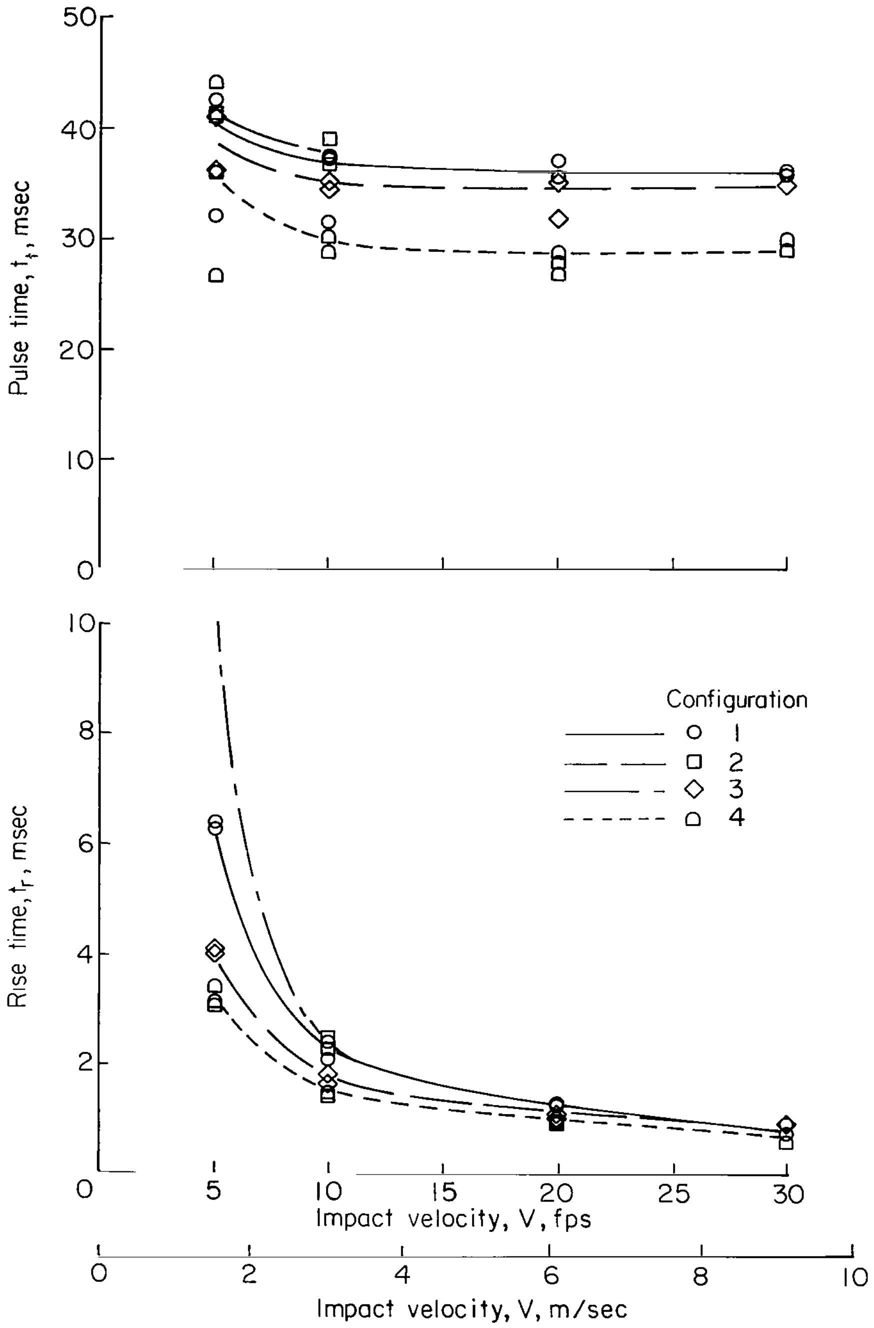

(f) $l = 65\mu$; $\gamma = 107$ lb/ft^3 (1714 kg/m^3).

Figure 11.- Continued.

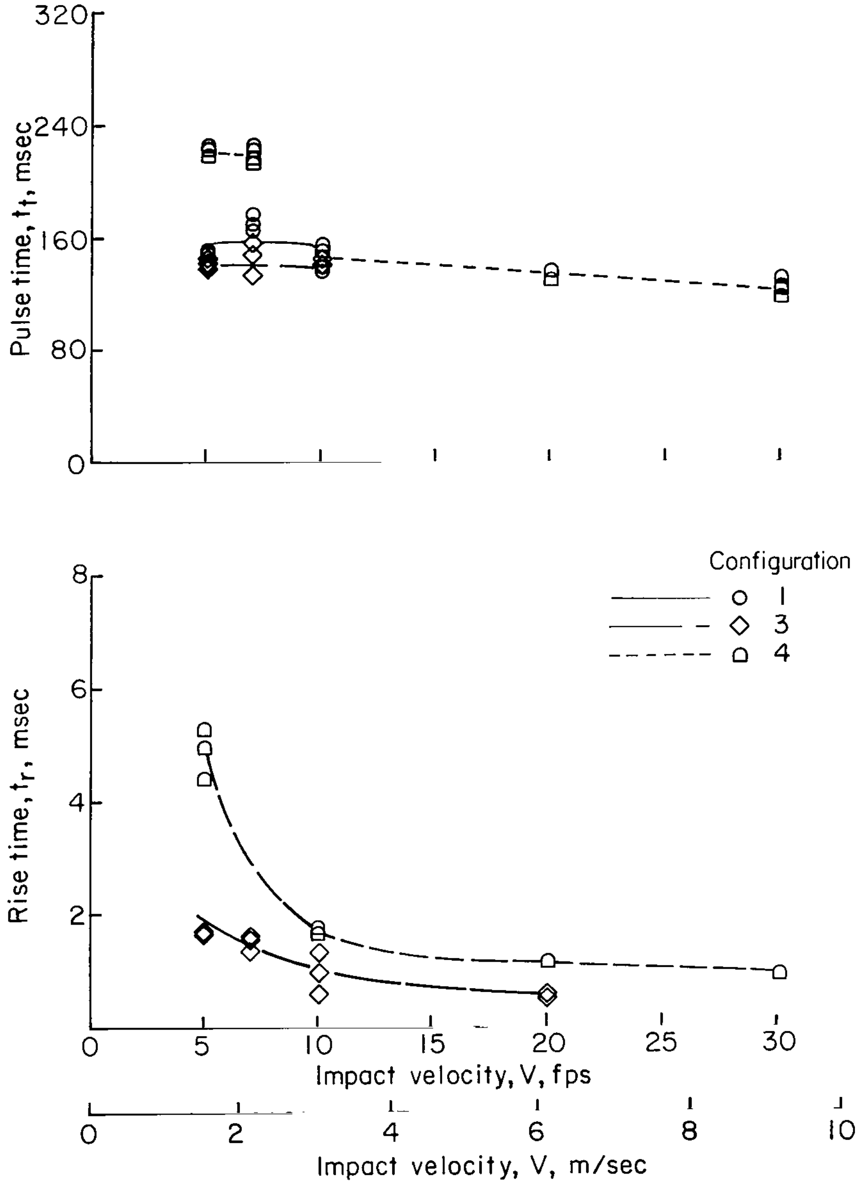

(g) $l = 27\mu$; $\gamma = 93$ lb/ft^3 (1490 kg/m^3).

Figure 11.- Continued.

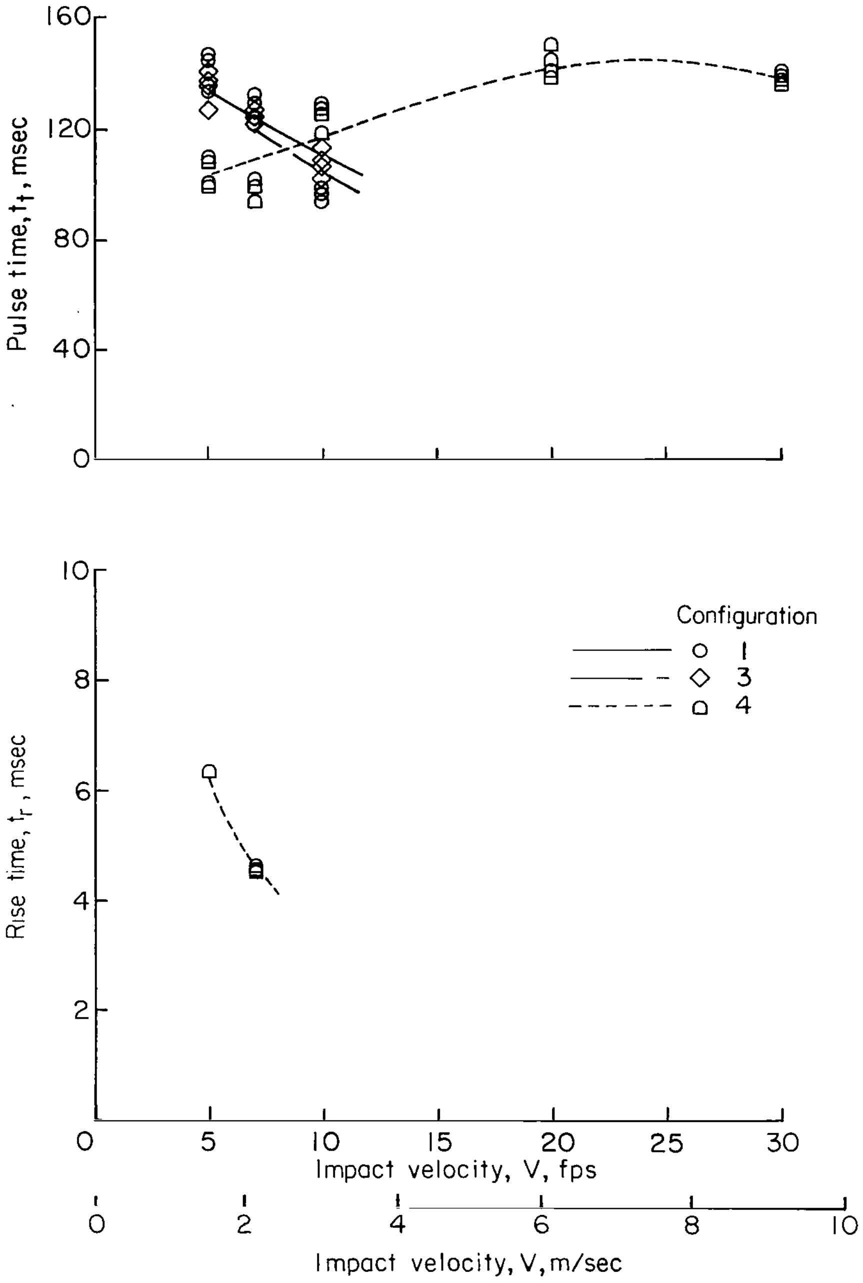

(h) $l = 5\mu$; $\gamma = 73$ lb/ft^3 (1169 kg/m^3).

Figure 11.- Continued.

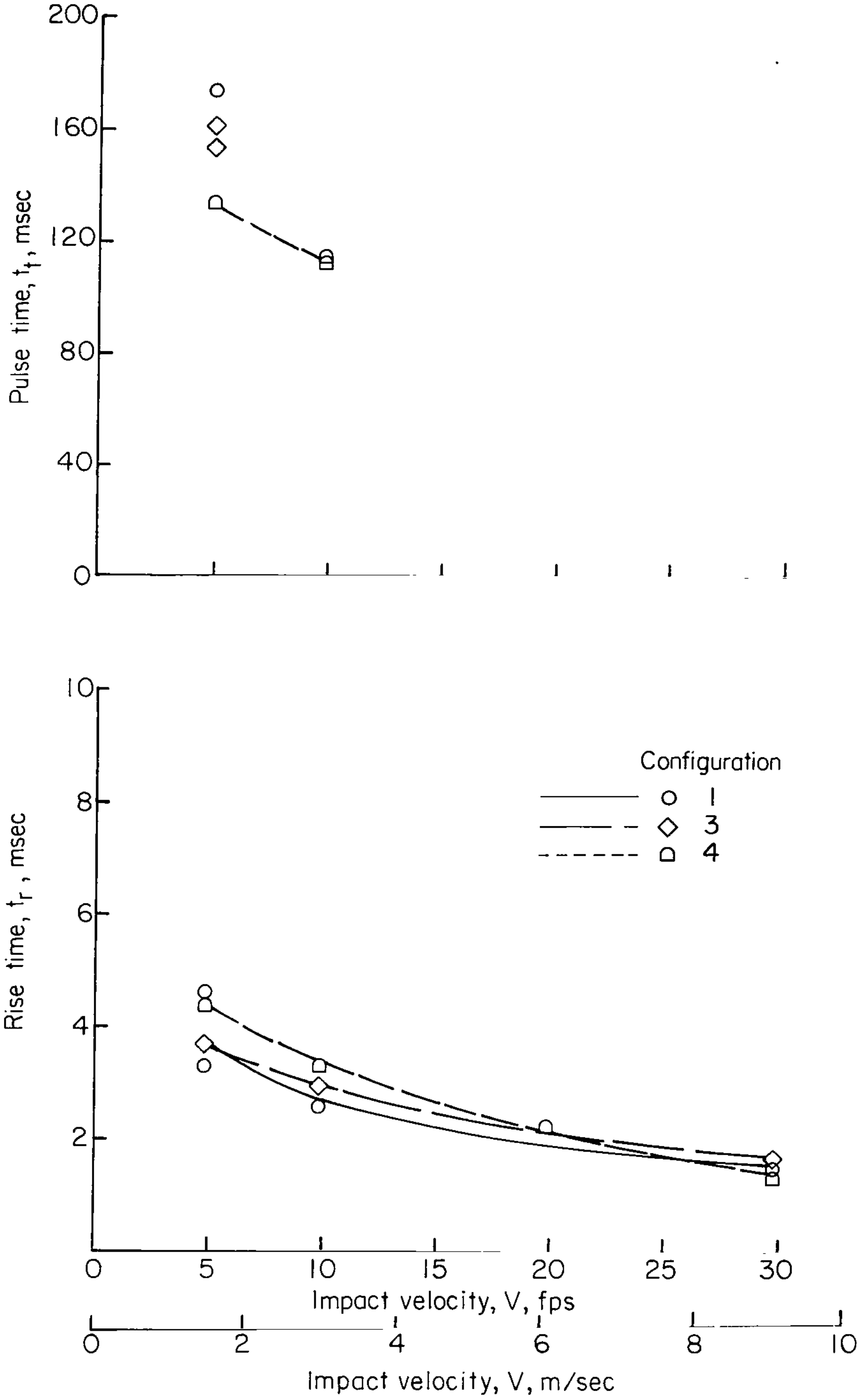

(i) Pumice; l = 68μ; γ = 37 lb/ft^3 (593 kg/m^3).

Figure 11.- Continued.

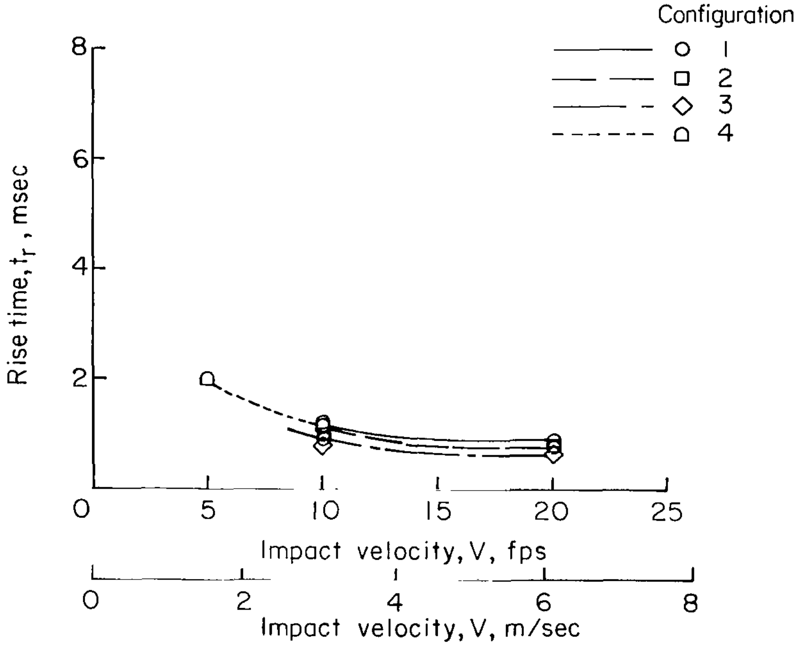

(j) Water.

Figure 11.- Concluded.

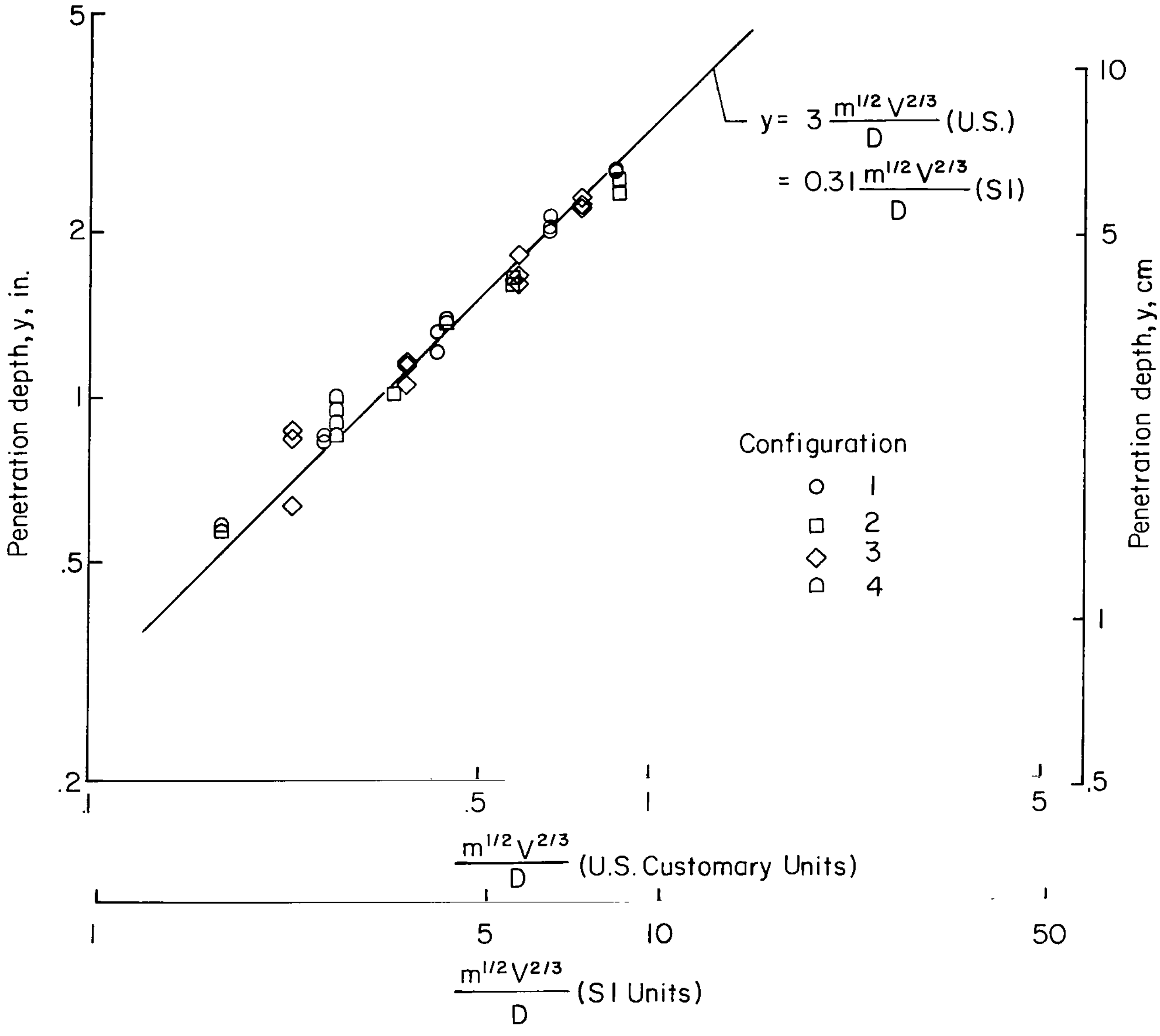

(a) $l = 936\mu$; $\gamma = 116$ lb/ft^3 (1858 kg/m^3).

Figure 12.- Summary of penetration data from penetrometer impact tests.

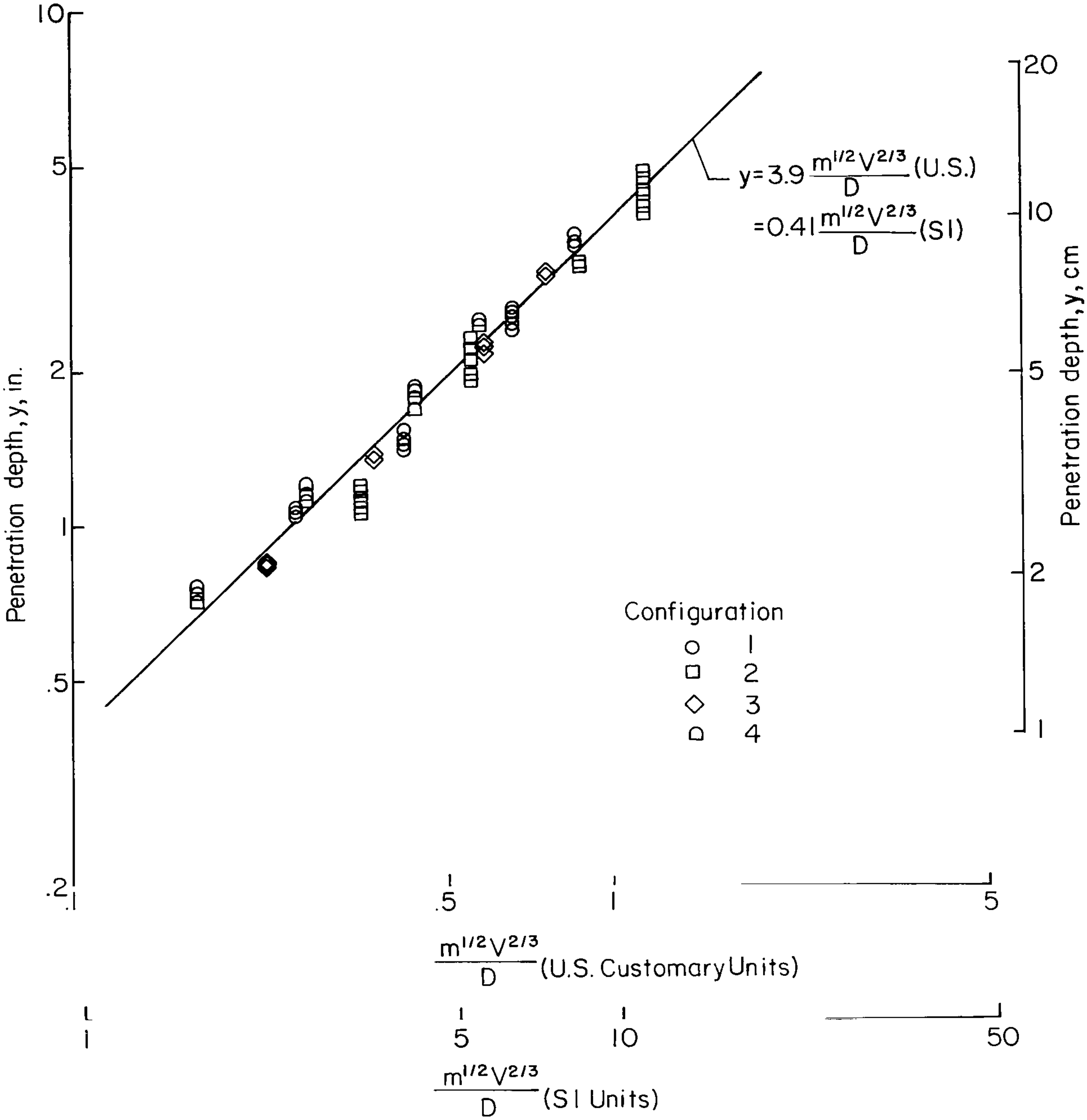

(b) l = 550μ; γ = 119 lb/ft^3 (1906 kg/m^3).

Figure 12.- Continued.

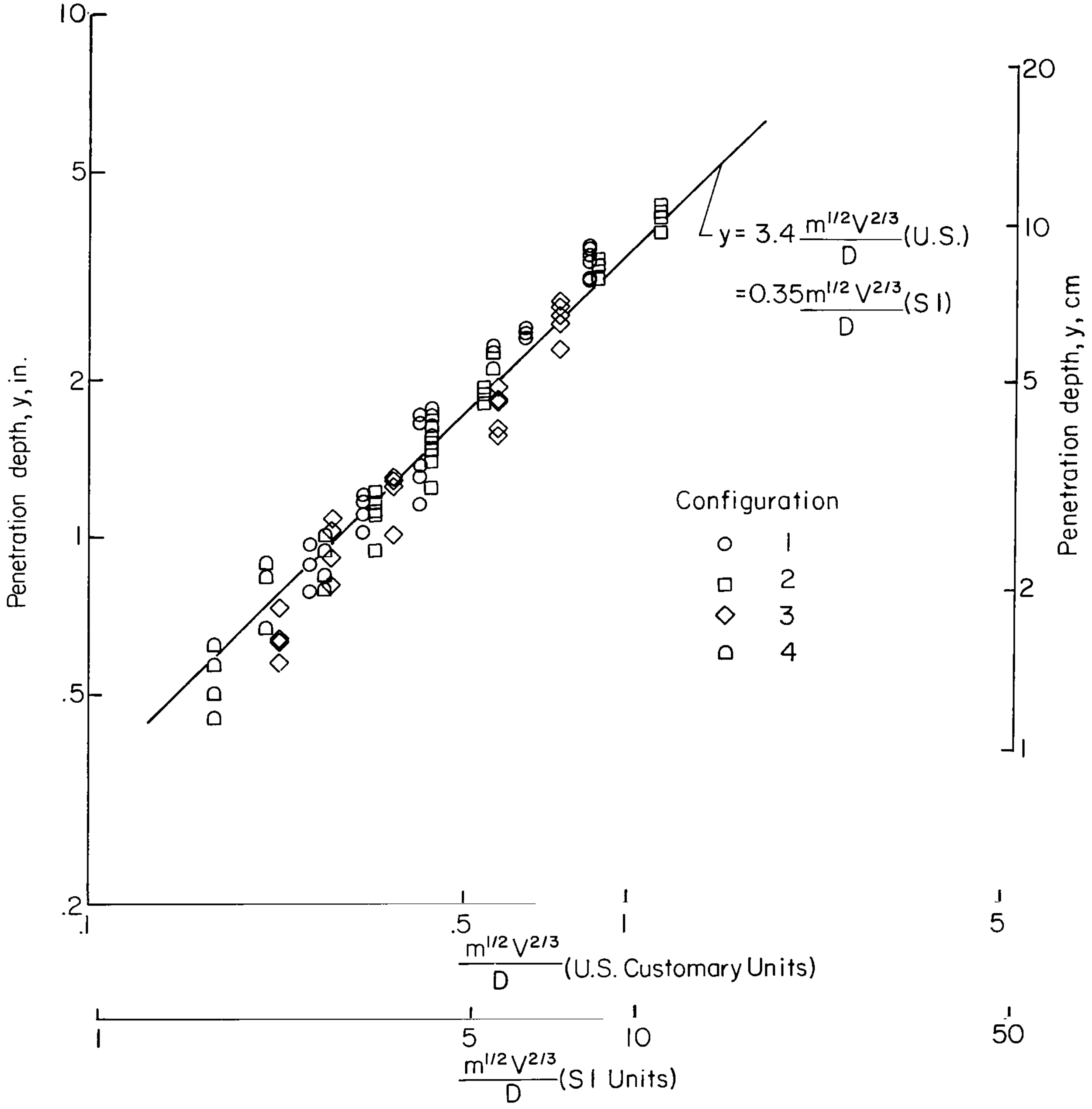

(c) l = 187μ; γ = 120 lb/ft^3 (1922 kg/m^3).

Figure 12.- Continued.

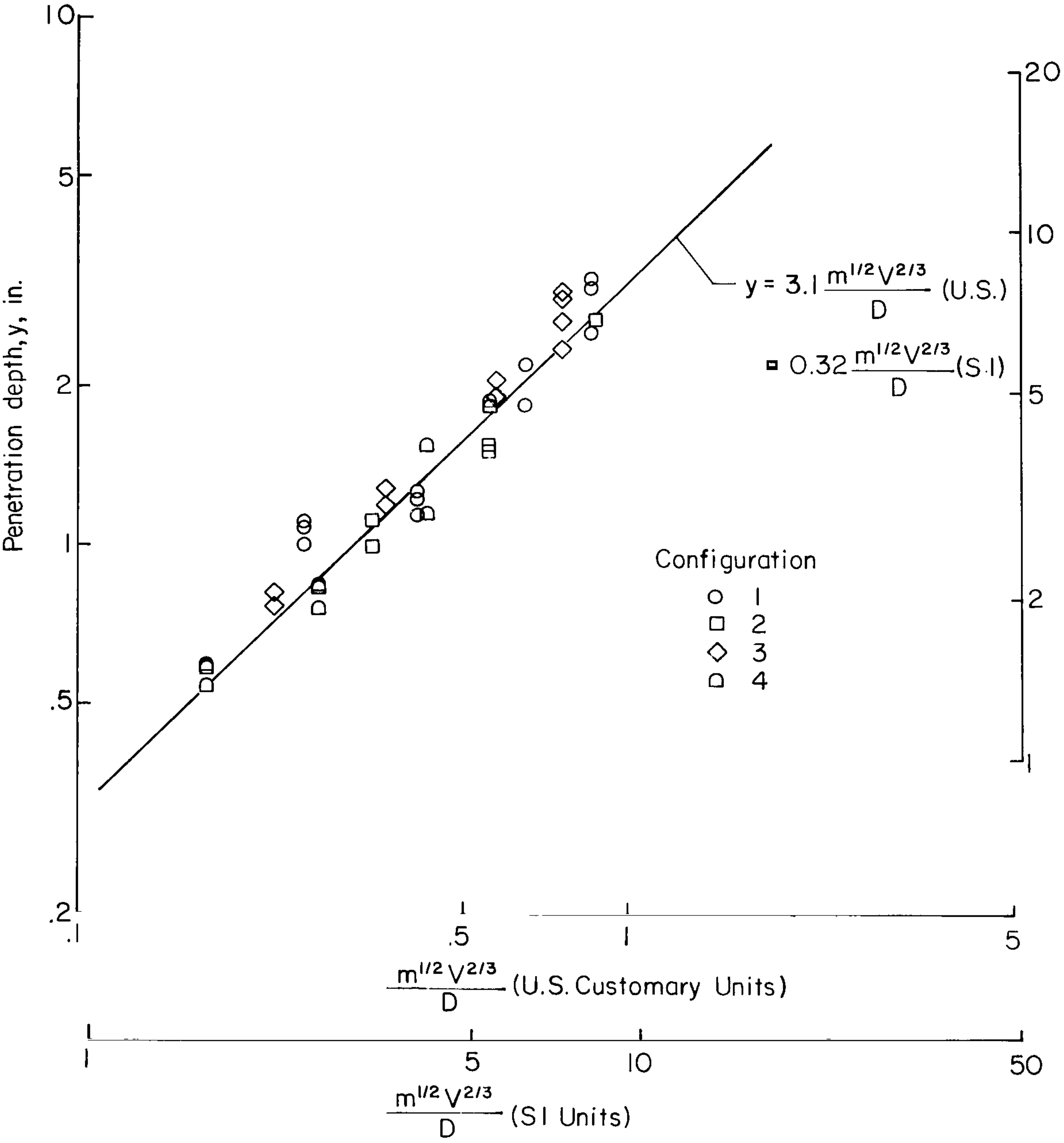

(d) l = 149μ; γ = 114 lb/ft^3 (1826 kg/m^3).

Figure 12.- Continued.

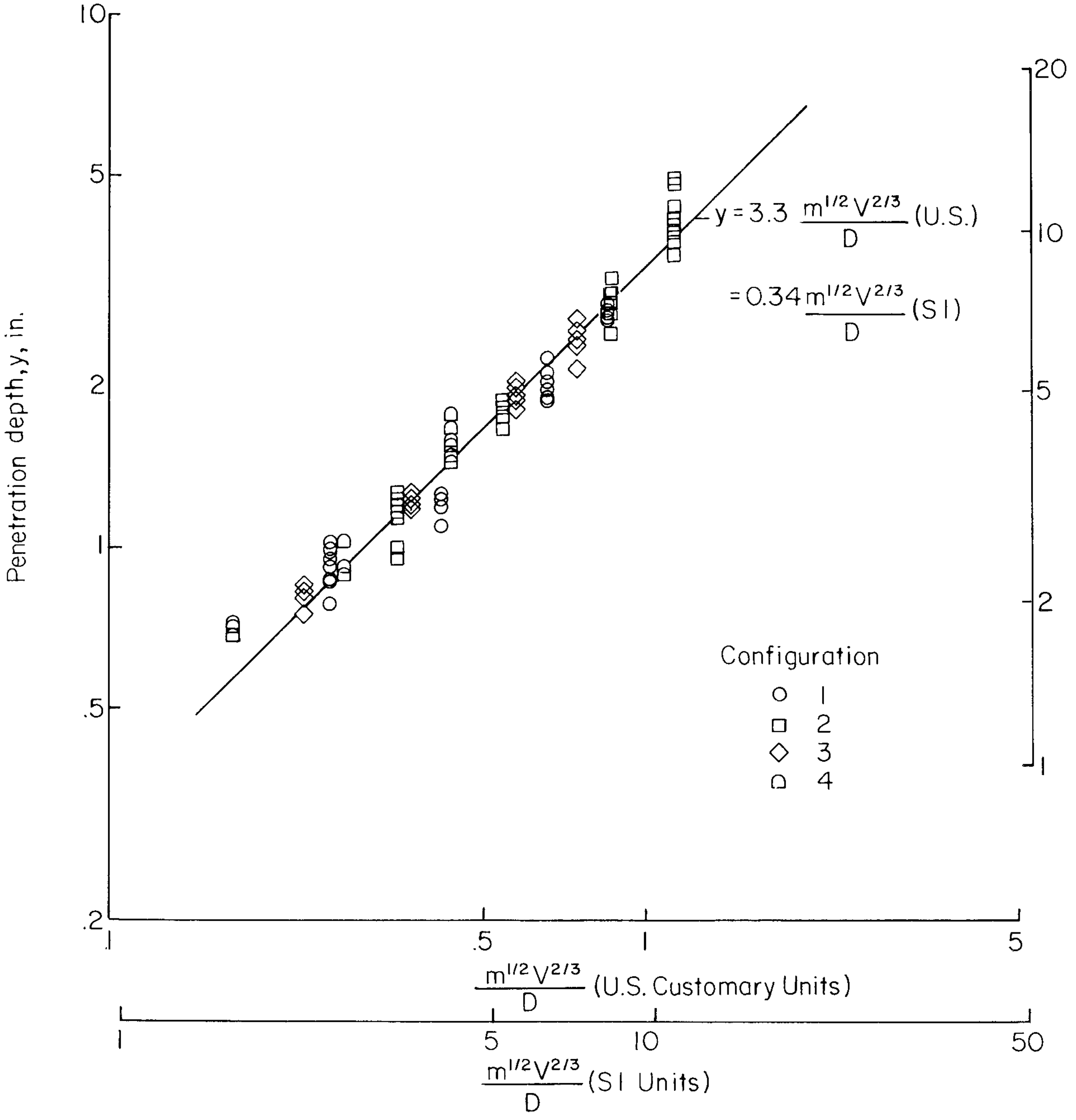

(e) l = 75μ; γ = 112 lb/ft^3 (1794 kg/m^3).

Figure 12.- Continued.

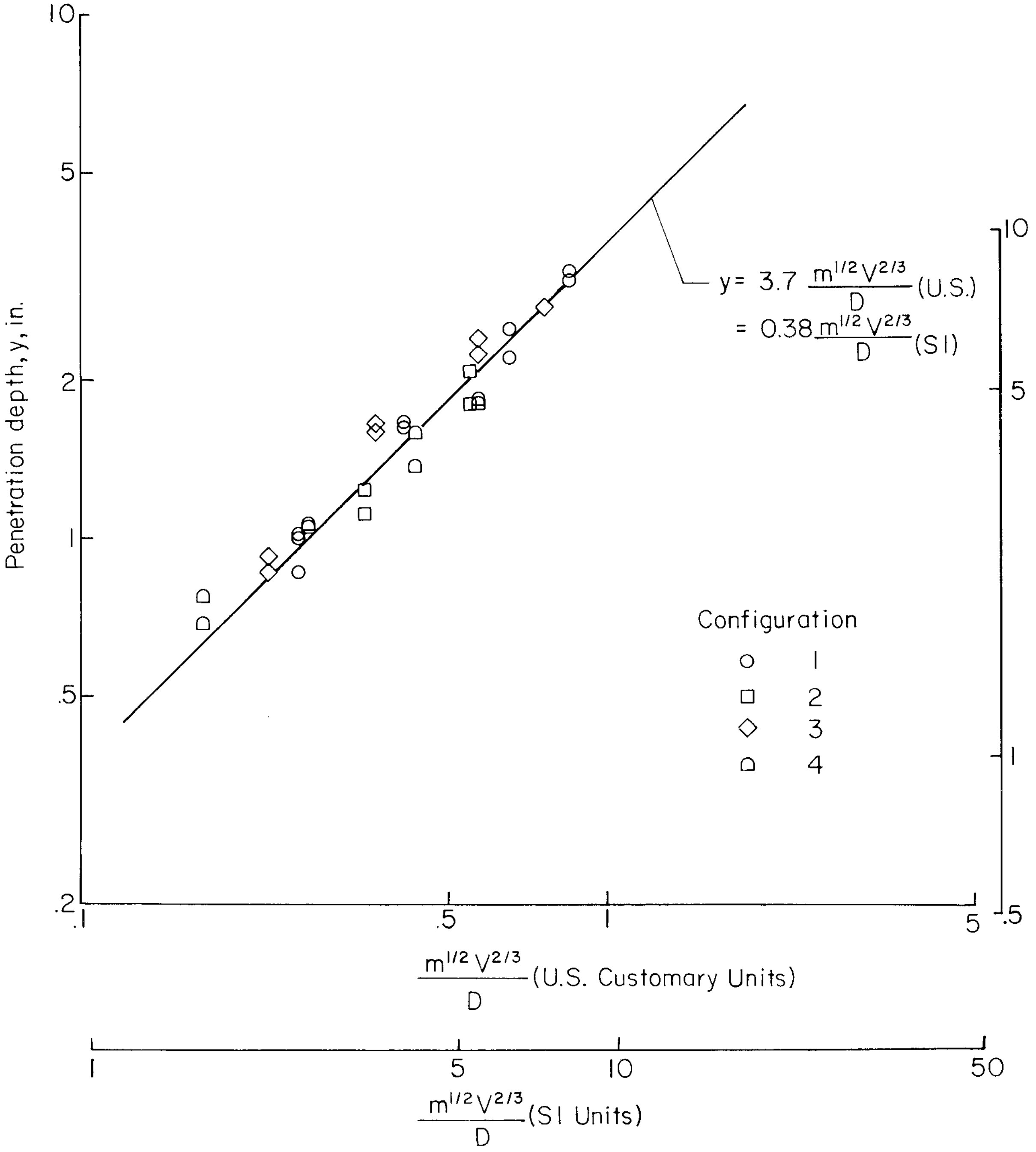

(f) l = 65μ; γ = 107 lb/ft^3 (1714 kg/m^3).

Figure 12.- Continued.

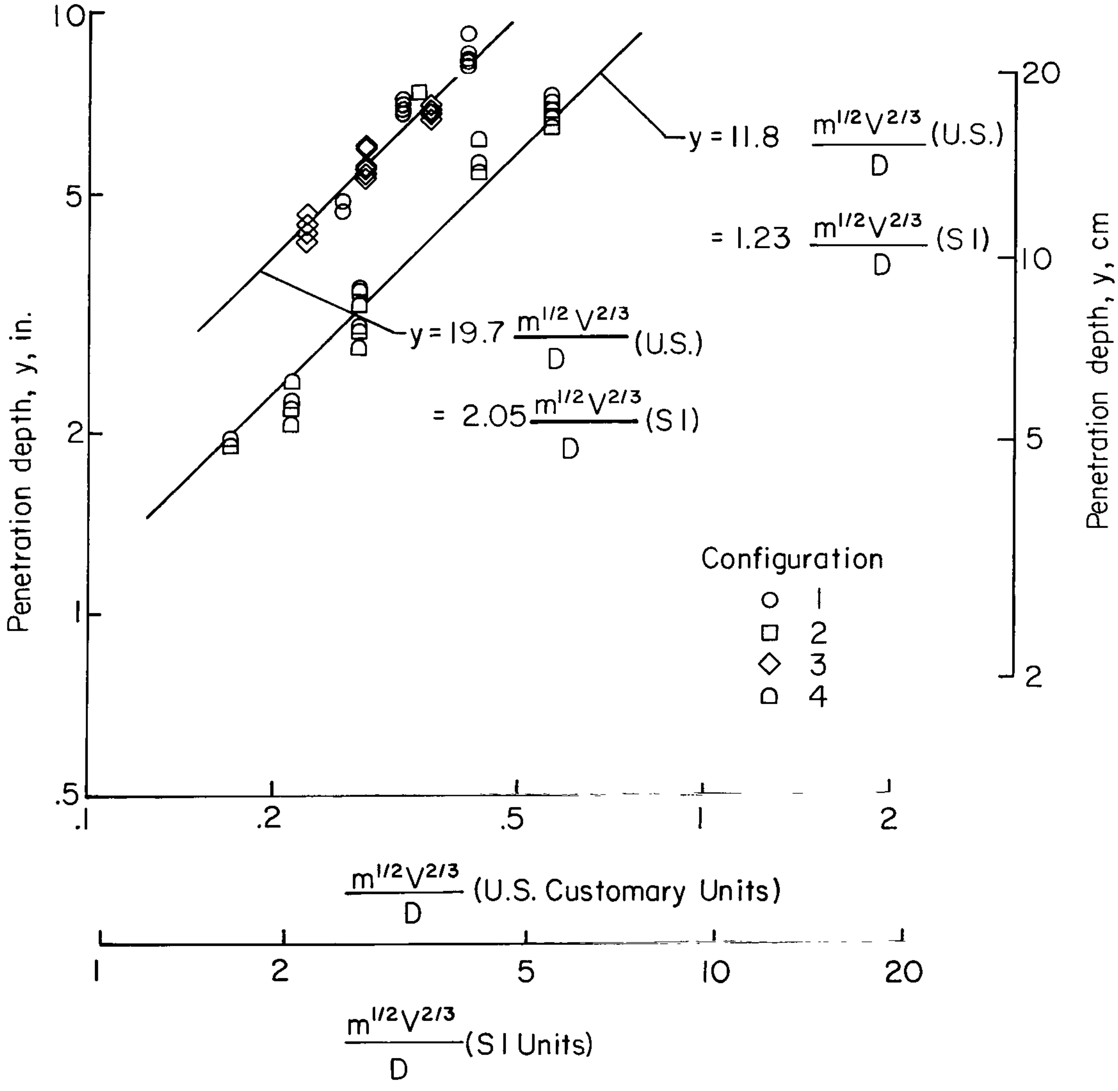

(g) l = 27μ; γ = 93 lb/ft^3 (1490 kg/m^3).

Figure 12.- Continued.

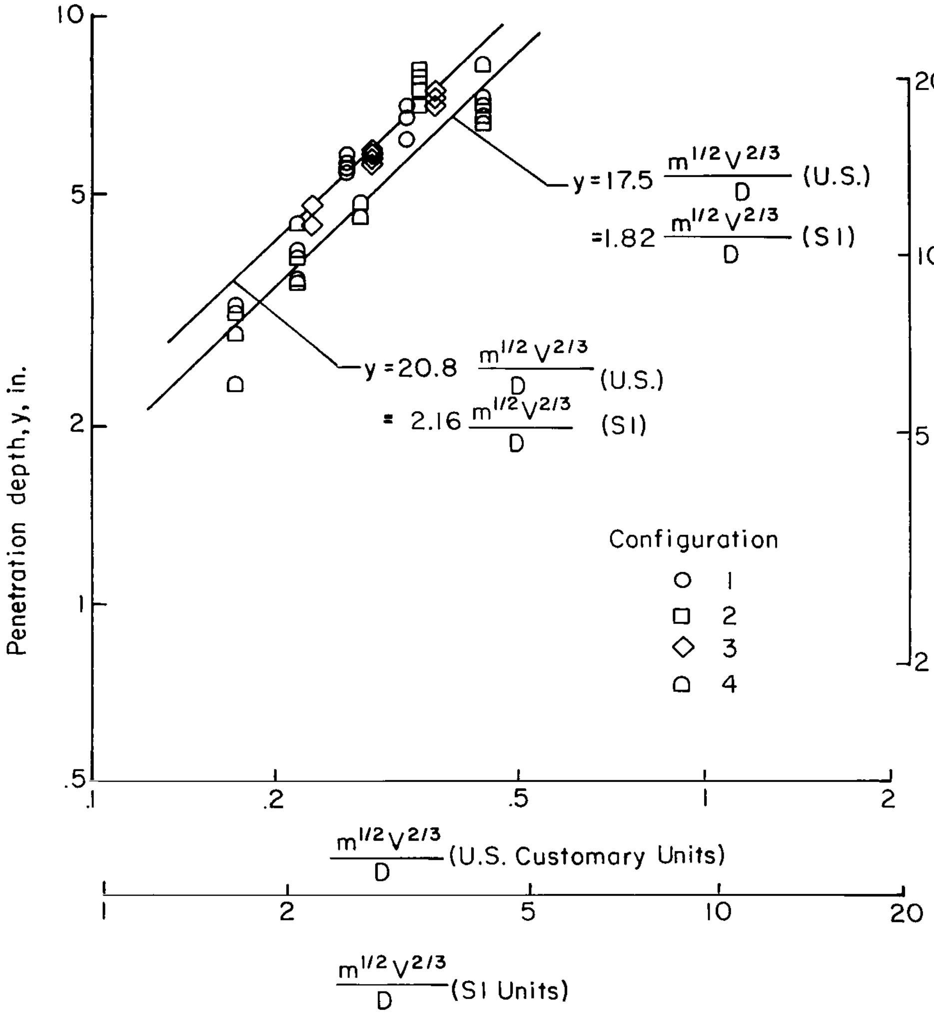

(h) $l = 5\mu$; $\gamma = 73$ lb/ft^3 (1169 kg/m^3).

Figure 12.- Continued.

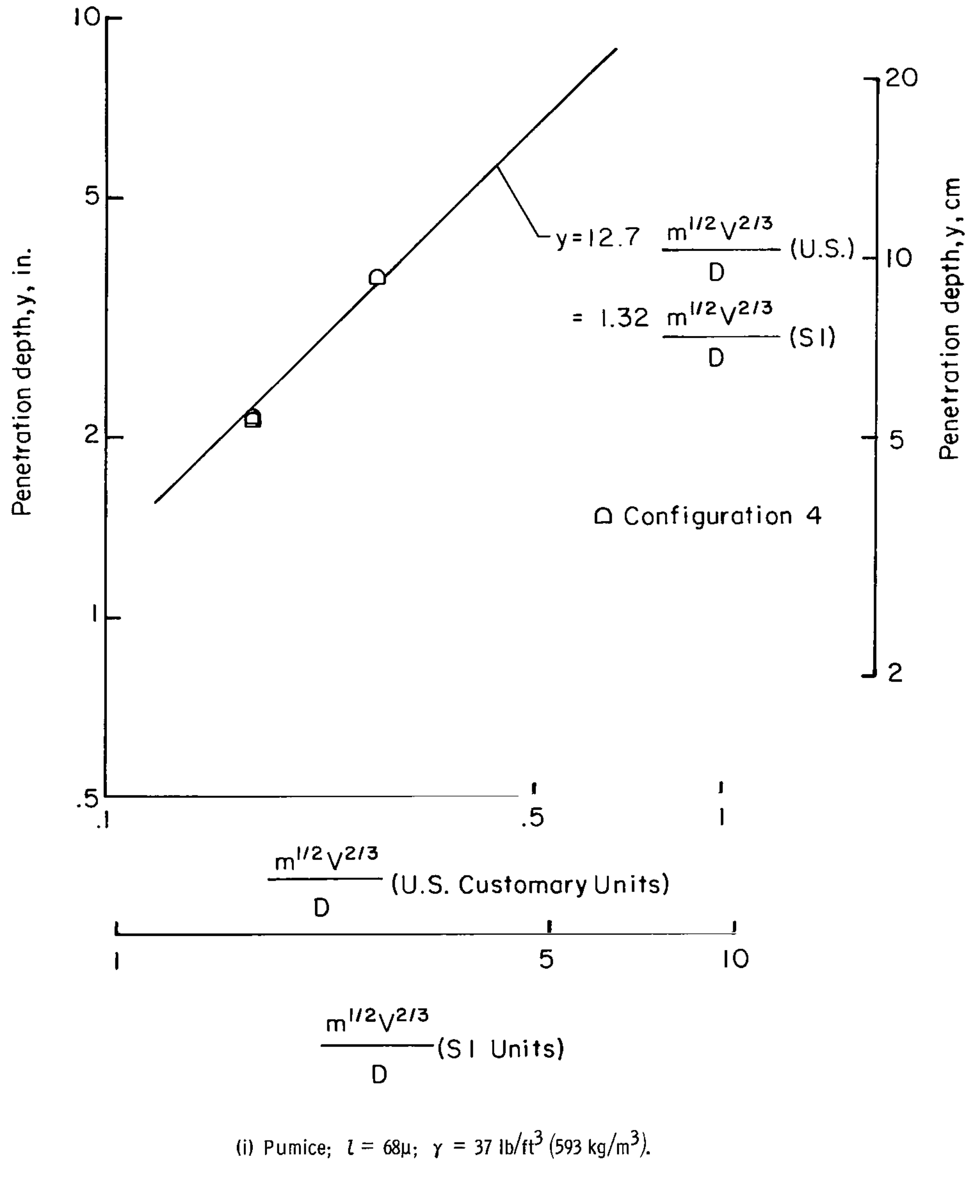

(i) Pumice; l = 68μ; γ = 37 lb/ft^3 (593 kg/m^3).

Figure 12.- Concluded.

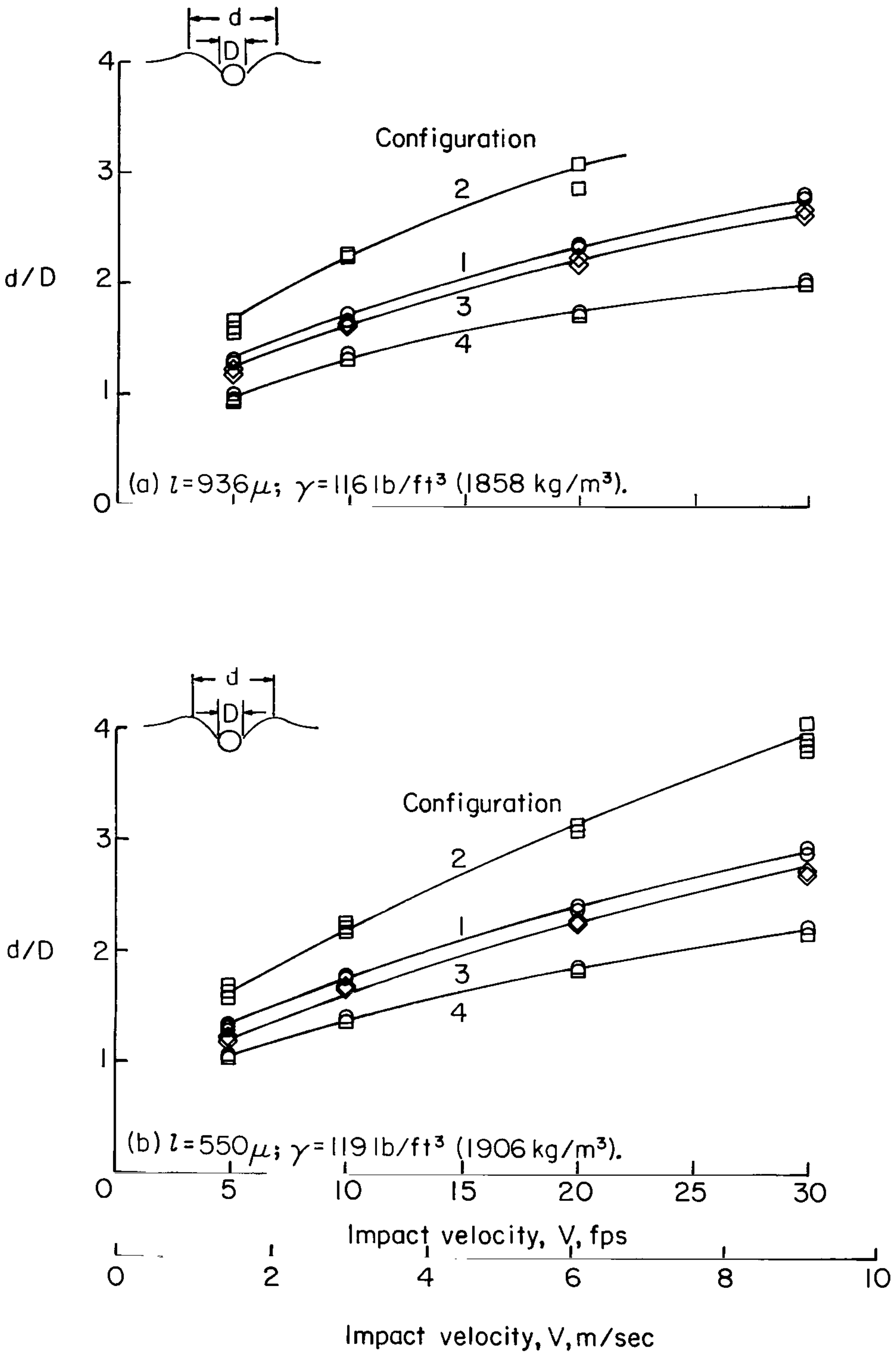

Figure 13.- Summary of blast crater data from penetrometer impact tests.

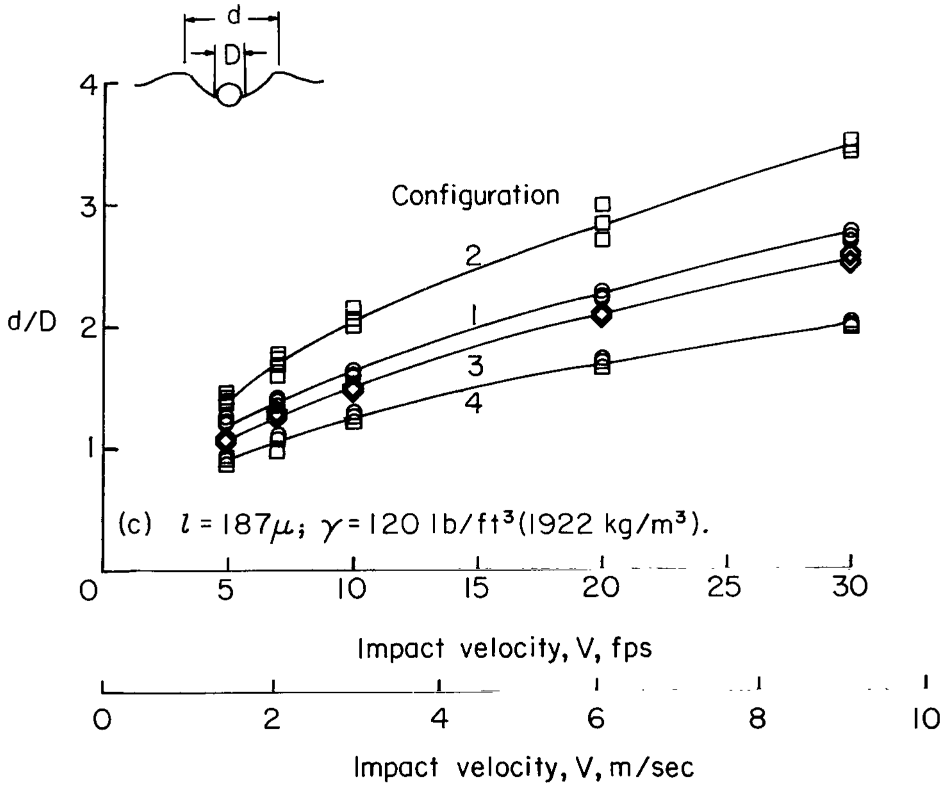

Figure 13.- Concluded.

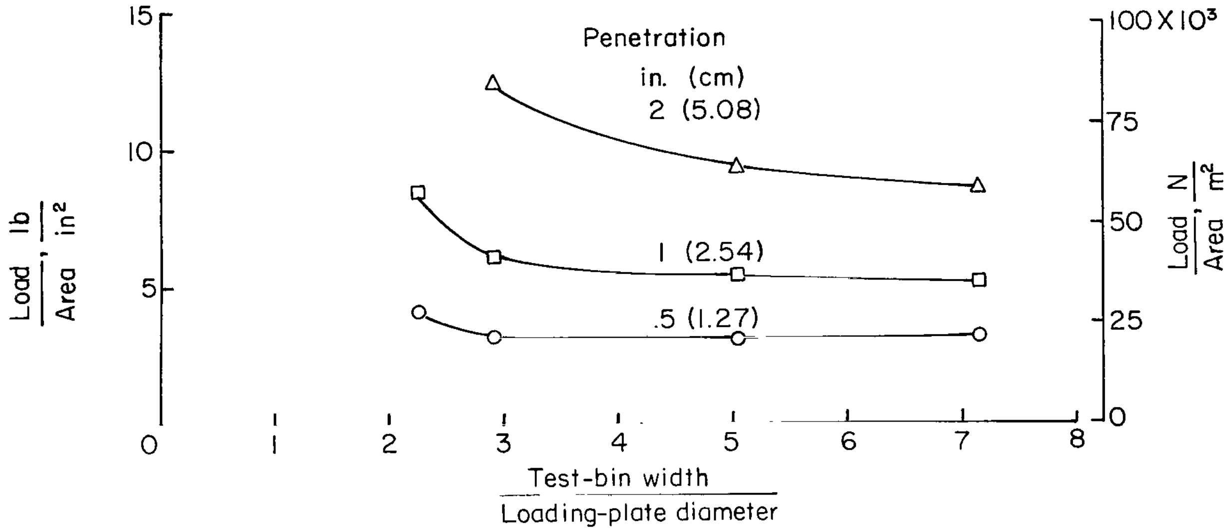

(a) Fixed test-bin width of 18 in. (45.72 cm); varying loading-plate diameter.

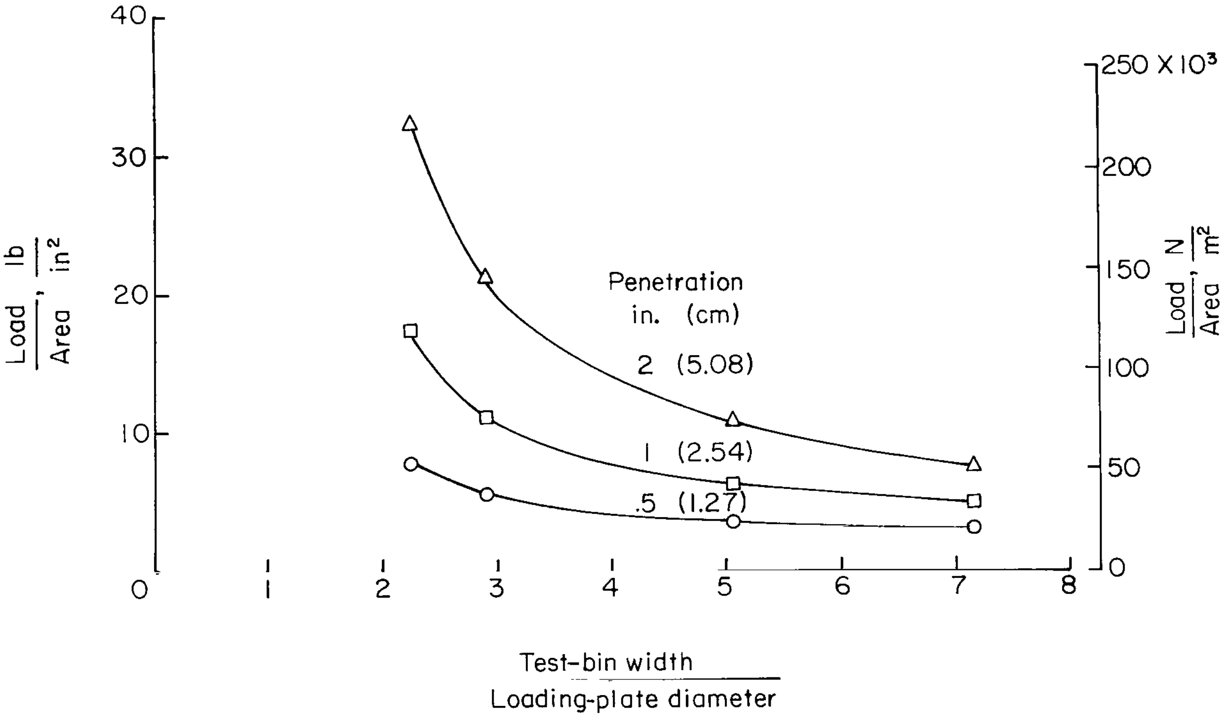

(b) Fixed loading-plate diameter of 2.52 in. (6.40 cm); varying test-bin width.

Figure 14.- Effect of test-bin size on bearing-strength measurements. l = 187μ.

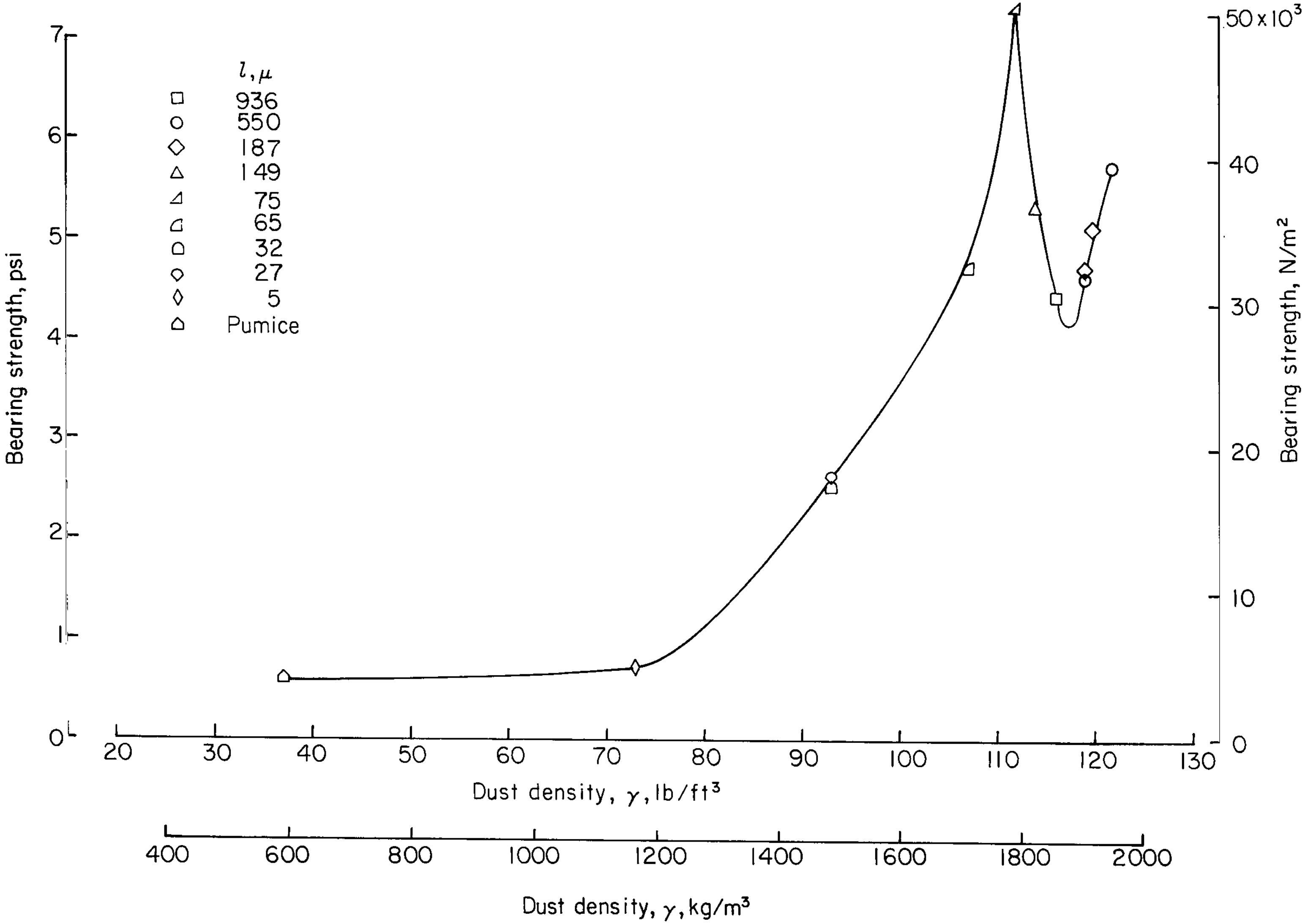

Figure 15.- Variation of bearing strength with dust density.

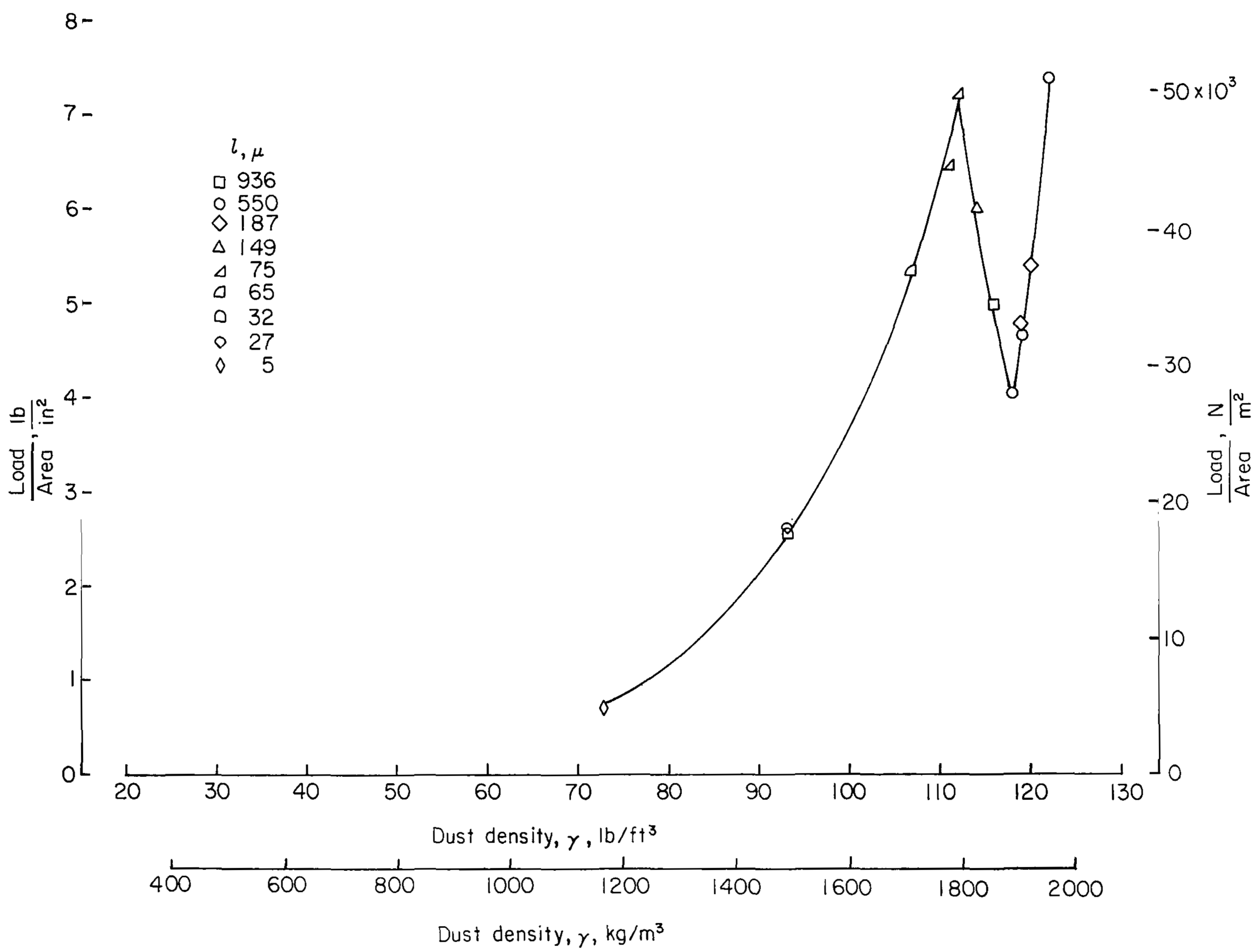

Figure 16.- Load per unit area as function of dust density for 10 in^2 (64.52 cm^2) plate at 1-in. (2.54 cm) penetration.

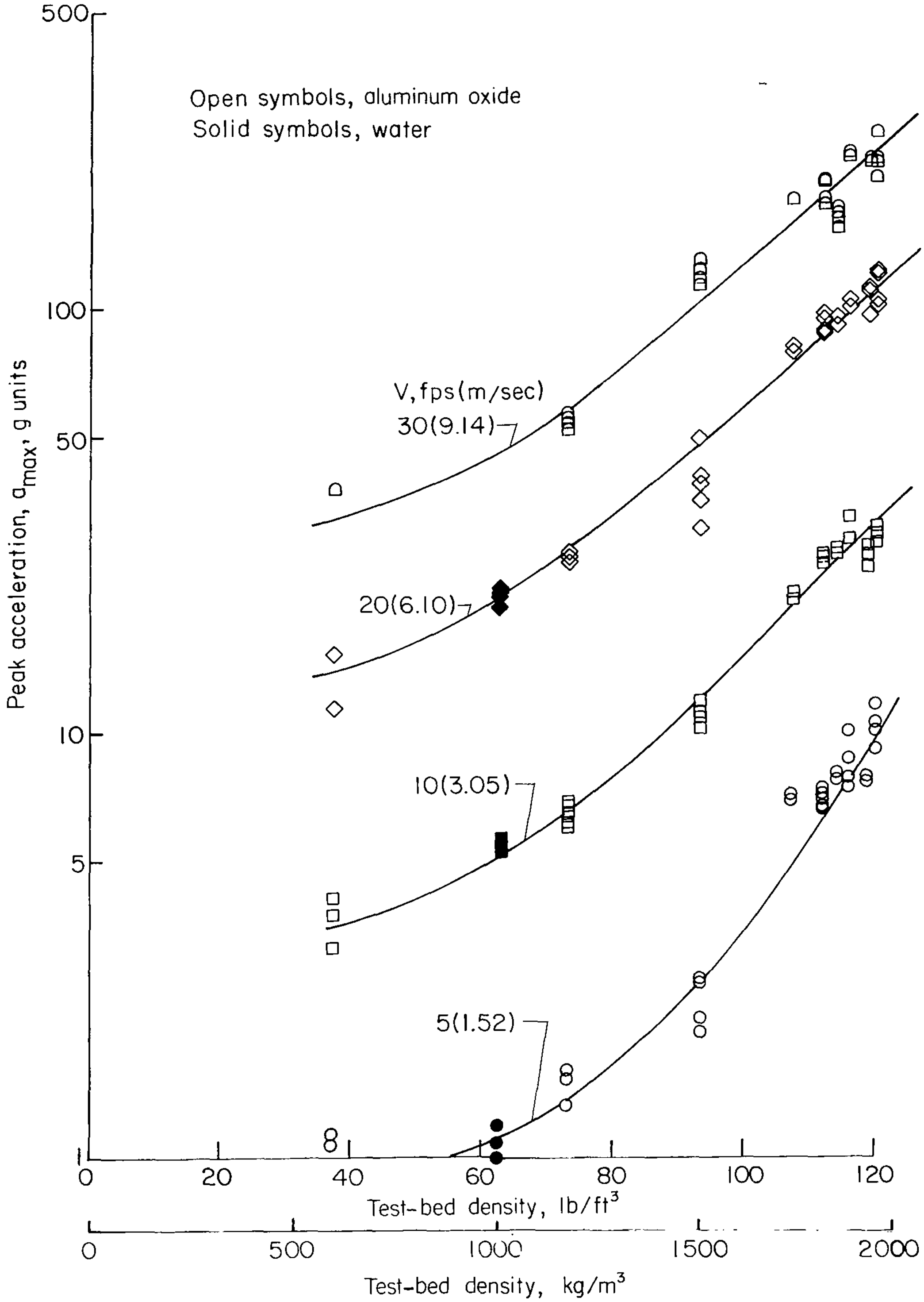

Figure 17.- Variation of peak impact accelerations with test-bed density for configuration 3.

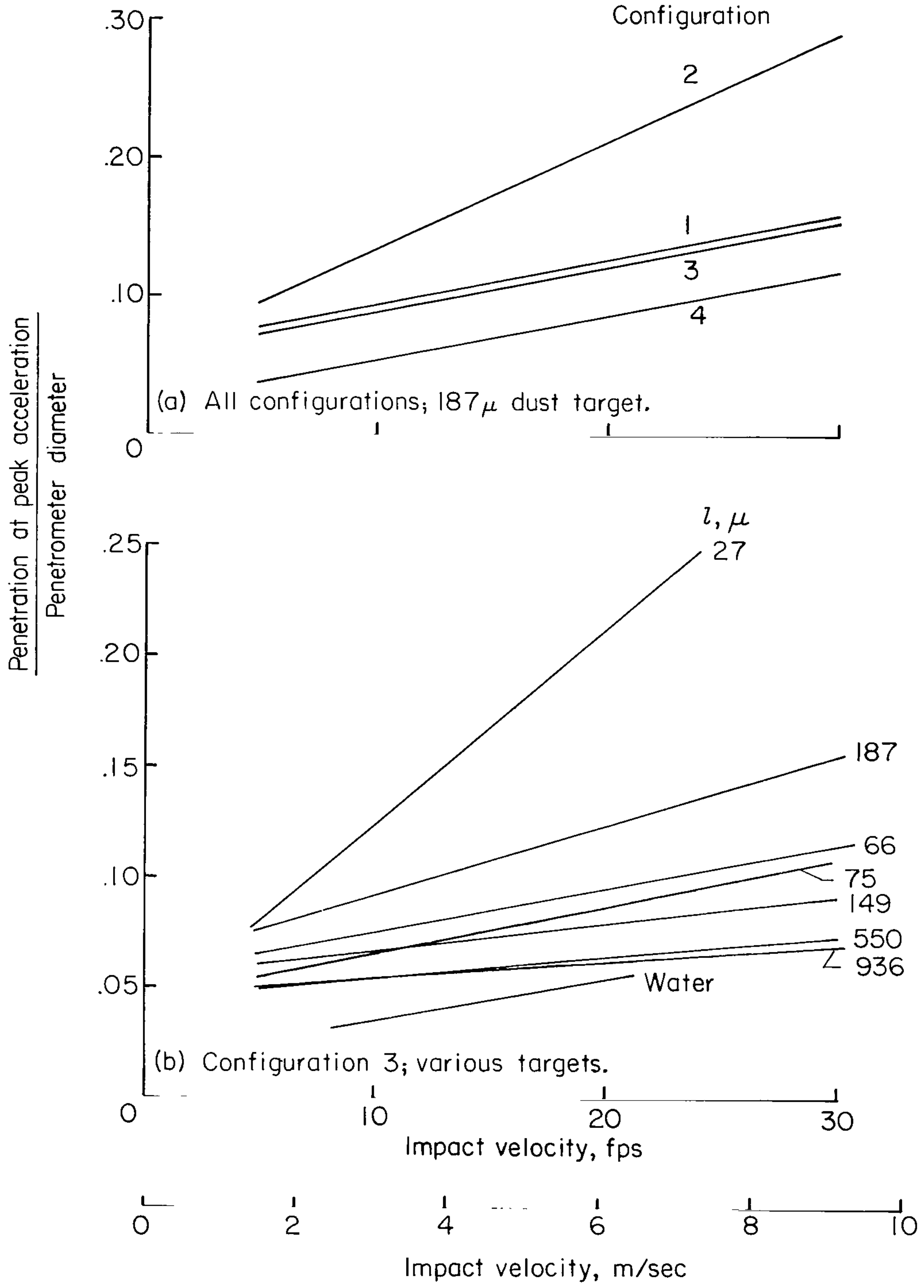

Figure 18.- Depth of penetrometer penetration at time of peak impact acceleration.

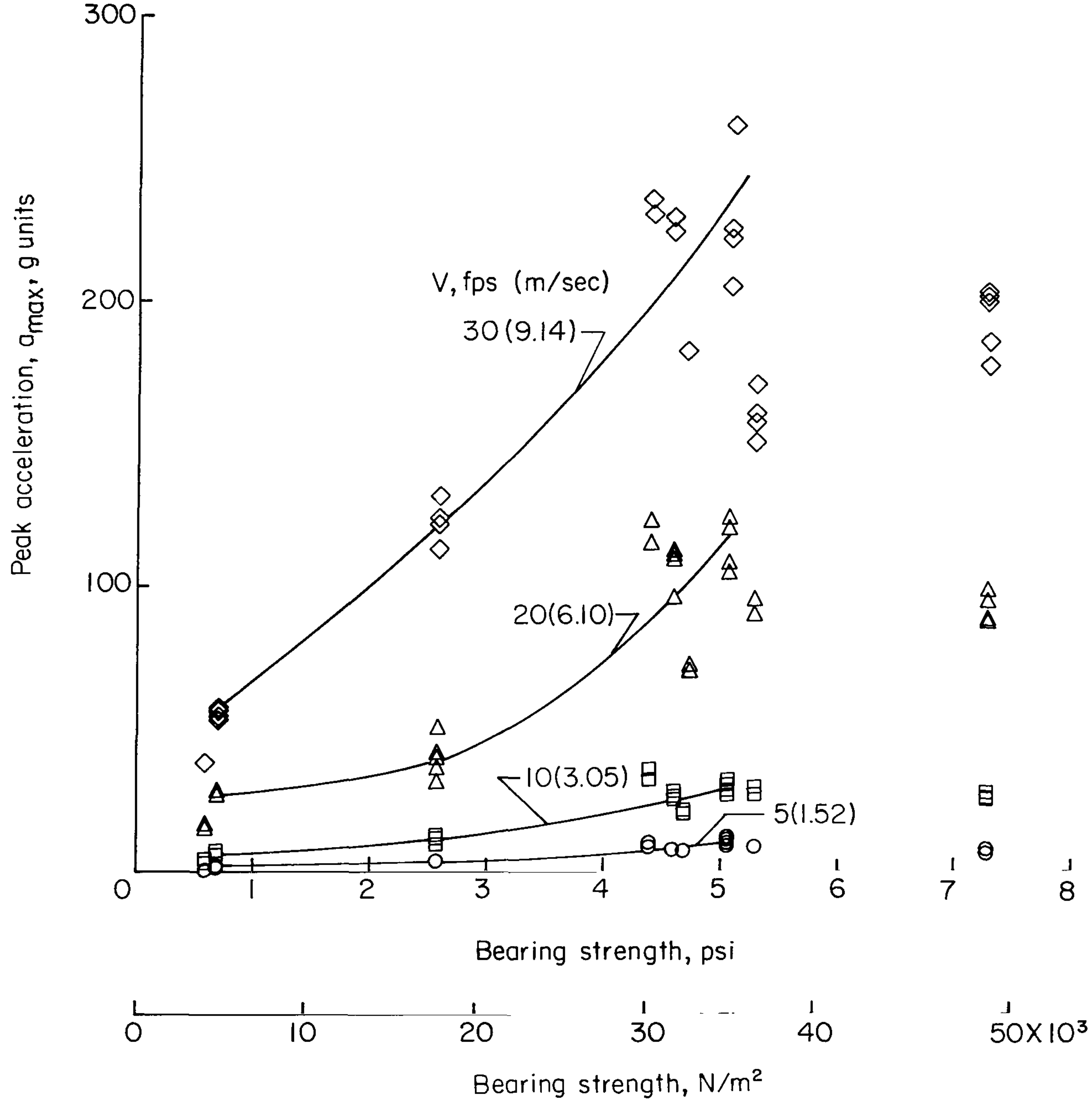

Figure 19.- Variation of peak impact accelerations with bearing strength for configuration 3.

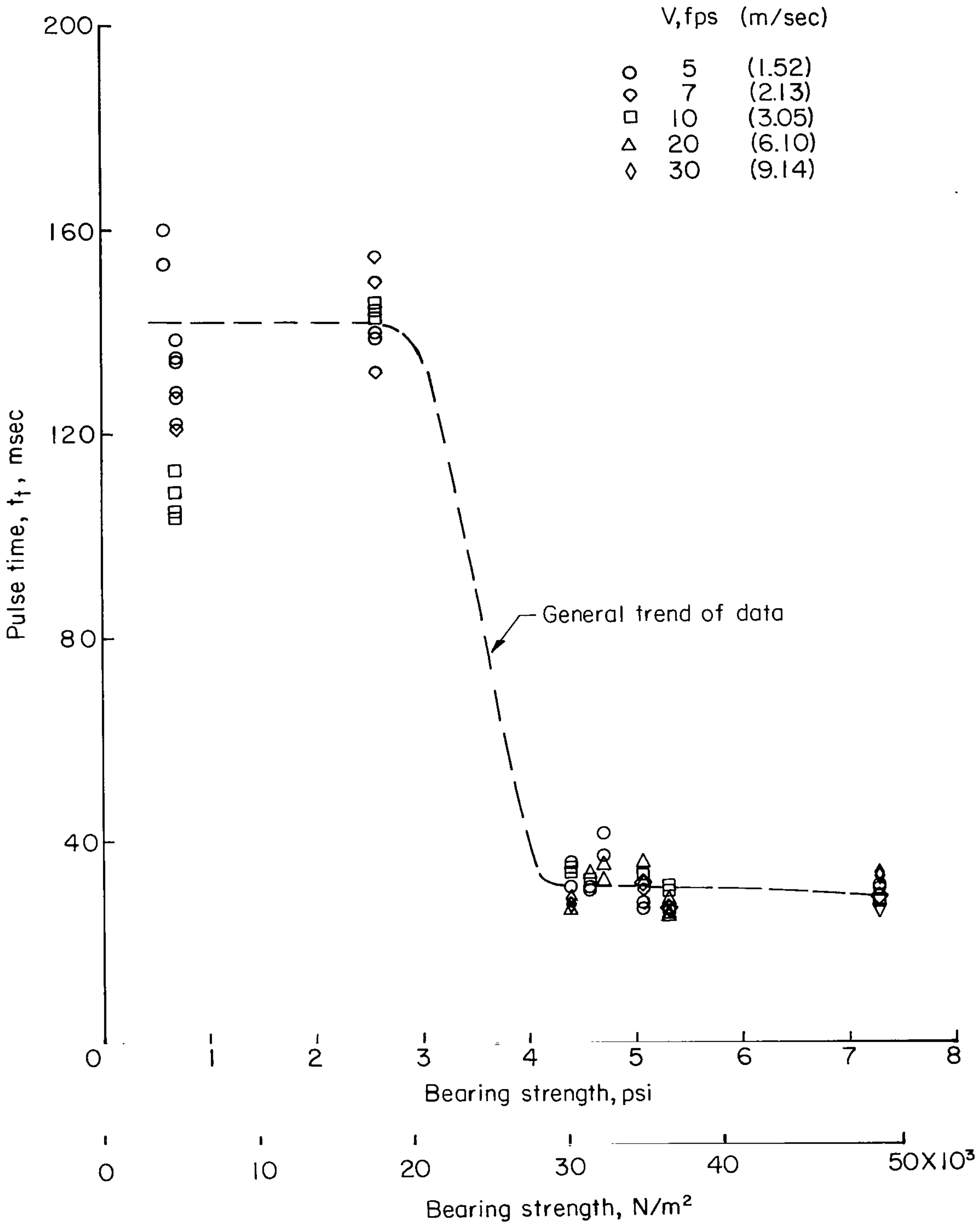

Figure 20.- Variation of pulse time with bearing strength for configuration 3.

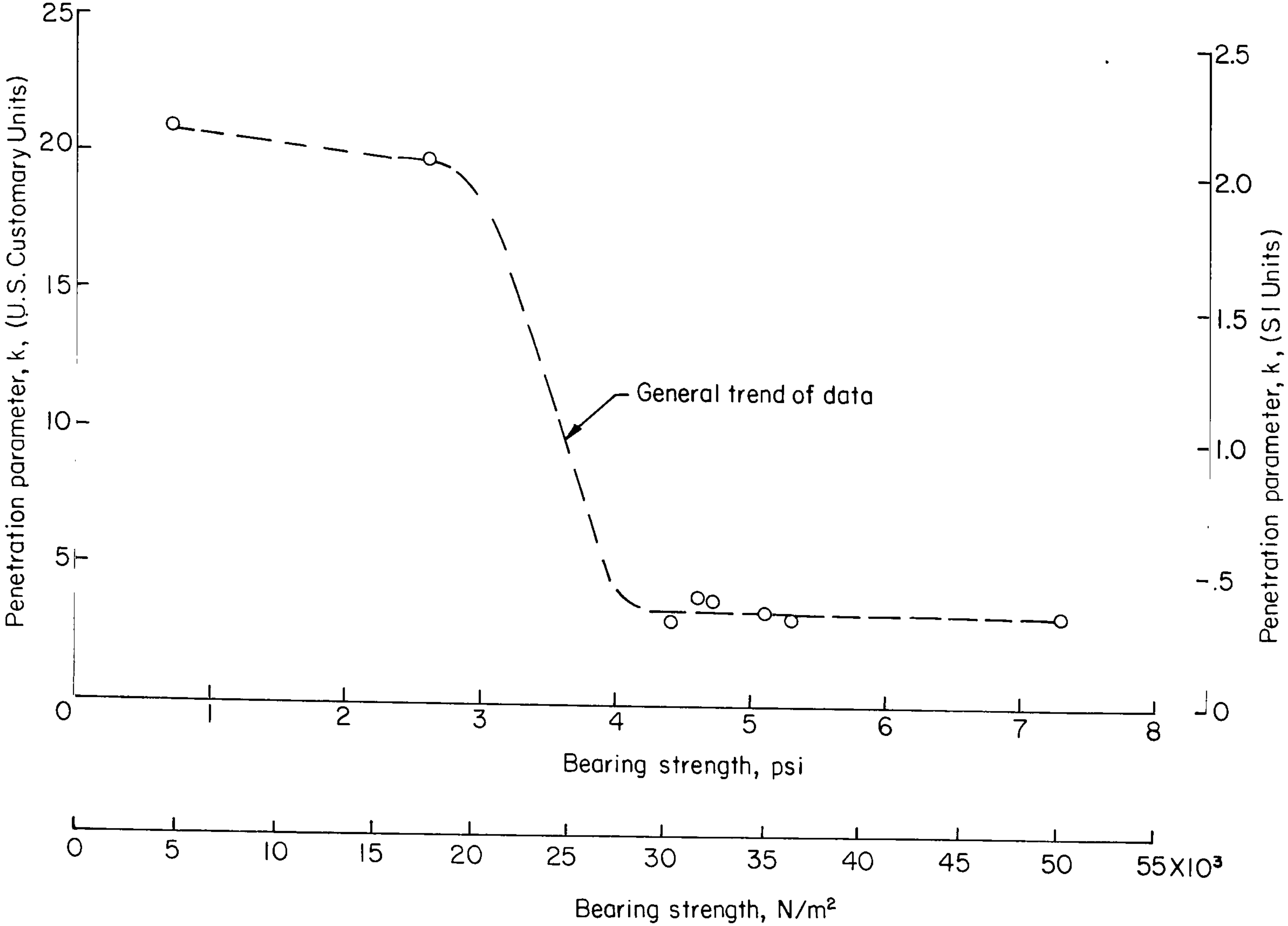

Figure 21.- Variation of penetration parameter with bearing strength. $k = \frac{y}{\frac{m^{1/2}V^{2/3}}{D}}$.

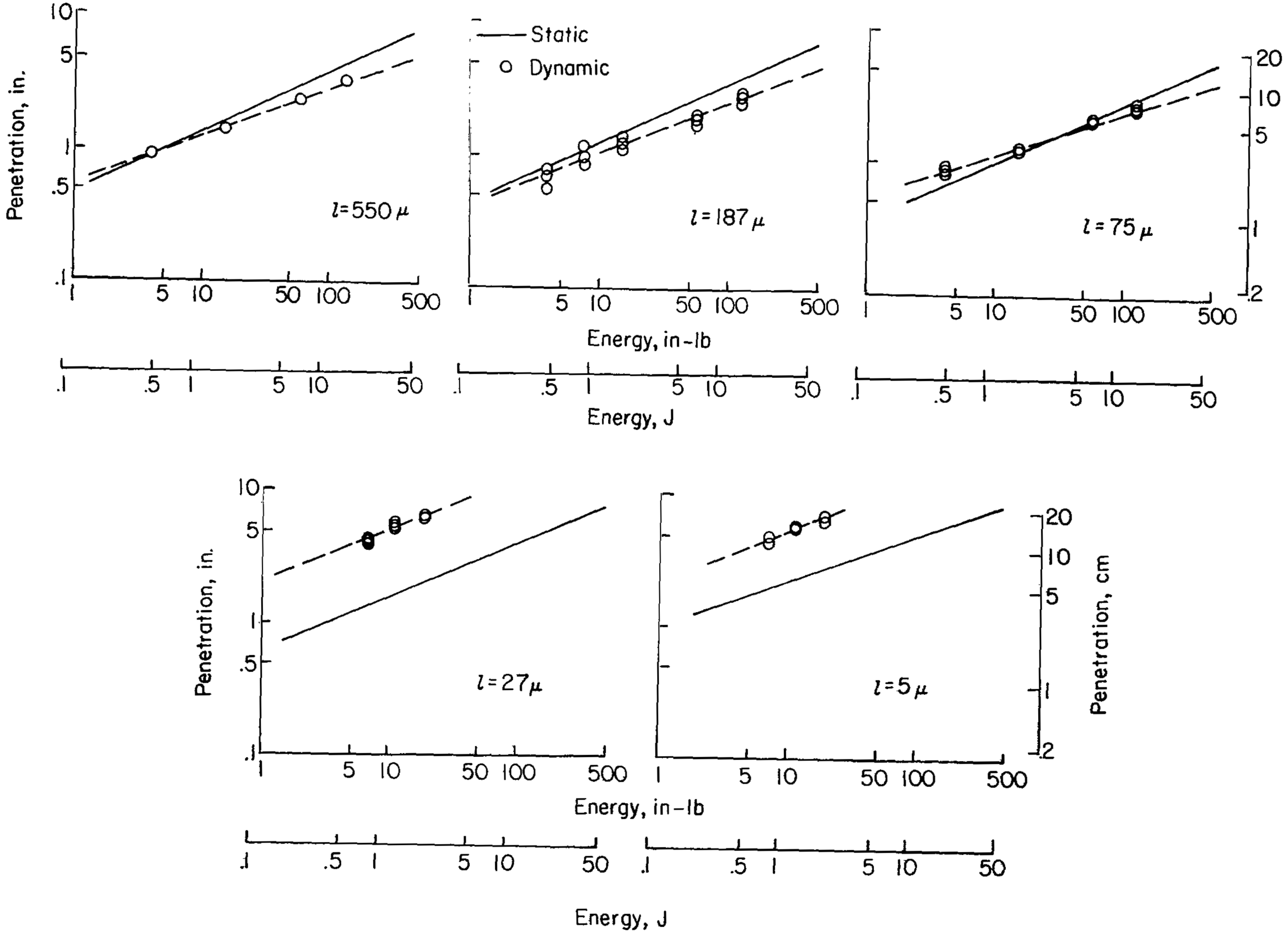

Figure 22.- Static and dynamic penetrations in various dusts as a function of expended energy for configuration 3.

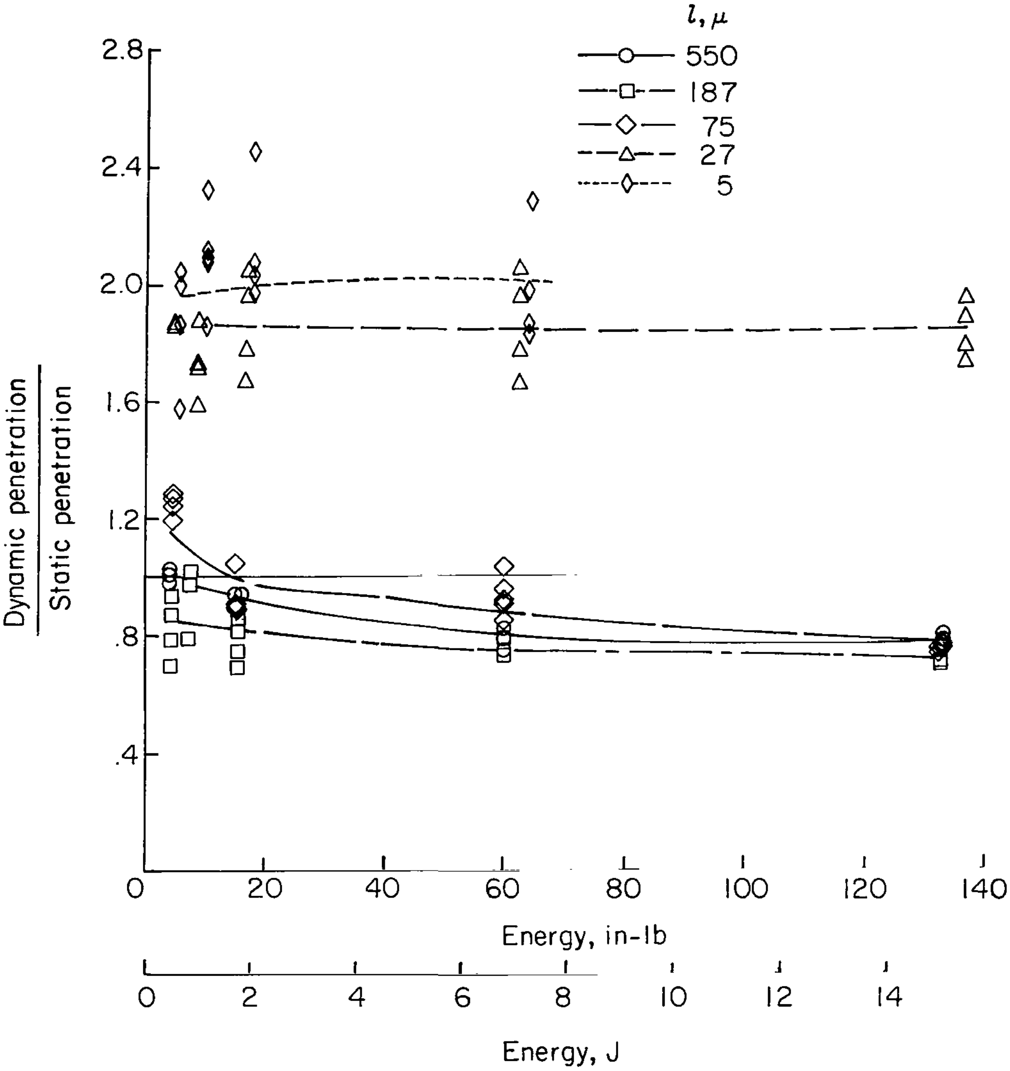

(a) Configuration 4.

Figure 23.- Ratio of penetrometer dynamic to static penetrations into various dust sizes at corresponding expended energies.

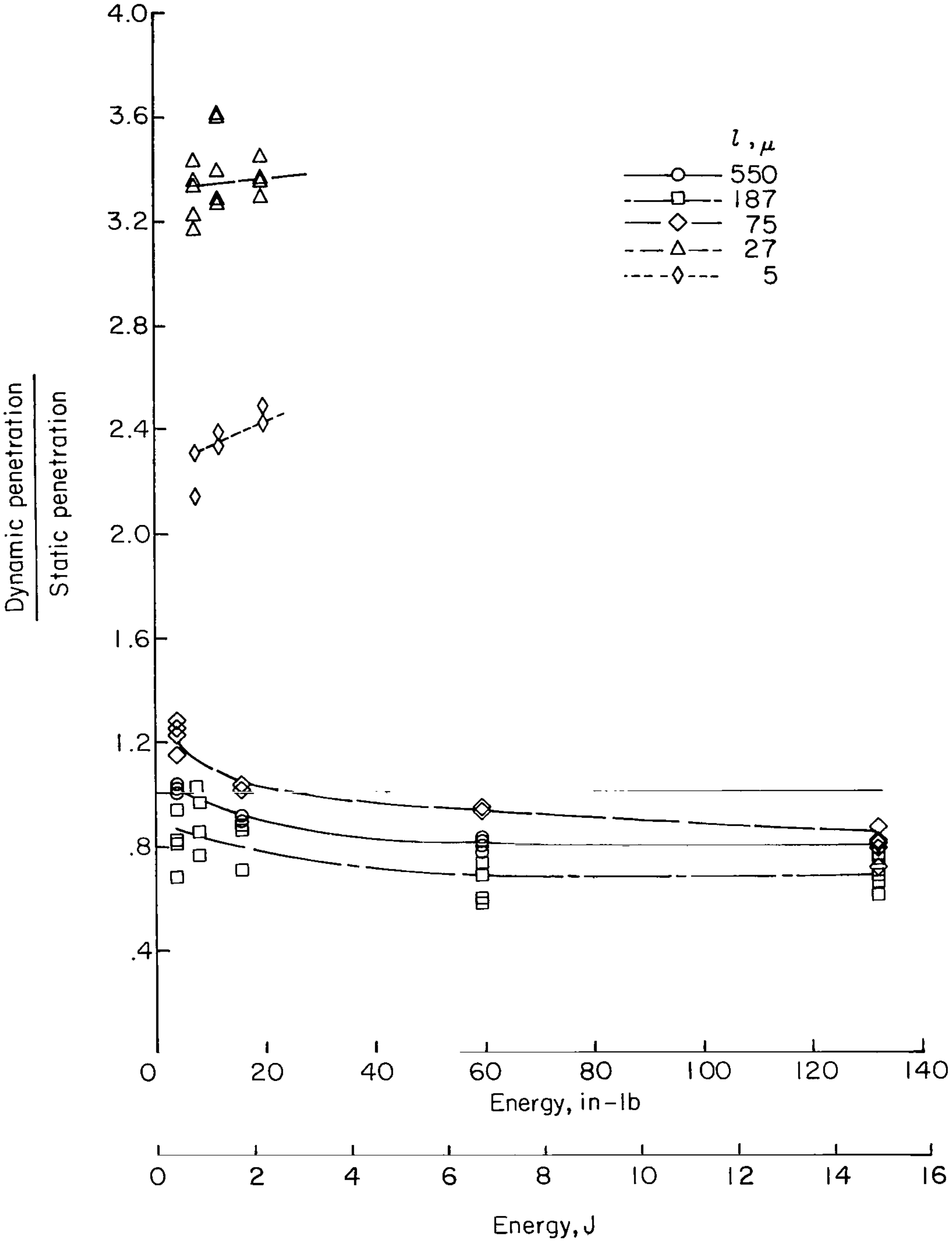

(b) Configuration 3.

Figure 23.- Continued.

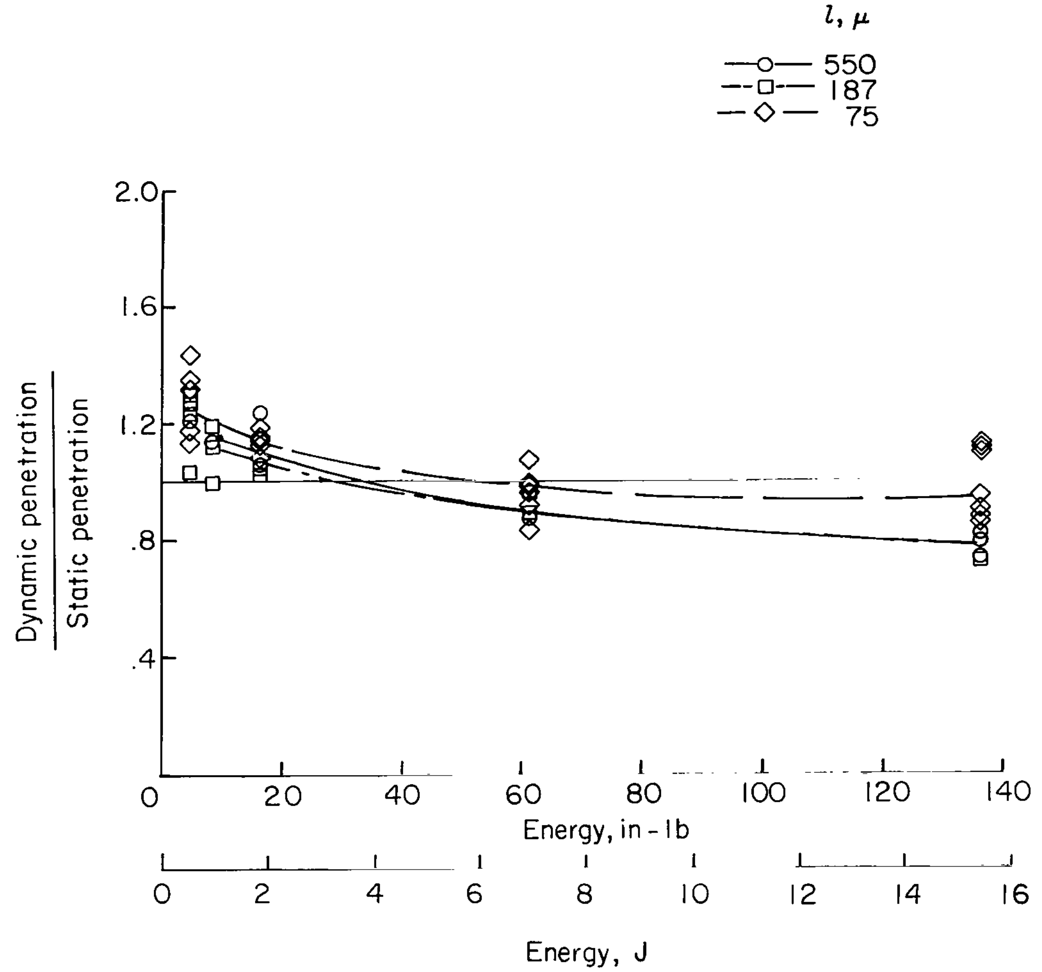

(c) Configuration 2.

Figure 23.- Continued.

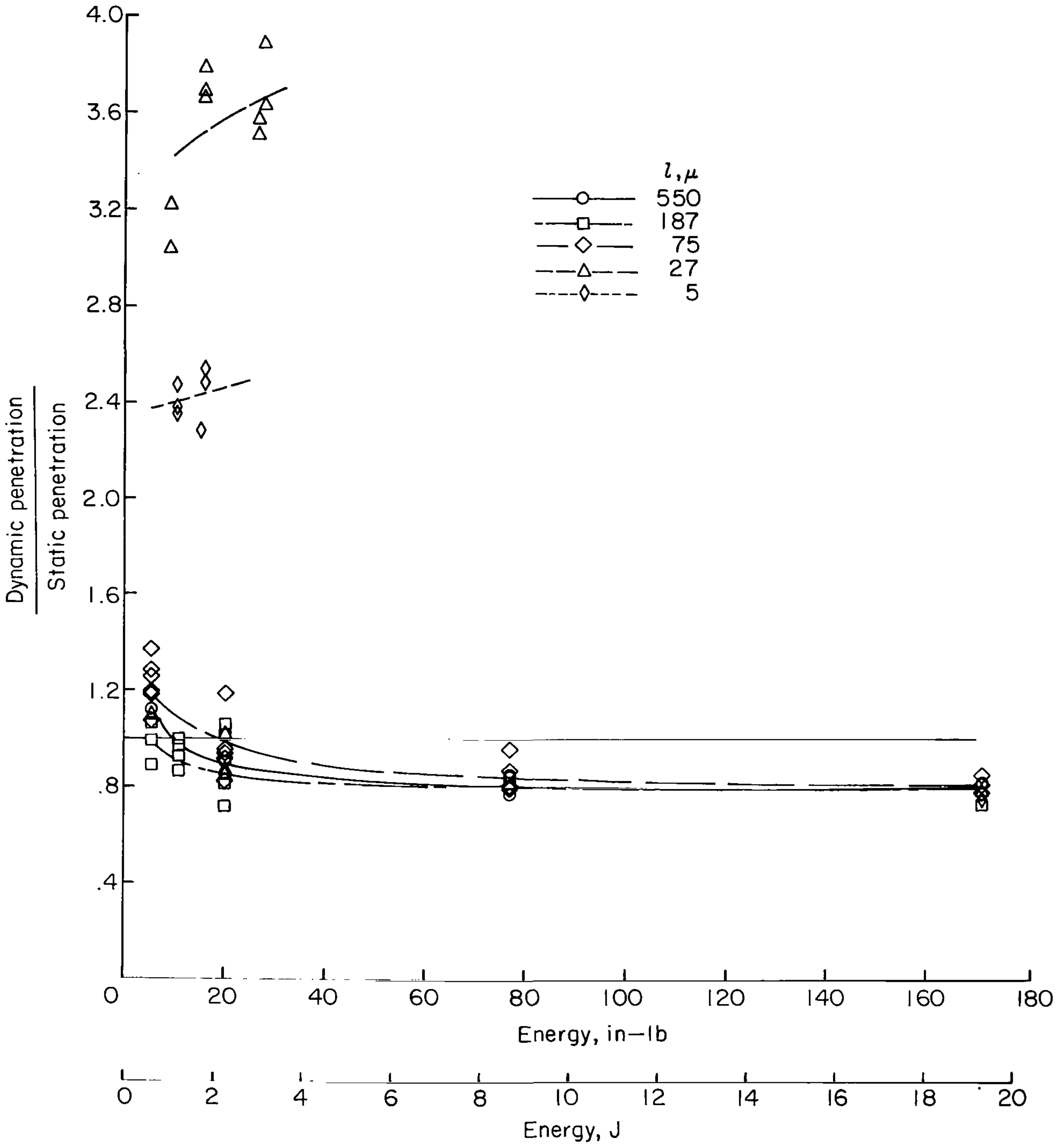

(d) Configuration 1.

Figure 23.- Concluded.